Interference Modelling and Management for Cognitive Radio Networks

by

Zengmao Chen

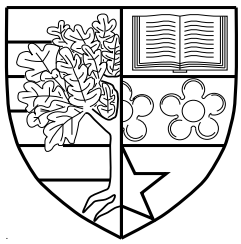

A thesis submitted in partial fulfilment for the degree of
Doctor of Philosophy

at

Heriot-Watt University
School of Engineering and Physical Sciences

May 2011

Abstract

Radio spectrum is becoming increasingly scarce as more and more devices go wireless. Meanwhile, studies indicate that the assigned spectrum is not fully utilised. Cognitive radio (CR) technology is envisioned to be a promising solution to address the imbalance between spectrum scarcity and spectrum underutilisation. It improves the spectrum utilisation by reusing the unused or underutilised spectrum owned by incumbent systems (primary systems). With the introduction of CR networks, two types of interference originating from CR networks are introduced. They are the interference from CR to primary networks (CR-primary interference) and the interference among spectrum-sharing CR nodes (CR-CR interference). The interference should be well controlled and managed in order not to jeopardise the operation of the primary network and to improve the performance of CR systems. This thesis investigates the interference in CR networks by modelling and mitigating the CR-primary interference and analysing the CR-CR interference channels.

Firstly, the CR-primary interference is modelled for multiple CR nodes sharing the spectrum with the primary system. The probability density functions of CR-primary interference are derived for CR networks adopting different interference management schemes. The relationship between CR operating parameters and the resulting CR-primary interference is investigated. It sheds light on the deployment of CR networks to better protect the primary system.

Secondly, various interference mitigation techniques that are applicable to CR networks are reviewed. Two novel precoding schemes for CR multiple-input multiple-output (MIMO) systems are proposed to mitigate the CR-primary interference and maximise the CR throughput. To further reduce the CR-primary interference, we also approach interference mitigation from a cross-layer perspective by jointly considering channel allocation in the media access control layer and precoding in the physical layer of CR MIMO systems.

Finally, we analyse the underlying interference channels among spectrum-sharing CR users when they interfere with each other. The Pareto rate region for multi-user MIMO interference systems is characterised. Various rate region convexification schemes are examined to convexify the rate region. Then, game theory is applied to the interference system to coordinate the operation of each CR user. Nash bargaining over MIMO interference systems is characterised as well.

The research presented in this thesis reveals the impact of CR operation on the resulting CR-primary network, how to mitigate the CR-primary interference and how to coordinate the spectrum-sharing CR users. It forms the fundamental basis for interference management in CR systems and consequently gives insights into the design and deployment of CR networks.

To my parents & sisters

Acknowledgements

This dissertation could not have been completed without the help of my supervisors, colleagues, friends and family. I would like to take this opportunity to express my sincere thanks to them.

My greatest appreciations go to my supervisor - Dr. Cheng-Xiang Wang. Thank him for introducing me into the research realm of wireless communications, the patient guidance, encouragement and advices he has provided throughout my PhD study. My heartfelt thanks also go to my second supervisors - Dr. John Thompson and Dr. Sergiy A. Vorobyov who cared about my work so much and responded to my questions and queries so promptly. I feel extremely lucky to have them as supervisors.

I am enormously grateful to my colleagues in our research group, Xuemin Hong, Xiang Cheng, Omar Salih, Ivan Ku, Yi Yuan, Margaret Anyaegbu, Raul Hernandez, Ammar Ghazal, Yu Fu and Fourat Haider. Many thanks for their kindly help and company during my PhD study. Thank them for making such a wonderful group for work and for life.

My special gratitude goes to my parents and sisters for their firm support, steady encouragement and continuous love.

Contents

List of Figures

List of Tables

Abbreviations

1G	First Generation
2G	Second Generation
3G	Third Generation
4G	Fourth Generation
AIC	Akaike Information Criterion
AWGN	Additive White Gaussian Noise
BS	Base Station
CPE	Customer Premises Equipment
CR	Cognitive Radio
CSI	Channel State Information
CSMA/CA	Carrier Sense Multiple Access with Collision Avoidance
DoF	Degrees of Freedom
DSA	Dynamic Spectrum Access
DVB-T	Digital Video Broadcasting – Terrestrial
EVD	Eigenvalue Decomposition
FCC	Federal Communications Commission (of United States)
FDM	Frequency Division Multiplexing
FP	Full Projection
FRESH	FREquency SHift Filter
GPS	Global Position System
i.i.d.	independent and identically distributed
IA	Interference Avoidance
IC	Interference Cancellation
IM	Interference Mitigation

INR	Interference-to-Noise Ratio
IR	Interference Region
ISM	Industrial, Scientific and Medical
IWF	Iterative Water Filling
JFI	Jain's Fairness Index
JICAP	Joint Iterative Channel Allocation and Precoding
K-S	Kalai-Smorodinsky
MAC	Media Access Control
MAI	Multi-Access Interference
MCO	Multiple Criteria Optimisation
MDL	Minimum Description Length
MH	Matern Hard-core
MIMO	Multiple Input Multiple Output
MISO	Multiple Input Single Output
MUD	Multi-User Detection
MUSIC	MUltiple SIgnal Classification
NB	Nash Bargaining
NE	Nash Equilibrium
NICAP	Non-Iterative Channel Allocation and Precoding
Ofcom	Office of Communications (of United Kingdom)
OSA	Opportunistic Spectrum Access
OFDM	Orthogonal Frequency Division Multiplexing
PDF	Probability Density Function
PIC	Parallel Interference Cancellation
PP	Partial Projection
PSD	Positive Spectrum Density
QoS	Quality of Service
QPSK	Quadrature Phase Shift Keying
RF	Radio Frequency
Rx	Receiver
SER	Symbol Error Rate

SIC	Successive Interference Cancellation
SINR	Signal-to-Interference-plus-Noise Ratio
SIR	Signal-to-Interference Ratio
SISO	Single Input Single Output
SNR	Signal to Noise Ratio
SOI	Signal Of Interest
SP	Sensing and Projection
STFT	Short-Time Fourier Transform
SVD	Singular Value Decomposition
TDD	Time Division Duplexing
TDM	Time Division Multiplexing
TDIR	Trivial over Dominant Interference Ratio
TV	Television
Tx	Transmitter
TFRs	Time-Frequency Representations
UMTS	Universal Mobile Telecommunications System
UWB	Ultra Wide Band
WRAN	Wireless Regional Area Network

Symbols

$(\cdot)^T$	transpose of a matrix
$(\cdot)^H$	Hermitian transpose of a matrix
$(\cdot)^\dagger$	pseudoinverse of a matrix
$\mathtt{tr}[\cdot]$	trace of a matrix
$\mathbb{E}[\cdot]$	statistical expectation operator
$\mathtt{rank}(\cdot)$	rank of a matrix
$\mathbb{C}^{x\times y}$	the space of $x \times y$ complex matrices
$\cup$	union of sets
$\cap$	intersection of sets
$\sum$	summation
$\prod$	production
A_i	channel allocation for ith CR transmitter
$\mathscr{A}$	channel allocation for all active CR transmitters
$C(x, r)$	a disk centred at point x with radius r
d_{nn}	nearest neighbour distance
$d_{\min}$	minimum distance between two CR transmitters
D	radius of a grey space
$f_{\mathrm{p}}(\cdot)$	PDF of the transmission power
$f_{\tilde{\lambda}}(\tilde{\lambda}_1, \tilde{\lambda}_2, \cdots, \tilde{\lambda}_{M_{\min}})$	joint PDF of $\{\tilde{\lambda}_1, \tilde{\lambda}_2, \cdots, \tilde{\lambda}_{M_{\min}}\}$
$\mathbf{F}$	precoding matrix
$\mathbf{F}_d$	precoding matrix for CR during primary downlink
$\mathbf{F}_{i,A_i}$	precoding matrix for the ith CR transmitter at the sub-channel A_i

$g(r_j)$	pathloss function at distance r_j
$\mathbf{G}_k$	channel matrix from the CR transmitter to the kth primary user
$\mathbf{G}_{U,i,A_i},\ \mathbf{G}_{D,j,A_j}$	interference channels from the primary user to the ith CR transmitter during uplink and from the primary BS to the jth CR receiver during downlink
h_j	channel gain from jth CR Tx to the primary Rx
$\mathbf{H}$	MIMO channel matrix
$\mathbf{H}_{\text{ur}}$	primary-CR Rx interference channel during uplink
$\mathbf{H}_{\text{ut}}$	primary-CR Tx interference channel during uplink
$\mathbf{H}_{\text{dr}}$	primary-CR Rx interference channel during downlink
$\mathbf{H}_{\text{dt}}$	primary-CR Tx interference channel during downlink
$\mathbf{H}_{\perp}$	effective CR channel matrix after projection
$\mathbf{H}_{i,j}$	channel matrix from the Tx i to the Rx j
$\mathbf{H}_{i,j,A_i}$	channel matrix from the ith CR Tx to the jth CR Rx over sub-channel A_i
i	$\sqrt{-1}$
$i,\ j$	index for CR users
$I_i(\mathbf{Q})$	mutual information for user i with transmit covariance matrices $\mathbf{Q}$
I_i^{NE}	mutual information for user i at NE
Int_i	average interference caused by the ith CR transmitter to the primary user
Int_l	CR-primary interference at low CR INRs
Int_h	CR-primary interference at high CR INRs
Int_h^{FP}	CR-primary interference due to FP precoding at high CR INRs
Int_h^{PP}	CR-primary interference due to PP precoding at high CR INRs
$\mathbf{I}$	identity matrix
J	Jain's fairness index

k_n	nth cumulant of the aggregate interference
K	total number of CR users
K_p	an estimate of active primary antenna numbers
l	radius of a disk centred at the primary receiver
L	radius of black space
L_S	length of sensing for SP precoding
L_{S1}	length of sensing during primary uplink
L_{S2}	length of sensing during primary downlink
L_T	length of transmission for SP precoding
L_{T1}	length of downlink transmission
L_{T2}	length of uplink transmission
m	Nakagami shape factor
M_t, M_r, M_{bs} and M_k	number of antennas for CR transmitter, CR receiver, primary base BS and the kth primary user
$M_{\min}$	minimum number of antennas
$M_{\max}$	maximum number of antennas
n	general index
$\mathbf{n}$	noise vector in MIMO channels
N	number of subchannels for primary networks
N_i^r	number of antennas at receiver i
N_i^t	number of antennas at transmitter i
p	transmission power under contention control
P_{cr}	maximum average CR transmission power
p_j	transmission power of the jth CR transmitter
P_p	transmission power of each primary user antenna
p_{pwc}	transmission power under power control
p_{hyb}	transmission power under hybrid control
$P_{\max}$	the maximum CR transmission power
q_{mh}	retaining probability of MH thinning
$\mathbf{Q}$	a set of transmit covariance matrices
$\mathbf{Q}_i$	transmit covariance matrix for user i

$\mathbf{Q}_u,\ \mathbf{Q}_d$	transmit covariance matrix for primary user during uplink and downlink
r_{cc_j}	nearest neighbouring CR-CR distance for jth CR
r_{cp}	distance between CR Tx and primary Rx
r_{hyb}	power control range for hybrid control scheme
r_j	distance between the jth CR Tx and primary Rx
r_{p}	distance between the primary Tx-Rx pair
r_{pwc}	power control range for the power control scheme
$r_{t/d}$	maximum ratio of the resulting to nullified interference
$\mathbf{r}_{i,j,A_i}(t)$	the tth received signal at CR Rx j during the time slot of CR pair i at subchannel A_i
$\mathbf{r}_{\mathrm{ut}}(t)$	the tth received symbol at the CR transmitter
$\mathbf{r}_{\mathrm{ut},i,A_i}(t)$	the tth received symbol at the ith CR transmitter at subchannel A_i
R	radius of IR
R_i	rate for user i
$\mathbf{R}_{-i}$	INR covariance matrix for user i
$\mathbf{R}_{i,j,A_i}$	covariance matrix of $\mathbf{r}_{i,j,A_i}$
$\mathbf{R}_{\mathrm{ut}}$	covariance matrix of $\mathbf{r}_{\mathrm{ut}}$
$\hat{\mathbf{R}}_{\mathrm{ut}}$	estimated $\mathbf{R}_{\mathrm{ut}}$
$\mathbf{R}_{\mathrm{ut},i,A_i}$	covariance matrix of $\mathbf{r}_{\mathrm{ut},i,A_i}$
S	bargaining set
S_n	set of cochannel CR users
$\mathbf{s}$	the transmit information vector
t	time index
$\mathbf{U},\ \mathbf{U}_d,\ \mathbf{U}_n,\ \mathbf{U}_G,\ \mathbf{U}_\perp$	unitary matrices from SVD
$\mathbf{V},\ \mathbf{V}_d,\ \mathbf{V}_n,\ \mathbf{V}_G,\ \mathbf{V}_\perp$	unitary matrices from SVD
$\mathbf{x}_u$	transmitted signal vector of all the K primary users
$\mathbf{x}_d$	transmitted signal vector of the primary BS
$\hat{\mathbf{x}}_i^{(n)}$	decoded signal vector at the receivers i
$\mathbf{y}$	received signal vector

Y	aggregated CR-primary interference
$\mathbf{z}$	interference signal vector
$\mathbf{Z}$	interference covariance matrix
α	power control exponent
β	pathloss exponent
ϕ_{Y}	characteristic function of the aggregate interference
η_{ji}	normalised INR from transmitter j to receiver i
λ	density of a stationary Poisson point process
λ_i	the ith eigenvalue of a matrix
μ	mean value
μ_Ω	standard mean of a log-normal distribution
ρ_i	normalised SNR for user i
σ^2	variance value
σ_Ω^2	standard variance of a log-normal distribution
τ	fraction of convex combination
θ	the angle between the line joining primary Tx and CR Tx and the line joining primary Tx-Rx pair
ω	variable in frequency domain
Φ	stationary Poisson point process
Φ_{th}	thinned stationary Poisson point process
Φ_{mh}	Matern hard-core point process
Γ_k	interference temperature limit for primary user k
$\mathbf{\Lambda}^{1/2},\ \mathbf{\Lambda}_d^{1/2},\ \mathbf{\Lambda}_n^{1/2},\ \mathbf{\Lambda}_G^{1/2},\ \mathbf{\Lambda}_\perp^{1/2}$	diagonal eigenvalue vectors from SVD

Chapter 1

Introduction

1.1 Problem Statement

Wireless communication is one of the few technologies that have significantly changed lives of human beings. In 1901, Marconi convincingly demonstrated the practicality of wireless communication by sending the first radio signal across the Atlantic, and a new era was born ever since then. After evolving over a century, wireless communication can find its applications in various aspects of our lives nowadays, ranging from highly commercialised cellular and satellite communication systems to privately used amateur radio, from daily used WiFi networks to rarely seen deep space communication systems, from infrastructure-based radio and television broadcast systems to ad hoc-oriented wireless microphones and Bluetooth devices. New wireless applications are still keeping emerging as the demand for them never stops.

Radio spectrum, the indispensable media underpinning a wireless communication system, is conventionally assigned to each wireless application for exclusive use by regulatory bodies like Federal Communications Commission (FCC) in the USA and Office of Communications (Ofcom) in the UK. It is becoming increasingly scarce as more and more devices go wireless. Meanwhile, studies indicate that there is a vast amount of spectrum not fully utilised in the domain of time, frequency and space [6]. Measurement campaigns have shown that up to 85% of the spectrum is wasted temporally

in some bands below 3 GHz [2, 7]. The imbalance between the plausible spectrum scarcity and eventual spectrum underutilisation has inspired a revolutionary paradigm shift on spectrum access by allowing the spectrum to be shared and reused in a dynamic manner, which is known as dynamic spectrum access (DSA) [3]. Cognitive radio (CR) is a prominent candidate technology enabling the DSA. It is capable of sensing its surrounding environment and adapting its operational parameters dynamically and autonomously to coexist with the incumbent systems (primary systems) in a nonintrusive manner [6]. It is envisioned as a promising solution to greatly improve the spectrum utilisation by reusing the underutilised spectrum owned by primary systems.

Interference is one of the key factors affecting the wireless network performance and has been a long-lasting problem coupling wireless communication systems. It is by no means an exaggeration to say that wireless communication is nothing but combating interference and impairment of wireless channels. In the context of CR networks, the interference issues are extremely important. Its paramount significance lies on two aspects. On one hand, CR holds the fundamental premise of not causing any detrimental interference to the primary system. On the other hand, CR performance may be limited by interference coming from either the primary or other CR nodes. Therefore, the interference related issues in CR networks deserve careful and comprehensive study, which is the main focus of this thesis.

1.2 Motivation

With the introduction of CR networks, two novel types of interference originating from CR networks are introduced. They are the interference from CR to primary networks (CR-primary interference) and the interference among spectrum-sharing CR nodes (CR-CR interference). The former is caused by spectrum sharing between CR and primary networks. While, the latter is due to spectrum sharing among CR nodes. Both types of interference should be well managed by CR networks in order not to

jeopardise the operation of the primary network and to improve the performance of CR systems. This motivates the research conducted in this thesis.

For the CR-primary interference, it is desirable to investigate how CR networks potentially affect the primary system. This requires interference modelling for CR networks to examine the impact of CR operation on the resulting CR-primary interference. It consequently gives clue for the deployment of CR networks aiming at minimising the CR-primary interference. Moreover, interference mitigation techniques applicable to CR networks are worth studying to further reduce the CR-primary interference. Physical layer signal processing has been widely used in interference mitigation. We can also perform the interference mitigation more effectively from a cross-layer perspective.

When multiple CR links share the spectrum, the CR-CR interference is inevitable. This naturally raises the problem of how to coordinate the mutually interfering CR nodes. The interference channels can be analysed by characterising the rate region of CR interference systems. Various signalling and interference mitigation techniques applicable to spectrum-sharing CR nodes need to be investigated by analysing their resulting rate regions.

1.3 Contributions

The key contributions of the thesis are summarised as follows:

- **Modelling the CR-primary interference:**

  We model the aggregate CR-primary interference by deriving its probability density function (PDF) for CR networks under different interference management mechanisms, including power control, contention control and hybrid power/contention control schemes. The impact of key CR operational parameters on the resulting CR-primary interference is investigated. The effect of hidden primary receiver on the CR-primary interference is examined as well.

- **Mitigating the CR-primary interference:**

  We first carry out a comprehensive review on a variety of interference mitigation techniques applicable to CR transmitters. Then, we focus on mitigating the CR-primary interference for CR multiple-input multiple-output (MIMO) systems. Two precoding-based interference avoidance schemes are proposed for CR MIMO systems to avoid interfering with the primary network and to boost the throughput of the CR system. To better mitigate the CR-primary interference, we perform the interference mitigation in a cross-layer manner by jointly considering precoding in the physical layer and channel allocation in the media access control (MAC) layer. Two distributed algorithms are proposed for the cross-layer interference mitigation.

- **Analysing the CR-CR interference channels:**

  We confine our attention to analysing multi-user CR MIMO interference systems. The Pareto rate region for MIMO interference systems are characterised by finding a sufficient condition for the convexity of the rate region. Then, various rate region convexification approaches including orthogonal signalling and interference mitigation techniques are examined and their resulting rate regions are analysed for the MIMO interference system. An achievable rate region is also given for multi-user MIMO interference systems. Finally, we apply Nash bargaining (NB) to coordinate the interfering CR users. The characteristics of the NB over MIMO interference systems such as the existence, uniqueness and optimality are studied.

The work presented in this thesis has led to the following publications:

Journals

1. **Z. Chen**, C.-X. Wang, X. Hong, J. Thompson, S. A. Vorobyov, F. Zhao, H. Xiao, and X. Ge, "Interference mitigation for cognitive radio MIMO systems based on practical precoding," *IEEE Trans. Wireless Commun.*, submitted for publication, 2011.

2. **Z. Chen**, S. A. Vorobyov, C.-X. Wang, and J. Thompson, "Convexification of Pareto region and Nash bargaining for rate control in MIMO interference systems via interference mitigation," *IEEE Trans. Autom. Control*, submitted for publication, 2011.

3. **Z. Chen**, C.-X. Wang, X. Hong, J. Thompson, S. A. Vorobyov, X. Ge, H. Xiao, and F. Zhao, "Aggregate interference modeling in cognitive radio networks with power and contention control," *IEEE Trans. Commun.*, accepted for publication, Mar. 2011.

4. X. Hong, **Z. Chen**, C.-X. Wang, and S. A. Vorobyov, "Cognitive radio networks: interference cancellation and management techniques," *IEEE Veh. Technol. Mag.*, vol. 4, no. 4, pp. 76–84, Dec. 2009.

Conferences

1. **Z. Chen**, C.-X. Wang, X. Hong, J. S. Thompson, S. A. Vorobyov, and D. Yuan, "Cross-layer interference mitigation for MIMO cognitive radio systems," in *Proc. IEEE ICC'11*, Kyoto, Japan, June 2011, accepted for publication.

2. **Z. Chen**, C.-X. Wang, X. Hong, J. Thompson, S. A. Vorobyov and X. Ge, "Interference modeling for cognitive radio networks with power or contention control," in *Proc. IEEE WCNC'10*, Sydney, Australia, Apr. 2010.

3. **Z. Chen**, S. A. Vorobyov, C.-X. Wang, and J. S. Thompson, "Nash bargaining over MIMO interference systems," in *Proc. IEEE ICC'09*, Dresden, Germany, June 2009.

1.4 Thesis Organisation

The remainder of this thesis is organised as follows:

Chapter 2 gives some essential background information for the research work presented in this thesis. We first give introduction on the concepts of the DSA. It is followed

by the introduction on CR technology including the operational mode and potential deployment of CR networks. Then, different types of interference involved in CR networks are analysed. At the end, the interference assessment for CR networks is introduced.

Chapter 3 presents the aggregate CR-primary interference modelling for CR networks under different interference management mechanisms. It begins with giving some mathematical preliminaries in stochastic geometry which is used to model the spatial distribution of CR nodes. Three interference management mechanisms adopted by CR networks including power control, contention control and hybrid power/contention control schemes are introduced as well. Then, the detailed interference modelling is given by deriving the interference PDFs via characteristic function- and cumulant-based approaches. Finally, we model the aggregate interference by taking the hidden primary receiver problem into account.

Chapter 4 focuses on the interference mitigation for CR networks. It first gives a comprehensive review on a family of interference mitigation techniques applicable to CR transmitters. Then, we confine our attention to CR-primary interference mitigation for CR MIMO systems. Two precoding-based interference avoidance schemes are proposed to proactively mitigate the CR-primary interference. Moreover, to better mitigate the CR-primary interference, we also propose two cross-layer interference mitigation algorithms by jointly considering precoding in the physical layer and channel allocation in the MAC layer.

Chapter 5 analyses the interference channels for spectrum-sharing CR networks. The Pareto rate region of multi-user MIMO interference systems is characterised by finding a sufficient condition which guarantees the convexity of the rate region. A variety of interference management techniques such as orthogonal signalling, interference cancellation at receivers and null space projection-based precoding at transmitters are analysed to convexify the rate region. An achievable rate region is also given for multi-user MIMO interference systems. Finally, NB is applied to coordinate the operation of interfering CR users. The characteristics of different NB solutions over MIMO interference systems such as uniqueness, existence and optimality are studied.

Chapter 6 concludes the thesis and suggests some future research topics.

Chapter 2

Background

2.1 Status Quo of Radio Spectrum

Radio spectrum refers to the part of electromagnetic spectrum corresponding to radio frequencies - that is, frequencies lower than around 300 GHz [8]. It is the transmission media carrying any wireless communication. By nature, radio spectrum is a precious and limited natural resource. For wireless systems operating in very low frequencies, the effective antenna size has to be very large, which is not feasible for portable wireless devices. As for spectrum with high frequencies, the wireless channel becomes too hostile for the propagation of electromagnetic waves. Therefore, only a limited range of spectrum is usable for wireless communications. This range of radio spectrum is usually divided into non-overlapping bands and assigned to different wireless applications for exclusive use to avoid mutual interference. The spectrum allocation is typically government regulated by regulatory agencies like FCC in the USA and Ofcom in the UK. Some bands are allocated to certain applications free of charge, e.g., the industrial, scientific, and medical (ISM) band for cordless telephones or wireless computer networks. Other bands are licensed or sold to private communication systems like cellular telephone operators and satellite communication companies.

The spectrum allocation in the USA is shown in Figure 2.1. Even a casual observer can easily tell from the figure that the radio spectrum has been fully "booked" due to

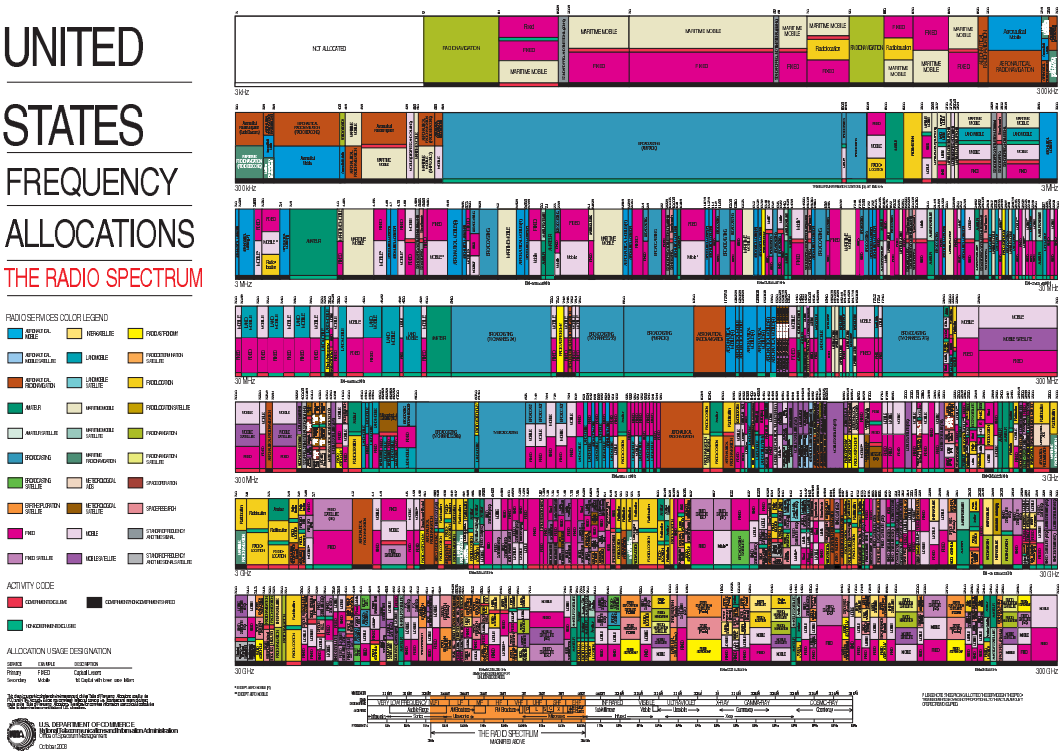

FIGURE 2.1: U.S. frequency allocations chart [1].

its "overcrowded" looking. It seems that the spectrum is too scarce to accommodate new wireless applications. The demand for bandwidth (radio spectrum), however, never stops by newly emerging wireless services. One representative example is cellular mobile communication, mobile communication systems have evolved from the voice oriented first generation (1G) and second generation (2G) to the multimedia-rich third (3G) and fourth generations (4G) over the last three decades. The technology evolution in mobile communication is driven by exponential increase in throughput demand and needs to acquire additional bands to operate on. The conflicts between spectrum availability and spectrum demand has incurred widely spread anxiety of spectrum scarcity. This can be reflected by the record-breaking auction of British 3G spectrum in early 2000. The UK 3G - Universal Mobile Telecommunications System (UMTS) spectrum licenses were sold for the extraordinary sums of £22 billions to five operators with only a 20-year tenure of use.

Despite the widely perceived spectrum scarcity, spectrum measurements unveil an astonishing fact on spectrum utilisation. Studies undertaken by the FCC [7] and

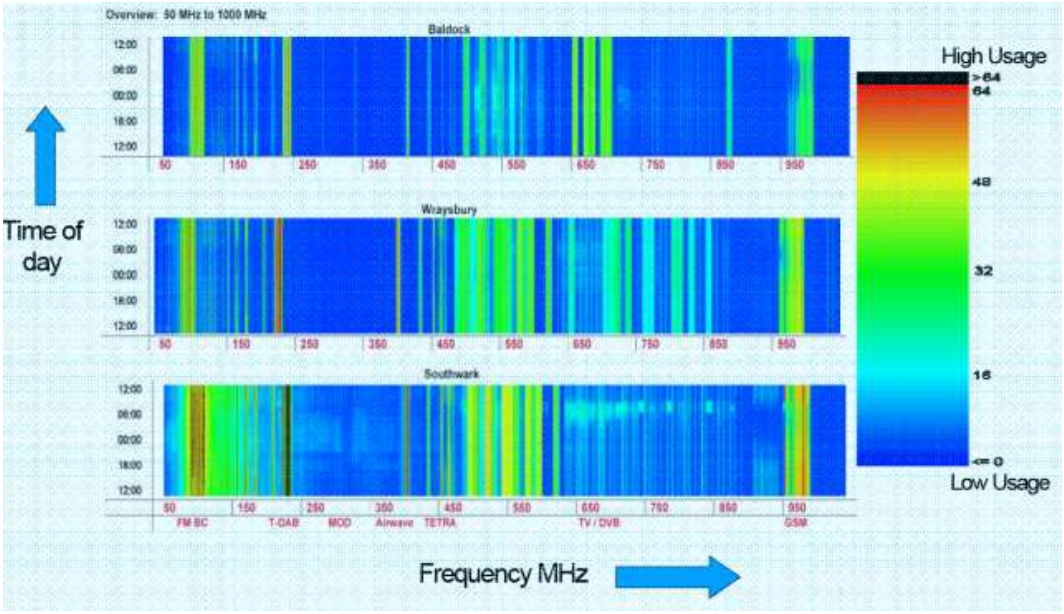

FIGURE 2.2: Spectrum occupancy measurements in a rural area (top), near Heathrow airport (middle) and in central London (bottom) [2].

the Ofcom [2] have revealed that the spectrum utilisation shows huge temporal and spatial variations ranging from 15 to 85% for spectrum below 3 GHz. An example of spectrum usage measurement in England is shown in FIGURE 2.2. These measurement campaigns indicate that a vast amount of spectrum bands are not fully used all the time or everywhere. In another word, the radio spectrum is eventually underutilised. It has been commonly accepted that the fixed spectrum allocation and the exclusive use of spectrum make the spectrum underutilised and appear scarce. There is potential to make considerably better use of spectrum if the spectrum is used in a more dynamic and flexible manner.

2.2 Dynamic Spectrum Access

The imbalance between plausible spectrum scarcity and eventual spectrum underutilisation has inspired enormous research on DSA. In contrast to the current fixed spectrum access policy where spectrum is allocated for exclusive use, DSA introduces a revolutionary paradigm shift on spectrum management by introducing much more flexibility into spectrum access. It allows the spectrum to be shared and reused

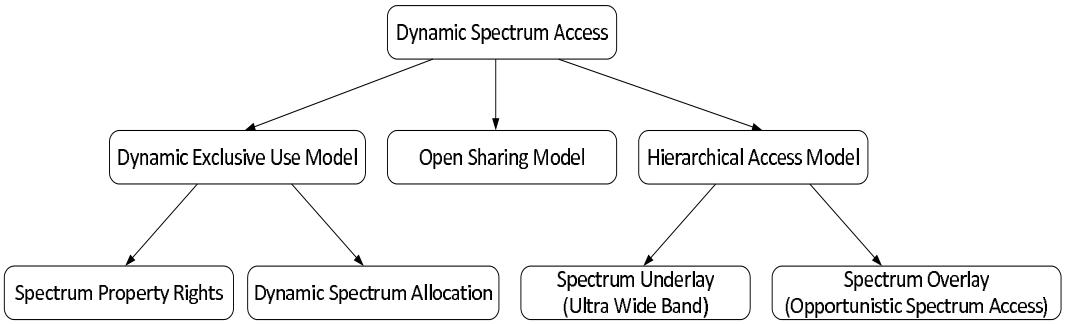

FIGURE 2.3: A taxonomy of dynamic spectrum access [3].

among different wireless applications on a negotiable or opportunistic basis. Therefore, it has the potential to greatly improve the spectrum utilisation. As illustrated in FIGURE 2.3, DSA can be broadly divided into three categories according its operation model [3].

- **Dynamic exclusive use model**

  It shares the similar philosophy with current fixed spectrum access in that the spectrum is rigidly for exclusive use once allocated, but it allows more flexibility in spectrum allocation. This can be achieved via either *spectrum property rights* or *dynamic spectrum allocation*. The former allows licensed spectrum holders lease or trade their spectrum freely with other wireless operators. For example, TV broadcasters may temporarily lease parts of TV bands to mobile operators to provide cellular network coverage for special festivals or events. While, the latter allocates the spectrum in a more dynamic manner in terms of time and location according to the traffic characteristics of different services. For instance, the spectrum allocation can be performed more frequently, e.g., hourly, for wireless applications with rapidly changing traffic load.

- **Open sharing model**

  In this model, peer users sharing the spectrum openly with equal access rights and priorities. An example of wireless network adopting this model is WiFi, which shares the ISM band freely and fairly with many other wireless systems like Bluetooth devices, cordless telephones, etc.

- **Hierarchical access model**

  This model differs from open sharing model in that spectrum users working in hierarchical access model have different priorities and are distinguished as primary and secondary users. Primary users who own the spectrum have the absolute privilege to use the spectrum. While, secondary users do not have the license to use the spectrum. They can reuse it only in a nonintrusive manner. To use an analogy, primary users are "hosts", while secondary users are like "guests". This model can be further divided into two subcategories: *spectrum underlay* and *spectrum overlay*. In spectrum underlay approach, the transmission power spectrum density (PSD) of secondary users is strictly constrained by a predefined spectral mask so that the PSD of secondary transmission is below that of the noise for primary users. Primary users can simply treat the secondary interference as background noise. Ultra wide band (UWB) systems is a representative example of this approach. They maintain a very low PSD for secondary transmission by spreading the secondary signals into a very wide band of spectrum [9]. Whereas, for spectrum overlay, no predefined PSD constraint is imposed on secondary users. Instead, secondary users can identify and exploit the spectrum opportunity without detrimentally interfering with primary users. This is also known as opportunistic spectrum access (OSA). The newly emerging CR serves as an enabling technology for OSA.

2.3 Cognitive Radio Technology

CR, first coined by Mitola in 1998 [10, 11], is a "smart" radio system aware of its surrounding operational environment by sensing and reasoning, and capable of dynamically and autonomously adjusting its radio operating parameters to coexist with the primary users in a nonintrusive manner [4, 6, 12]. CR is envisioned as a promising technology to improve the spectrum utilisation by sharing the underutilised spectrum with the legacy users in a hierarchical manner without causing detrimental interference to the primary network.

To facilitate the nonintrusive coexistence with primary users, a CR is supposed to have a set of cognitive capabilities as illustrated in FIGURE 2.4 [4]. The following three main capabilities need to be incorporated throughout the whole cognitive cycle.

- **Spectrum sensing**

  Intuitively, how to find out the available spectrum holes from a spectrum pool, is the first step for a CR. In this step, the radio environment is constantly monitored, and *spectrum holes* are detected by a CR. Spectrum holes, also known as frequency voids or *white spaces*, refer to frequency segments that are originally licensed to the primary network, but unused or partly occupied by the primary system temporally or in some geographical locations. Spectrum sensing can be performed by using energy detection [13] or cyclostationary feature detection [14] across the spectrum pool. Cooperative spectrum sensing has gained much recognition as a more appealing sensing technique in terms of detection accuracy [15].

- **Spectrum analysis**

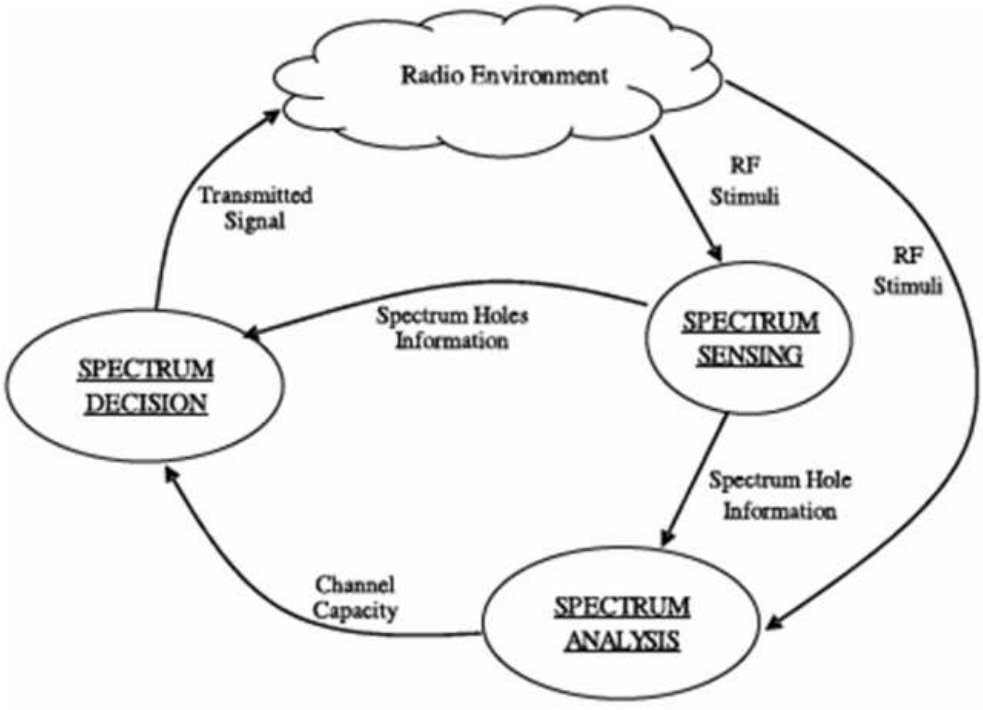

FIGURE 2.4: Cognitive cycle of CR systems [4].

The spectrum holes information is analysed in this phase. The characteristics of spectrum holes, such as the interference level they suffers and the channel capacity they can offer, are estimated and forwarded to the next also the final stage.

- **Spectrum decision**

  A CR network synthesises all the information from spectrum sensing, spectrum analysis and CR user demand to determine which spectrum band to choose and how the transmission should be carried out.

According to the way that CR systems reuse the spectrum, a CR network can operate on a *non-interfering* or *interference-tolerant* basis.

2.3.1 Non-interfering Cognitive Radio

For non-interfering (or interference-free) CR [16, 17], as the name suggests, theoretically it does not cause any interference to the primary system by only reusing spectrum holes that are not occupied by the primary users. That is, only white spaces of the primary system are exploited by the CR network. Obviously, CR working in a non-interfering manner is favourable to the primary network, since the quality-of-service (QoS) of primary network is not compromised at all. Moreover, the primary system does not need to be aware of the existence of the CR users, i.e., no modification is required in primary systems to accommodate CR applications, because CR systems always "avoid" the primary transmission "automatically". Therefore, non-interfering CR is chosen by the IEEE 802.22 working group as the enabling technique for the first standardised CR network - wireless regional area network (WRAN) [18].

WRAN aims at providing wireless broadband access service in lightly populated rural areas by using non-interfering CR technique to share the geographically unused TV bands licensed to television broadcasters [19]. The initial 802.22 standard specifies that a WRAN works in a point to multipoint manner. It consists of a base station (BS) and customer premises equipments (CPEs). Each CPE is attached to a BS. The

BS is a central controller managing the access of CPEs that attach to it. A WRAN can operate in two approaches. One approach is based on spectrum sensing. Each CPE performs independent sensing in the TV bands and reports the sensing result to the BS regularly. The BS gathers and analyses the sensing information from all the associated CPEs and instructs each CPE which band it should operate on. The other approach is geo-location based. All the BS and CPEs are capable of finding their own location using some location identification techniques like the Global Positioning System (GPS). With their location information, the BS determines the channels that the associated CPEs can use by regularly looking up an incumbent database. The incumbent database keeps the live information of licensed TV operation in any given geographical location and it is usually maintained by spectrum regulatory bodies.

2.3.2 Interference-Tolerant Cognitive Radio

In contrast to non-interfering CR, interference-tolerant CR [20–22] can share the whole spectrum with the primary system (including the bands that are being used by primary users), but the interference experienced at the primary receiver from CR networks must be maintained below a specific level without causing any outage on primary operation. In another word, the CR system can reuse the whole spectrum so long as the primary network can "tolerate" it. To implement an interference-tolerant CR, the primary receiver has to provide CR systems the information of how much interference it can tolerate across the spectrum, which is known as *interference temperature limit*. Thus, a real-time feedback mechanism from the primary to the CR networks is essential to inform the CR network of the interference temperature limit. In order to facilitate this functionality, some modification on the primary system is inevitable.

It is easy to understand that non-interfering CR is a transmitter-centric approach since it indirectly controls the potential CR-primary interference by regulating CR transmitters to only exploit spectrum holes. While, interference-tolerant CR is receiver-centric due to the fact that the primary receiver directly controls the CR-primary interference by giving CR networks the interference temperature limit. Moreover, interference-tolerant CR leads to higher spectrum utilisation than non-interfering CR,

since the former has more available spectrum than the latter. However, interference-tolerant CR needs the intervention of the primary network to acquire the interference temperature limit. The requirement for the primary network intervention makes interference-tolerant CR undesirable or even infeasible sometimes. Therefore, people commonly regard non-interfering CR as the first generation CR networks and interference-tolerant CR as a long-term evolution goal.

2.4 Interference in Cognitive Radio Networks

Interference involved in CR networks can be classified into two types: intra-network interference and inter-network interference. Intra-network interference, also known as self-interference, refers to the interference caused within one network (either a primary or CR network). Typical examples of intra-network interference include inter-symbol interference in frequency selective channels and multi-access interference (MAI) in multi-user networks. Intra-network interference exists to some extent in every wireless communication system and there is a wealth of techniques established to mitigate them effectively. On the other hand, inter-network interference refers to the mutual interference between the primary and CR networks. The problem of inter-network interference management is two-fold. First, CR transmitters need to carefully control their emissions to guarantee that the QoS of the primary network is not harmfully degraded by the CR-primary interference. Second, CR receivers should be able to effectively combat the primary-CR interference and provide useful QoS to the CR application. We first give an introduction on the characteristics of the inter-network interference.

2.4.1 CR-Primary Interference

To assess the CR-primary interference in interference-tolerant CR systems, a new metric - interference temperature has been proposed in [4]. Unlike traditional transmitter-centric approaches that seek to regulate interference indirectly by controlling the emission power, time, or locations of interfering transmitters, the interference temperature model takes a receiver-centric approach and aims to directly manage interference at primary receivers through interference temperature limits. The interference temperature limit characterises the "worst case" interfering scenario in a particular frequency band and at a particular geographic location for primary receivers [4, 23]. In other words, it represents the maximum amount of interference that the primary receiver can tolerate.

The interference temperature model serves as a useful tool to characterise the CR-primary interference. An ideal interference temperature model should account for the cumulative radio frequency (RF) energy from multiple CR transmissions and sets a maximum cap on their aggregate level. CR users are then allowed to use a frequency band as long as their transmissions do not violate the interference temperature limits. Implementation of such an ideal interference temperature model usually requires real-time interactions between CR transmitters and primary receivers and is therefore widely regarded as impractical. To this end, several modified interference models [5, 24] have been proposed as more practical models for the CR-primary interference received at primary receivers.

In [24], the interference was defined as the expected fraction of primary users with services disrupted by nearby CR transmitters. Factors such as CR signal modulation, antenna gains, and power control were considered in this model. However, this model only accounted for the case where the primary services were disrupted by a single CR user and it did not consider the aggregate effect of multiple CR transmissions. In [5], the aggregate effect was taken into account and complex stochastic models were built to characterise the exact PDF of the accumulated interference power. Moreover, the interference avoidance ability of CR transmitters was considered by introducing the concept of an exclusion region. As illustrated in FIGURE 2.5, an exclusion region is

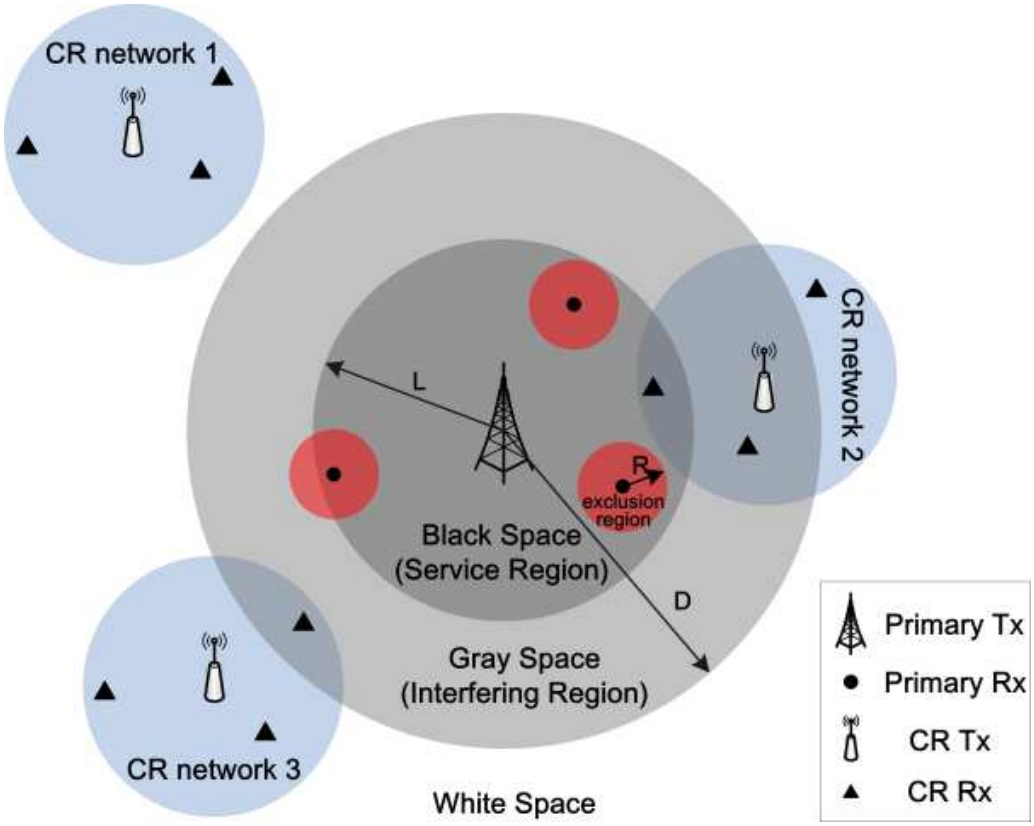

FIGURE 2.5: Coexistence of a primary network and randomly distributed CR networks with illustrations of the exclusion region, black space (service region), grey space (interfering region), and white space.

defined as a disk centred at a primary receiver with a radius R. Any CR transmitter within the exclusion region is regarded as a harmful interferer and is therefore forbidden to transmit. When the locations of CR transmitters follow a Poisson point process with a density λ, the PDF of the aggregate interference can be computed as a function of R. As shown in FIGURE 2.6, it is found that a slight increase of R can effectively reduce both the mean and variance of the received interference power. The CR-primary interference modelling is further extended in [25] by taking into account interference management schemes for CR networks including power and contention control. The detailed modelling will be presented in Chapter 3. To combat the CR-primary interference, several interference mitigation schemes will be proposed in Chapter 4.

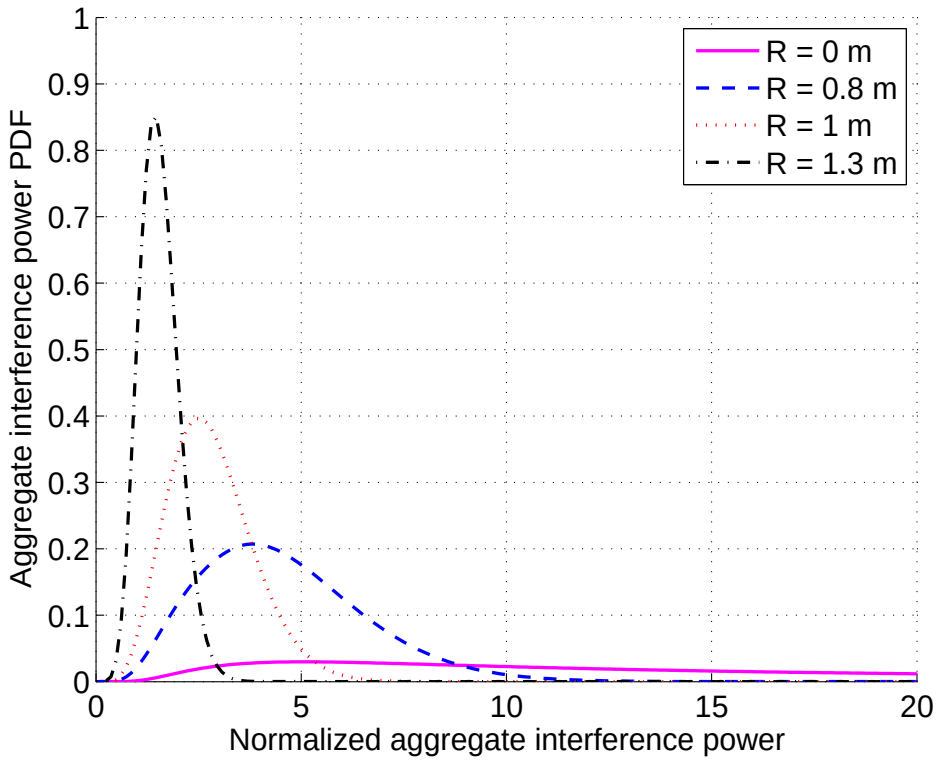

FIGURE 2.6: PDFs of the aggregate interference power (normalised to the transmit power of the interferers) with different values of the exclusion region radius R (CR transmitter density $\lambda = 1$) [5].

2.4.2 Primary-CR Interference

The interference from primary to CR networks can be directly measured by CR receivers with passive sensing techniques. Based on the PSD of the interfering primary signals, we can broadly classify the spectra into three categories: (i) *Black spaces* are spectra occupied by high-power primary signals, which have high probability to be decoded by CR receivers; (ii) *Grey spaces* refer to spectra with low to medium power primary signals, which are too weak to be decoded satisfactorily but are still significant sources of interference to the CR network; (iii) White spaces refer to spectra where primary signals have negligible power and can be simply treated as background noise.

Characterising the distributions of white/grey/black spaces across frequency, time, and space domains are of great importance for assessing the interference faced by CR

receivers. To date, such a characterisation has mainly been conducted empirically by a number of measurement campaigns [6], which show that the radio spectrum consists of a high percentage of white space. A theoretical model was recently proposed in [26] to characterise the spatial distributions of white/grey/black spaces in the presence of a random primary network with homogeneous nodes. There, it was assumed that every active primary transmitter uniquely defines a black space area and a grey space area. As illustrated in FIGURE 2.5, the black space area, often considered as the service region of the primary transmitter, is given by a circular disk with radius L centred at the primary transmitter. The grey space area, on the other hand, is an outer ring with radius D surrounding the service region and is regarded as the interfering region to CR systems. Under an intra-network interference constraint that prohibits two active primary transmitters to lie closer than a minimum distance of $L + D$, in [26] it was found that white/grey spaces are naturally abundant but geographically fragmented. For example, when $D = 2L$, the spectra will be detected as white spaces on more than 56% of the plane and as grey spaces on more than 34% of the plane [26].

Intuitively, white spaces are the most desirable resources for CR networks to exploit, while grey spaces can also be reused to further improve the spectrum utilisation. There is a widespread perception that black spaces are not exploitable by CR networks due to the presence of strong interfering primary signals.

2.4.3 CR-CR Interference

The intra-network interference can be further classified into two types: interference within primary networks and CR-CR interference. The interference within primary networks has nothing to do with CR networks. Therefore, it is out of the scope of this thesis. As for CR-CR interference, it has no fundamental difference from intra-network interference within other networks, except that CR users hold the premise of not detrimentally interfering with the primary system in the first place. CR-CR interference is a main source limiting the performance of spectrum-sharing CR networks. In Chapter 5, we will evaluate the performance of CR-CR interference channels and

investigate how to coordinate multiple CR users using different interference management schemes.

Chapter 3

Interference Modelling for Cognitive Radio Networks

3.1 Introduction

Due to the spectrum sharing nature, a CR network can utilise the spectrum more efficiently when coexisting with a primary system on the interference-tolerant basis. In this case, the CR-primary interference should be carefully managed and well maintained below a certain level by the CR network to protect the primary system. Therefore, it is desirable to model the CR-primary interference to reveal how the service of the primary network is deteriorated and how CR networks may be deployed. This chapter aims to model and analyse the characteristics of the CR-primary interference when multiple CR nodes coexist with the primary system. The relationship between CR operating parameters and the resulting CR-primary interference is investigated. Moreover, some insights are given on the deployment of the CR network to better protect the primary system.

In the literature, the existing research on interference modelling for CR networks mainly falls into three categories: spatial, frequency-domain and accumulated interference modelling. For spatial interference modelling, as the name suggests, the interference is examined according to the geographical location. The fraction of white

spaces available for CR networks was investigated in [27] and [26]. In [28], the region of interference for CR receivers and region of communication for CR transmitters were studied for the case where a CR network coexists with a cellular network. The interference from CR devices to wireless microphones operating in TV bands was analysed in [29], where the loss of reliable communication area of a wireless microphone due to the existence of CR devices was examined.

CR interference can also be modelled in the frequency domain. For example, an experimental study on the interference due to out-of-band emission of a WRAN was reported in [30]. On one hand, the interference received at the neighbouring bands of the WRAN operation band was evaluated via measurements. On the other hand, the maximum allowable radiated power for WRAN end-user devices in each neighbouring band of a digital television (TV) receiver was determined.

Finally, as for accumulated interference modelling, the aggregate interference in a given location and at a given frequency band is modelled. Usually, the PDF of the aggregate interference and the outage probability of a primary receiver due to the interference are two commonly-used statistics for the aggregate interference modelling. In [31], the aggregate interference power from a sea of CR transmitters surrounding a primary receiver was derived. The performance of a primary system was evaluated in [32] in terms of outage probability caused by the interference from CR networks. The outage probability was derived for both underlay and overlay spectrum sharing cases. In [33] the aggregate interference from multiple CR transmitters following a Poisson point process was approximated by a Gamma distribution and the probability of interference at a primary receiver was also given. It is worth noting that only pathloss was assumed for the interfering channel in [31–33]. Their work was extended by taking both shadowing and fading into account in [5] and [34]. Moreover, the PDF for accumulated interference and outage probability due to the aggregate interference from CR nodes were also derived in [5] and [34], respectively.

However, in all the previous works [5, 26–34], the CR transmitters were assumed to transmit at a fixed power level, i.e., no power control for CR transmitters was considered. Moreover, the CR nodes were all assumed to communicate with each other

simultaneously. Thus, no contention control scheme was employed at the cognitive MAC layer. In this chapter, we extend the aggregate interference modelling employing various interference management mechanisms, e.g., power/contention control schemes. The contribution of this chapter can be summarised as follows.

- A realistic power control scheme is proposed, and a hybrid power/contention control scheme is introduced.
- The PDFs of interference perceived at a primary receiver from a CR network are derived numerically for the cases of power or contention control. The interference distribution of the hybrid control scheme is also analysed and compared with that of the pure power control and pure contention control schemes by simulations.
- To reduce the complexity of the numerical interference PDF's computation, cumulant-based approximations are applied to fitting the interference distributions for the first two interference management schemes.
- The impact of the hidden primary receiver problem on the aggregate interference is investigated for all the three interference management schemes.

The interference modelling presented in this chapter considers several basic interference management schemes, which forms a fundamental basis for the development of other advanced interference models for CR networks. Secondly, it gives insights into CR deployment by figuring out how to optimise CR operation parameters. Finally, the interference modelling lays a foundation for performance evaluation of primary networks, e.g., outage capacity of primary systems can be derived based on the interference PDFs.

The remainder of this chapter is organised as follows. The system model is elaborated in Section 3.2. Some preliminaries in stochastic geometry which underpins the interference modelling are introduced in this section as well. The detailed interference modelling is presented in Section 3.3 when perfect knowledge of the primary system is known to the CR network. In Section 3.4, the hidden primary receiver problem is

taken into account for the interference modelling, i.e., scenarios with imperfect primary system knowledge. The impact of several key parameters on the interference is analysed via numerical studies in Section 3.5. Finally, Section 3.6 concludes this chapter.

3.2 System Model

The system model is illustrated in FIGURE 3.1. It consists of a CR network coexisting with a primary transmitter-receiver pair. The *interference region* (IR) is adopted by the primary network to protect itself against interference from the CR network. No CR transmission is allowed within the IR. There exist two main types of techniques to identify the IR for a primary network: geo-location technique and spectrum sensing [35]. For geo-location-based CR networks, the GPS can be incorporated within the CR network. It enables CR transmitters to determine whether they are located far enough outside the protected service contour of the primary system. The geo-location technology usually leads to a circular IR around the primary system. As for spectrum-sensing-based CR, the IR is usually not circular but more irregular than that of the geo-location-based CR due to fading and/or imperfect sensing. In this chapter, we focus on the former type and thus, a circular IR with a radius R is considered.

The underlying interference channels from CR transmitters to the primary receiver experience pathloss, shadowing and fading. The pathloss function $g(r_j)$ is

$$g(r_j) = r_j^{-\beta} \tag{3.1}$$

where r_j is the distance between the jth ($j = 1, 2, \cdots$) active CR transmitter and the primary receiver and β is the pathloss exponent. The composite model for shadowing and fading can be expressed as the product of the long term shadowing and the short term multipath fading. In this chapter, log-normal shadowing and Nakagami fading are considered. Let h_j denote the channel gain for the composite shadowing and fading of the interference channel from the jth active CR transmitter to the primary

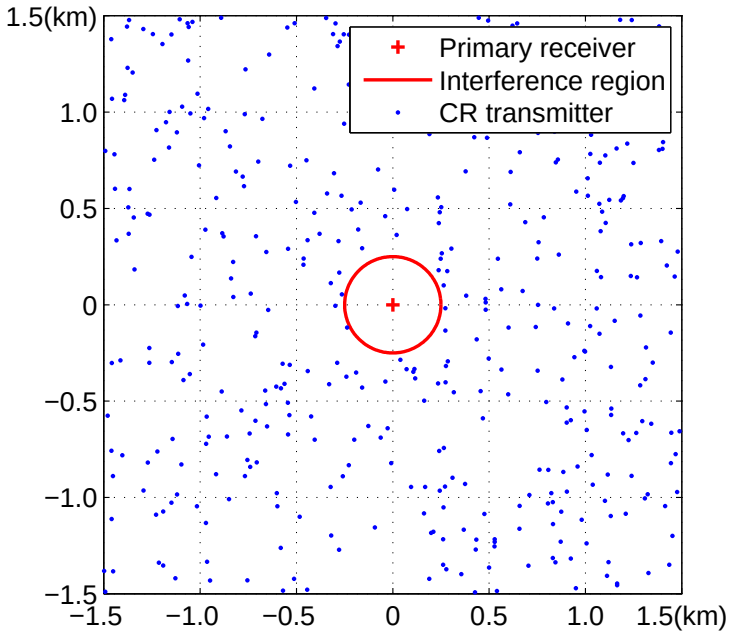

FIGURE 3.1: System model for CR networks coexisting with a primary network (CR with power control, $\lambda = 50$ user/km^2 and IR radius $R = 250$ m).

receiver. The PDF of the composite channel gain h_j can be approximated by the following log-normal distribution [36]

$$f_{\mathrm{h}}(x) \approx \frac{1}{\sqrt{2\pi}\sigma x} \exp\left\{-\frac{(\ln(x)-\mu)^2}{2\sigma^2}\right\} \tag{3.2}$$

where the mean μ and variance σ^2 can be expressed as

$$\mu = \left(\sum_{k=1}^{m-1} \frac{1}{k} - \ln(m) - 0.5772\right) + \mu_\Omega \tag{3.3}$$

$$\sigma^2 = \sum_{k=0}^{\infty} \frac{1}{(m+k)^2} + \sigma_\Omega^2 \tag{3.4}$$

with m being an integer and standing for the Nakagami shape factor, and μ_Ω and σ_Ω^2 denoting the standard mean and variance of the log-normal distribution, respectively.

Let p_j denote the transmission power of the jth active CR transmitter. The accumulated power of the instantaneous interference received at the primary receiver can be

expressed as

$$Y = \sum_{j=1}^{\infty} p_j g(r_j) h_j. \tag{3.5}$$

It worth noting that the average attenuation due to both path loss and shadowing is incorporated into the path loss model $g(r_j)$ in (3.5). In this case the shadowing model h_j superimposed on the path loss model should have zero mean, i.e., $\mu = 0$. However, if the shadowing model incorporates path loss via its mean or if the path loss model does not incorporate average attenuation due to shadowing, then μ will be negative [37]. In this chapter, we investigate the characteristics of the aggregate interference from all CR transmitters employing the following three different interference management schemes: (i) power control, (ii) contention control, and (iii) hybrid power/contention control.

3.2.1 Preliminaries in Stochastic Geometry

Before detailing the interference management schemes adopted by the CR transmitters, we introduce some preliminaries in *stochastic geometry* [38]. Stochastic geometry emerges as a mathematical tool to provide mathematical models and methods for the statistical analysis of various geometrical patterns. We will use stochastic geometry to model the spatial distribution of active CR transmitters.

Stationary Poisson point process

Random point patterns, also known as, *point processes* play an exceptionally important role in stochastic geometry. The Poisson point process is the simplest and also the most common random point pattern. A stationary Point point process Φ is characterised by two fundamental properties: (i) Poisson distribution of point counts, the number of points of Φ falling into a closed area A has a Poisson distribution with mean λA, where λ is the *density* of the stationary Poisson point process Φ; (ii) Independent scattering, the numbers of points of Φ in k disjoint areas form k independent

random variables. Property (ii) can be interpreted as the 'complete randomness' or 'pure randomness' of points of Φ.

The distribution of the nearest neighbour distance is one of the most commonly-used statistics of a stationary Poisson point process Φ. It describes the distribution of the distance from a typical point x of Φ to the nearest neighbouring point in $\Phi \backslash x$. The PDF of the nearest neighbour distance d_{nn} is given by [38]

$$f_{nn}(d_{nn}) = 2\pi\lambda d_{nn} e^{-\lambda\pi d_{nn}^2}. \tag{3.6}$$

Thinnings

A thinning operation uses some definite rules to delete points of a point process Φ, thus yielding a *thinned point process* Φ_{th}. As a random closed set Φ_{th} is a subset of Φ, i.e., $\Phi_{th} \subset \Phi$. The simplest thinning is $p-thinning$, where each point of Φ has probability $1-p$ to be deleted. The deletion of a point in $p-thinning$ is independent of both its location and the deletions of any other points of Φ. Therefore, it is called *independent thinning*. Alternatively, when the deletion of a point in a thinned point process depends on its location and/or the deletions of any other points, the thinning is termed as *dependent thinning*.

Matern hard-core point process

A hard-core point process is a point process where the constituent points are forbidden to lie closer together than a certain minimum distance $d_{\min}$. These hard-core models are used to describe patterns produced by the locations of centres of non-overlapping circles or spheres of radius $d_{\min}/2$. The points in a hard-core point process can be considered as the centres of hard-core circles or spheres. *Matern hard-core (MH) process* [39] is a hard-core process with high eventual density of points. An MH process Φ_{mh} is essentially the result of dependent thinning applied to a stationary Poisson point process Φ with density λ. The mathematical expression of the MH

process Φ_{mh} is given by [38]

$$\Phi_{\text{mh}}=\{x \in \Phi : m(x) < m(y) \text{ for all } y \text{ in } \Phi \cap C(x, d_{\min})\}. \tag{3.7}$$

Each point x in the original Poisson point process Φ is marked with a random variable $m(x)$ uniformly distributed in (0,1), while $C(x, d_{\min})$ is a disk centred at point x with the radius $d_{\min}$. The *retaining probability* q_{mh} for the MH process, which is the probability of a point of Φ surviving the thinning process, is given by [38]

$$q_{\text{mh}} = \frac{1 - e^{-\lambda \pi d_{\min}^2}}{\lambda \pi d_{\min}^2}. \tag{3.8}$$

3.2.2 Power Control

In this scenario, the distribution of active CR transmitters shown in FIGURE 3.1 follows a Poisson point process with a density parameter λ for the density of CR transmitters on the plane.

The transmission power of a CR transmitter is governed by the following proposed power control law

$$p_{\text{pwc}}(r_{\text{cc}_j}) = \begin{cases} \left(\frac{r_{\text{cc}_j}}{r_{\text{pwc}}}\right)^{\alpha} P_{\max}, & 0 < r_{\text{cc}_j} \leq r_{\text{pwc}} \\ P_{\max}, & r_{\text{cc}_j} > r_{\text{pwc}} \end{cases} \tag{3.9}$$

where r_{cc_j} is the distance from the jth active CR transmitter to its nearest neighbouring active CR transmitter. From the nearest neighbour distance distribution function of a Poisson point process (3.6), the PDF of r_{cc_j} can be written as

$$f_{\text{cc}}(r_{\text{cc}_j}) = 2\pi\lambda r_{\text{cc}_j} e^{-\lambda \pi r_{\text{cc}_j}^2}. \tag{3.10}$$

In (3.9), α is the power control exponent, $P_{\max}$ is the maximum transmission power for CR transmitters, and r_{pwc} is the power control range, which determines the minimum r_{cc_j} leading to maximum CR transmission power $P_{\max}$. The parameter r_{pwc} is introduced here to adjust the range of the power control.

We assume that the power control exponent α is equal to the pathloss exponent β in (3.1) throughout this chapter. The above proposed power control scheme is designed in such a manner that the interference caused by the jth active CR transmitter to its nearest active CR transmitter due to pathloss is $p_{\text{pwc}}(r_{\text{cc}_j})g(r_{\text{cc}_j})$. It is clear that within the power control range r_{pwc}, this interference is equal to a constant $P_{\max}/r_{\text{pwc}}^{\alpha}$. But beyond the power control range, the interference is smaller than that constant. That is, at any CR transmitter the interference from the nearest neighbouring CR transmitter is capped and independent of the nearest neighbour distance within the power control range.

A CR network can be deployed as either an infrastructure or an ad hoc network[12]. For a CR infrastructure network, the above power control scheme is applicable to CR base stations (BSs), whose transmission powers are usually determined by their coverages. Moreover, the CR BSs locations are usually fixed, which minimises the network planning load to determine the transmission power of CR BSs.

3.2.3 Contention Control

Unlike the aforementioned power control scheme, for the case of contention control every active CR transmitter has fixed transmission power p, but their transmission is governed by a contention control protocol to determine which CR transmitters can transmit at a given time. We assume that the multiple access protocol - carrier sense multiple access with collision avoidance (CSMA/CA) is employed, like in IEEE 802.11 networks. Every CR transmitter senses the medium before transmission. If the medium is busy, namely, the CR transmitter detects transmission from other CR transmitters within its contention region, it defers its transmission. Otherwise, the CR transmitter starts its transmission. As a result of the contention control, all the active CR transmitters are separated from each other by at least the contention distance, which is the minimum distance $d_{\min}$ between two concurrent CR transmitters. The distribution of the active CR transmitters under the contention control can be modelled as an MH point process [40]. A CR network adopts the contention control scheme is demonstrated in FIGURE 3.2, which is the result of the application of the

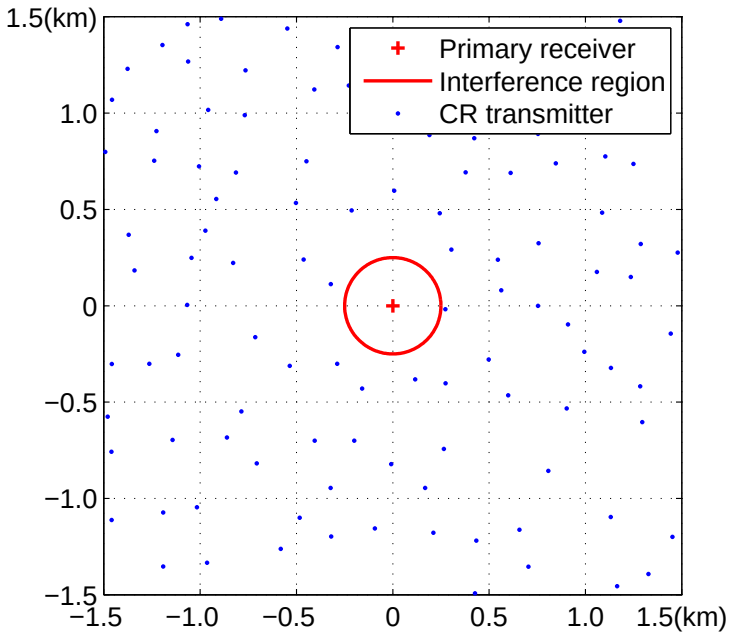

FIGURE 3.2: A CR network under contention control or hybrid control scheme coexists with a primary network ($\lambda = 50$ user/km^2, $d_{\min} = 150$m, $R = 250$ m).

CSMA/CA to the CR system shown in FIGURE 3.1. The contention control scheme can be applied to either a CR ad hoc network or distributed multiple-access users of a CR infrastructure network.

3.2.4 Hybrid Power/Contention Control

A natural extension of the above two interference management schemes is to implement both schemes in the same system. This is termed hybrid power/contention control and it works in the following manner. The contention control scheme is first applied, resulting in a set of active CR transmitters following an MH point process (as shown in FIGURE 3.2). Then, a power control scheme similar to (3.9) is employed to adjust the transmission power of each active CR transmitter according to the distance to the nearest neighbouring active transmitter. The following power control law is

adopted in the hybrid control scheme

$$p_{\text{hyb}}(r) = \begin{cases} \left(\frac{r}{d_{\min}}\right)^{\alpha} p, & d_{\min} \leq r \leq r_{\text{hyb}} \\ \left(\frac{r_{\text{hyb}}}{d_{\min}}\right)^{\alpha} p, & r > r_{\text{hyb}} \end{cases} \tag{3.11}$$

where r is the distance from an active CR transmitter to its nearest neighbouring active CR transmitter, α is the power control exponent as in (3.9), and r_{hyb} is the power control range similar to r_{pwc} in (3.9) except that it also determines the maximum transmission power, i.e., $\left(\frac{r_{\text{hyb}}}{d_{\min}}\right)^{\alpha} p$. It is obvious that a larger r_{hyb} leads to a larger maximum CR transmission power and, consequently, longer communication range for CR transmitters. The above power control law (3.11) guarantees that when a pathloss channel is considered for each active CR transmitter, the perceived interference caused by its nearest neighbouring CR transmitter is $p_{\text{hyb}}(r)g(r)$, which is (i) a constant $p/d_{\min}^{\alpha}$ within the power control range r_{hyb} and (ii) less than the constant $p/d_{\min}^{\alpha}$ when the distance r is larger than the power control range.

3.3 Interference Modelling with Perfect Primary System Knowledge

In this section, we intend to model the aggregate interference from CR transmitters employing the three different interference management schemes introduced in Section 3.2 by finding their corresponding PDFs. We first consider the scenarios where the knowledge of the primary receiver location is known to the CR network. Therefore, the interference exclusion region can be created precisely by the CR network as shown in FIGURES 3.1 and 3.2.

3.3.1 Characteristic Function-Based Approach

To derive a PDF for a random variable, the characteristic function-based method used in [5] and [41] is a widely-used approach. In this subsection, we apply this method

to the derivation of PDFs of the aggregate CR-primary interference. Firstly, the characteristic functions of the interference under different system models are derived. Then, the PDFs of the aggregate interference are obtained by performing an inverse Fourier transform on their characteristic functions.

Power control

When all the CR transmitters follow a Poisson point process distribution and employ the power control scheme proposed in (3.9), we can adopt the characteristic function-based method as in [5, 41–43] and obtain the following characteristic function $\phi_{\mathrm{Y}}(\omega)$ of the aggregate interference Y at a primary receiver from all CR transmitters [5]

$$\phi_{\mathrm{Y}}(\omega) = \exp\left(\lambda\pi \int_H f_{\mathrm{h}}(h) \int_P f_{\mathrm{p}}(p) T(\omega p h) dp\, dh\right) \tag{3.12}$$

where $f_{\mathrm{p}}(\cdot)$ is the PDF of the CR transmission power $p_{\mathrm{pwc}}(r_{\mathrm{cc}_j})$ of a CR transmitter defined in (3.9) and

$$T(\omega p h) = R^2(1 - e^{i\omega g(R) p h}) + i\omega p h \int_0^{g(R)} [g^{-1}(t)]^2 e^{i\omega t p h} dt. \tag{3.13}$$

In (3.13), $g^{-1}(\cdot)$ denotes the inverse function of $g(\cdot)$ in (3.1). For the derivation of (3.12), the following fact is used: for a given number of CR transmitters in an annular ring area, the distances from the jth CR transmitter to the primary receiver r_j $(j = 1, 2, \cdots)$ have independent and identical uniform distributions [41]. Their PDFs have the following form [41]

$$f_{\mathrm{r}}(x) = \begin{cases} 2x/(l^2 - R^2), & R \le x \le l \\ 0, & \text{otherwise} \end{cases} \tag{3.14}$$

when CR transmitters are distributed within an annular ring with inner radius R and outer radius l. In (3.12), p is a function of r_{cc} as shown in (3.9), so the expectation of $T(\omega p h)$ over p equals that of $T(\omega p_{\mathrm{pwc}}(r_{\mathrm{cc}}) h)$ over r_{cc}. Using the PDF of r_{cc} given in

(3.10), (3.12) can be rewritten as

$$\phi_{\mathrm{Y}}(\omega) = \exp\left(\lambda\pi \int_H f_{\mathrm{h}}(h) \int_{r_{\mathrm{cc}}} f_{\mathrm{cc}}(r) T(\omega p_{\mathrm{pwc}}(r_{\mathrm{cc}})h) dr dh\right). \tag{3.15}$$

Moreover, (3.15) can be written as (see Appendix A for the detailed derivation procedure)

$$\begin{aligned}\phi_{\mathrm{Y}}(\omega) = \exp\Bigg\{\lambda\pi \int_H f_{\mathrm{h}}(h) \int_0^{r_{\mathrm{pwc}}} f_{\mathrm{cc}}(r) \Bigg[R^2\left(1 - e^{\frac{i\omega r^{\alpha} P_{\max} g(R) h}{{r_{\mathrm{pwc}}}^{\alpha}}}\right) \\ + \frac{i\omega r^{\alpha} P_{\max} h}{{r_{\mathrm{pwc}}}^{\alpha}} \int_0^{g(R)} t^{-\frac{2}{\beta}} e^{\frac{i\omega t r^{\alpha} P_{\max} h}{{r_{\mathrm{pwc}}}^{\alpha}}} dt\Bigg] dr dh \\ + \lambda\pi \int_H f_{\mathrm{h}}(h) \int_{r_{\mathrm{pwc}}}^{\infty} f_{\mathrm{cc}}(r) \left[R^2\left(1 - e^{i\omega g(R) P_{\max} h}\right) + i\omega P_{\max} h \int_0^{g(R)} t^{-\frac{2}{\beta}} e^{i\omega t P_{\max} h} dt\right] dr dh\Bigg\}.\end{aligned} \tag{3.16}$$

Finally, we obtain the PDF of the interference by performing the inverse Fourier transform on $\phi_{\mathrm{Y}}(\omega)$ as

$$f_{\mathrm{Y}}(y) = \frac{1}{2\pi} \int_{-\infty}^{+\infty} \phi_{\mathrm{Y}}(\omega) e^{-2\pi i \omega y} d\omega. \tag{3.17}$$

Equations (3.16) and (3.17) serve as general expressions for the characteristic function and PDF, respectively, of the interference under the power control scheme. As a special case, when the pathloss exponent $\beta = 4$ and the radius of the interference region $R = 0$, the PDF $f_Y(y)$ can be further simplified through similar steps to that used in [41] and obtained as

$$f_{\mathrm{Y}}(y) = \frac{\pi}{2} K \lambda y^{-3/2} \exp\left(-\frac{\pi^3 \lambda^2 K^2}{4y}\right) \tag{3.18}$$

where

$$K = \sqrt{P_{\max}} \int_H f_{\mathrm{h}}(h) \sqrt{h}\, dh \left[\int_0^{r_{\mathrm{pwc}}} 2\pi r \lambda e^{-\lambda\pi r^2} \left(\frac{r}{r_{\mathrm{pwc}}}\right)^{\frac{\alpha}{2}} dr + e^{-\lambda\pi {r_{\mathrm{pwc}}}^2}\right]. \tag{3.19}$$

The detailed derivation procedure for K can be found in Appendix B.

Contention control

As mentioned in Section 3.2.3, the distribution of CR transmitters can be modeled as an MH point process when the contention control is adopted. The MH process is a dependent thinning process from the original Poisson point process, which means that the positions of CR transmitters are correlated to each other. However, it is very difficult to obtain a distribution function like (3.14) for an MH point process in order to model the distance from an active CR transmitter to the primary receiver. Alternatively, the dependent thinning can be approximated by a process with the following two steps: (i) An independent thinning with retaining probability q_{mh} given by (3.8); (ii) With the primary receiver being the pole in a polar coordinate, the position of each retaining point is then adjusted by only changing its angular coordination to fulfill the minimum distance $d_{\min}$ separation requirement. It is worth noting that the rotation in the second step is possible for low CR density cases. The approximated thinning process preserves the statistical properties of two crucial parameters for the MH process, i.e., the total number of active CR transmitters and the distances between active CR transmitters and the primary receiver. Therefore, we can approximate the MH point process as an independent thinned Poisson point process with retaining probability q_{mh}. To this end, the contention control scheme can be interpreted as follows: all the CR transmitters still follow the original Poisson point process with intensity λ, but the jth CR transmitter has probability q_{mh} (or $1-q_{\text{mh}}$) to transmit at power level p (or 0). The characteristic function of the accumulated interference can be found as

$$\phi_{\text{Y}}(\omega) = \exp\left(\lambda\pi q_{\text{mh}} \int_{H} f_{\text{h}}(h) T(\omega p h) dh\right). \tag{3.20}$$

The detailed derivation of (3.20) is presented in Appendix C. The accuracy of the approximation for the dependent thinning is evaluated in Section 3.3.2.

Moreover, the PDF of the interference can be obtained from (3.20) and (3.17). As a special case, when $R = 0$, i.e., no IR is implemented, and the pathloss exponent

$\beta = 4$, this PDF can be simplified as (3.18) with

$$K = q_{\text{mh}} \int_H f_h(h) \sqrt{ph}\, dh. \tag{3.21}$$

Hybrid power/contention control

So far, the PDFs of the interference received at a primary receiver from a CR network employing the power control and contention control schemes have been derived. In order to model the aggregate interference under the hybrid control scheme, the nearest neighbouring distance distribution function analogous to (3.10) for active CR transmitters is indispensable to evaluate the transmission power designated in (3.11). Unfortunately, there is no closed-form expression for the nearest neighbour distance distribution function for an MH point process [44]. Alternatively, several estimators have been used to statistically estimate the nearest neighbour distance distribution function in practice [45]. However, statistical estimation is not practical for deriving the characteristic function in our case. Thus, we approach this problem numerically.

The PDF for the aggregate interference under the hybrid control scheme is simulated in FIGURE 3.3, where the interference PDFs for power and contention control are given as well for the purpose of comparison. It can be seen from this figure that both the mean and variance of the aggregate interference increase for the hybrid control scheme compared to either power or contention control schemes. However, the boosted interference is paid off by the increased CR communication area (coverage) for the hybrid control scheme. We define the coverage of each CR transmitter as a circular disk centred at a CR transmitter with radii being $\texttt{min}(r/2, r_{\text{pwc}}/2)$, $d_{\min}/2$ and $\texttt{min}(r/2, r_{\text{hyb}}/2)$ for power control, contention control and hybrid power/contention control schemes, respectively. Then, the received signal power at cell edge of a CR transmitter due to pathloss is $2^\beta P_{\max}/{r_{\text{pwc}}}^\beta$, $2^\beta p/d_{\min}^\beta$ and $2^\beta p/d_{\min}^\beta$ for the above three aforementioned schemes. For the sake of comparison, let $r_{\text{pwc}} = d_{\min}$ and $P_{\max} = p$, which guarantees that the strength of the received signal power at cell edge of a CR transmitter is the same for all the three schemes. The overall coverage of the CR network under different control schemes can be investigated numerically. With this

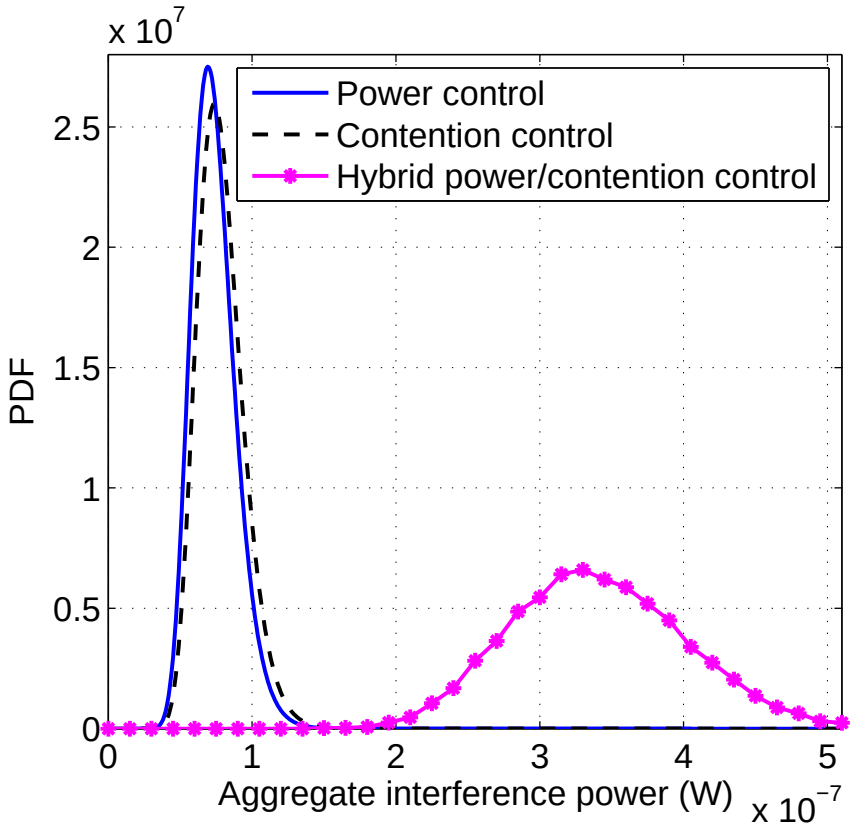

FIGURE 3.3: Comparison of interference distributions for power, contention and hybrid power/contention control schemes (R =100 m, λ =300 user/km^2, β =4, $r_{\text{pwc}} = 20$ m, $\alpha = 4$, $P_{\max} = 1$ W, $p = 1$ W, $d_{\min} = 20$ m and $r_{\text{hyb}} = 30$ m)

setup, the overall coverage ratio for the power control, contention control and hybrid power/contention control is 1.0093, 1, and 2.0229, respectively. Two interesting facts are unveiled from this experiment. Firstly, the power control scheme leads to slightly smaller interference and slightly lager coverage compared to the contention control scheme, which suggests that power control is preferable to contention control in terms of lower resulting interference and larger coverage if the CR system can afford the complexity introduced by implementing the power control scheme. Secondly, the hybrid scheme tends to cause higher interference, but it greatly enlarges the coverage compared to the power and contention control schemes.

3.3.2 Analytical Approximation

In Section 3.3.1, the characteristic function-based method has been used to derive the PDFs for the aggregate interference. This interference modelling approach is extremely computation-intensive, since generally closed-form expressions are not admitted for either the characteristic function or the inverse Fourier transformation, and the computations for both steps have to be performed numerically. It is desirable to model the aggregate interference with less complexity. An alternative approach with greatly reduced complexity is to approximate interference PDFs as certain known distributions. Observations from FIGURE 3.3 suggest that the interference distribution for either power or contention control is positively skewed and heavy-tailed, which suggests a log-normal distribution. Thus, in this section, we fit the aggregate interference under power and contention control schemes to log-normal distributions. The theory behind the log-normal fitting is based on the following two facts. It has been shown that the sum of interference from uniformly distributed interferers in a circular area is asymptotically log-normal [34, 46]. This ensures that the aggregate interference in these two schemes can be approximated as log-normal distributed. Meanwhile, the sum of randomly weighted log-normal variables can be modeled as a log-normal distribution as well [47], which guarantees that the aggregate interference is still log-normal distributed even if the effect of shadow fading (3.2) is taken into account. In what follows, the log-normal fitting is performed using a cumulant-matching approach [48], where the first two order cumulants of the aggregate interference Y in (3.5) are used to estimate the mean and variance of the log-normal distribution function. Therefore, the exact PDFs of interference can be obtained. Fortunately, these cumulants have closed-form expressions for both control schemes. Consequently, it significantly reduces the complexity compared to the characteristic function-based interference modelling carried out in Section 3.3.1. Moreover, compared to the characteristic function-based method, the relationship between CR system parameters and the resulting interference becomes much clearer for the cumulant-based PDFs approximation.

For a log-normal random variable x, its mean μ and variance σ^2 can be estimated using its first two order cumulants k_1 and k_2 as follows [49]:

$$\mu = \ln \frac{k_1}{\sqrt{\frac{k_2}{k_1^2}+1}} \tag{3.22}$$

$$\sigma^2 = \ln\left(\frac{k_2}{k_1^2}+1\right). \tag{3.23}$$

In the context of interference distribution fitting, the nth cumulant k_n of the aggregate interference Y can be obtained from its characteristic function $\phi_{\mathrm{Y}}(\omega)$ via the following equation

$$k_n = \frac{1}{i^n}\left[\frac{\partial^n \ln\phi_{\mathrm{Y}}(\omega)}{\partial\omega^n}\right]_{\omega=0}. \tag{3.24}$$

Power control

From (3.24) and the characteristic function in (3.16), the cumulants for aggregate interference under the power control scheme can be derived as (see Appendix D for detailed derivation)

$$k_n = \frac{2\lambda\pi P_{\max}^n e^{n\mu+\frac{n^2\sigma^2}{2}}}{(n\beta-2)R^{n\beta-2}}\left[\frac{n\alpha(n\alpha-2)\cdots 2}{{r_{\mathrm{pwc}}}^{n\alpha}(2\pi\lambda)^{\frac{n\alpha}{2}}}\left(1-e^{-\lambda\pi {r_{\mathrm{pwc}}}^2}\right) - \sum_{i=1}^{\frac{n\alpha}{2}-1}\frac{n\alpha(n\alpha-2)\cdots(n\alpha-2i+2)}{(2\pi\lambda {r_{\mathrm{pwc}}}^2)^i}{r_{\mathrm{pwc}}}^{n\alpha-2i}e^{-\lambda\pi {r_{\mathrm{pwc}}}^2}\right]. \tag{3.25}$$

It can be seen from (3.25) that k_n is proportional to $P_{\max}^n$ and $1/R^{n\beta-2}$, and all cumulants are most sensitive to the IR radius R since it has the highest exponent compared to other parameters. The power control range r_{pwc} and the density λ have similar impact on all cumulants, but the impact of the former is larger than that of the latter, since the former has a larger exponent.

To evaluate the accuracy of the approximation for the power control case, some comparisons are performed in FIGURE 3.4, where complementary cumulative distribution functions (CDFs) are used to improve readability. It can be seen from FIGURE 3.4

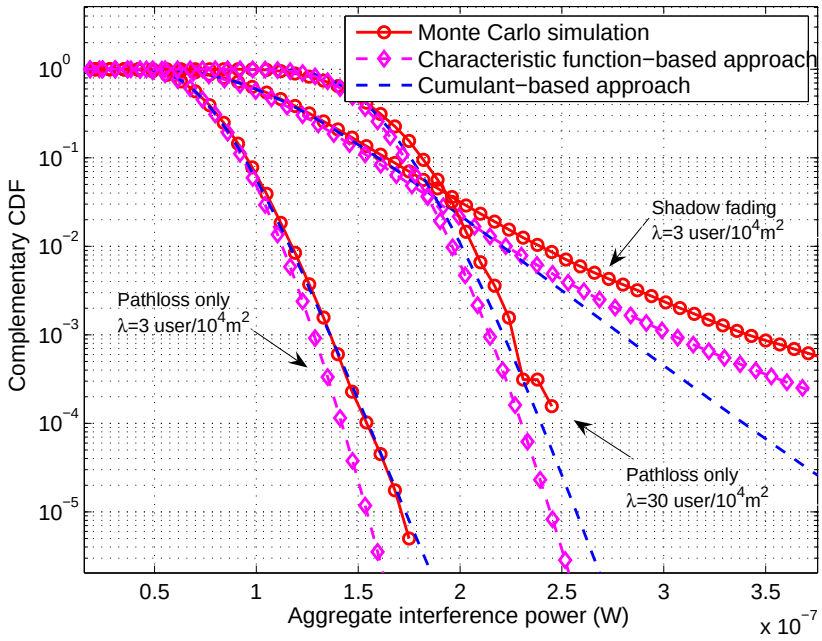

FIGURE 3.4: Log-normal approximation for interference distribution under power control (R =100 m, β =4, $r_{\text{pwc}} = 20$ m, $\alpha = 4$, $P_{\max} = 1$ W, $\mu = 0$ and $\sigma = 4$ dB).

that there is fairly good agreement among the interference CDFs derived in Section 3.3.1 (characteristic function-based approach), the approximated counterparts (cumulant-based approach) and the Monte Carlo simulation. Moreover, the pathloss-only scenario has better fit than shadow fading channels.

Contention control

Following the similar steps as in Appendix D and given the characteristic function (3.20) for the aggregate interference under contention control and also using (3.24), we can find the nth cumulant k_n of aggregate interference as

$$\begin{aligned} k_n &= \frac{\lambda\pi q_{\text{mh}}}{i^n}\int_H f_{\text{h}}(h)\left[-R^2\left(ipg(R)h\right)^n + n\left(iph\right)^n\int_0^{g(R)} t^{n-1-\frac{2}{\beta}}dt\right]dh \\ &= \lambda\pi q_{\text{mh}}\left(\frac{n}{n-\frac{2}{\beta}}g^{n-\frac{2}{\beta}}(R) - R^2g^n(R)\right)p^n\int_H f_{\text{h}}(h)h^n dh \\ &= \frac{2p^n\left(1-e^{-\lambda\pi d_{\min}^2}\right)e^{n\mu+\frac{n^2\sigma^2}{2}}}{(n\beta-2)d_{\min}^2R^{n\beta-2}}. \end{aligned} \tag{3.26}$$

As we can see from (3.26), k_n is linear to p^n and $1/R^{n\beta-2}$, which suggests that IR radius R is the most effective parameter to control the aggregate interference due to its highest exponent. The cumulants are not sensitive to the CR density λ for large λ. The contention range $d_{\min}$ has little impact on the cumulants when it is small. It can also be seen from (3.25) and (3.26) that shadow fading has the same impact on cumulants for the power and contention control schemes.

The accuracy evaluation of approximations under the contention control scheme is also performed and shown in FIGURE 3.5. It can be seen from this figure that the log-normal approximation is fairly accurate compared to the simulated interference CDFs for either pathloss-only or shadow fading channels. Moreover, it can be observed that the approximated thinning process tends to be less accurate as the CR density λ increases. This is due to the fact that some rotations in the second step of the approximated process might be impossible for a large λ.

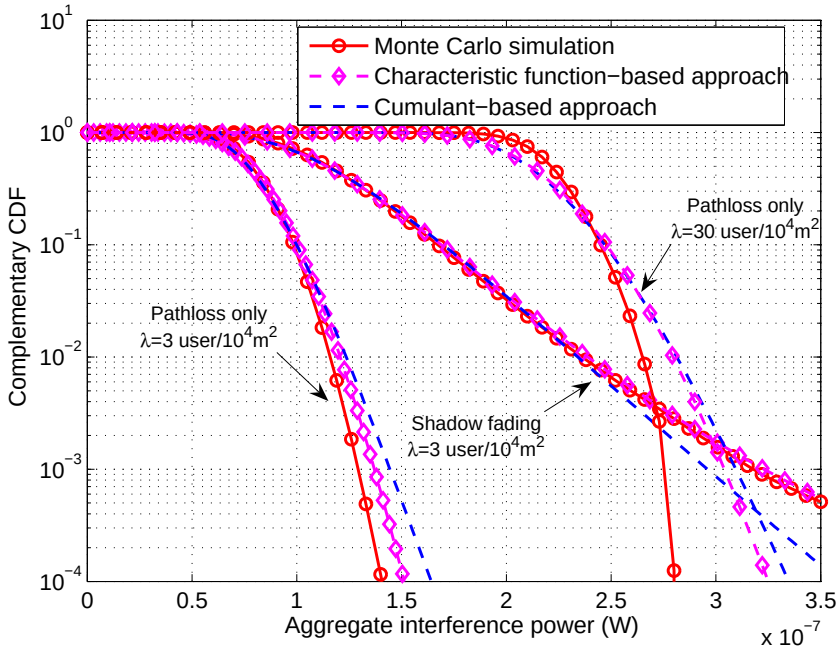

FIGURE 3.5: Log-normal approximation for interference distribution under contention control (R =100 m, β =4, $d_{\min}$ = 20 m, p = 1 W, μ = 0 and σ = 4 dB).

3.4 Interference Modelling with Imperfect Primary System Knowledge

In practice, some information about the primary system may not be perfectly known. One prominent example is the location of the primary receivers, which is usually required by CR networks in order to protect primary receivers from interfering CR transmitters. However, this information is not always available, especially in the case of passive primary receivers, i.e., when the primary receivers are hidden from CR networks. It is widely accepted that passive receiver detection techniques can be used or developed in the context of CR networks. For example, one of such primary receiver detection techniques is reported in [50]. Nevertheless, its applicability is still not convincingly viable since it requires deploying sensor nodes close to primary receivers and much coordination is involved between these sensors and CR networks as well. The most commonly used and also the simplest approach to protect the primary receiver is to regulate the transmission of the CR network based on primary transmitter sensing, assuming that primary receivers are in close proximity to the primary transmitter. In this section, we evaluate the effect of a hidden primary receiver on the resulting CR-primary interference.

Consider a primary and CR coexisting systems depicted in FIGURE 3.6, where an IR with radius R centred at the primary transmitter is introduced. All CR transmitters are distributed in the shaded concentric ring with inner radius R and outer radius l. Let θ be the angle between the line joining the primary transmitter and a CR transmitter and the line joining the primary transmitter-receiver pair. The distance from the CR transmitter to the primary transmitter is r and the distance between the primary transmitter-receiver pair is r_{p}. Then, the distance between the CR transmitter and the primary receiver r_{cp} can be expressed as

$$r_{\mathrm{cp}}(r,\theta) = \left[r^2 + r_{\mathrm{p}}^2 - 2rr_{\mathrm{p}}\cos(\theta)\right]^{\frac{1}{2}}, \quad r \in [R,l];\ \theta \in [0,2\pi] \tag{3.27}$$

where r is distributed as in (3.14) and θ is uniformly distributed in $[0,2\pi]$ if a Poisson point process is assumed for the CR transmitter distribution.

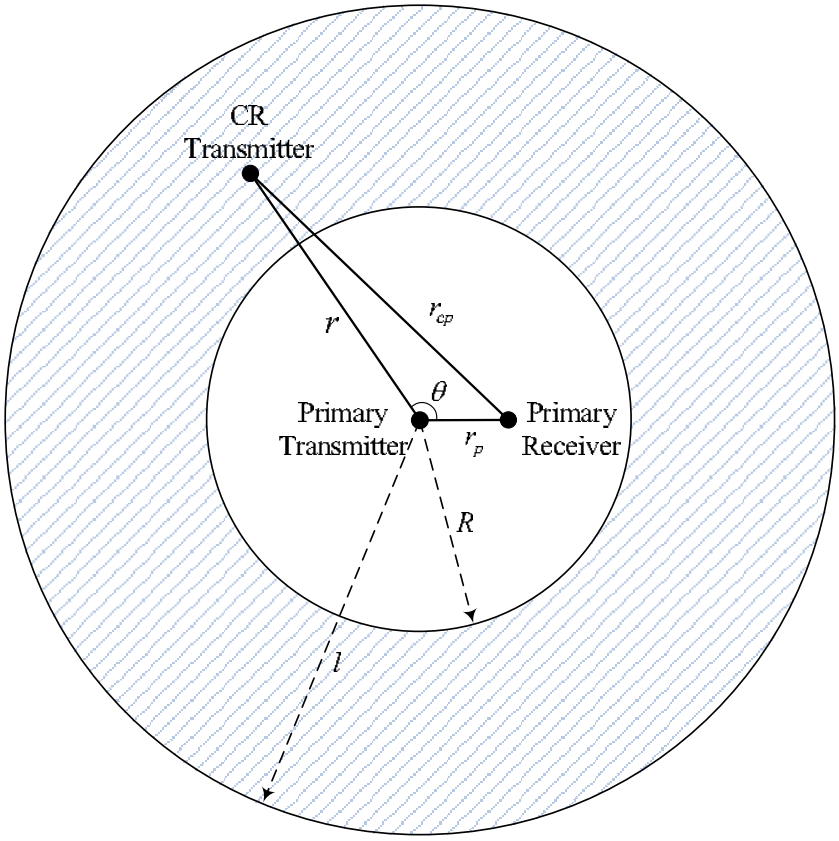

FIGURE 3.6: Imperfect knowledge of primary receiver location - the primary receiver is hidden from all CR transmitters distributed in the shaded region.

3.4.1 Power Control

Under the system model given in FIGURE 3.6 and the power control scheme proposed in Section 3.2.2, the characteristic function of aggregate interference $\phi_{\mathrm{Y}}(\omega)$ can be written as follows (see Appendix E for the detailed derivation):

$$\phi_{\mathrm{Y}}(\omega) = \lim_{l\to\infty} \exp\Bigg\{ \lambda \int_H f_{\mathrm{h}}(h) \int_0^{r_{\mathrm{pwc}}} f_{\mathrm{cc}}(x) \int_0^{2\pi} \int_R^l e^{i\omega \left(\frac{r}{r_{\mathrm{pwc}}}\right)^{\alpha} P_{\max}(x) g(r_{\mathrm{cp}}(r,\theta)) h} r - r \, dr \, d\theta \, dx \, dh + \lambda \int_H f_{\mathrm{h}}(h) \int_{r_{\mathrm{pwc}}}^{\infty} f_{\mathrm{cc}}(x) \int_0^{2\pi} \int_R^l e^{i\omega P_{\max}(x) g(r_{\mathrm{cp}}(r,\theta)) h} r - r \; dr \, d\theta \, dx \, dh \Bigg\}. \tag{3.28}$$

Applying the log-normal approximation method used in Section 3.3.2, we obtain the kth cumulant of the interference as

$$k_n = \lim_{l\to\infty} \lambda \left\{ \int_H f_{\mathrm{h}}(h) \int_0^{r_{\mathrm{pwc}}} f_{\mathrm{cc}}(x) \int_0^{2\pi} \int_R^l \frac{\left(r^\alpha P_{\max}(x) g(r_{\mathrm{cp}}(r,\theta))h\right)^n}{{r_{\mathrm{pwc}}}^{n\alpha}} r\,dr\,d\theta\,dx\,dh \right.$$
$$\left. + \int_H f_{\mathrm{h}}(h) \int_{r_{\mathrm{pwc}}}^{\infty} f_{\mathrm{cc}}(x) \int_0^{2\pi} \int_R^l \left[P_{\max}(x) g(r_{\mathrm{cp}}(r,\theta))h\right]^n r\,dr\,d\theta\,dx\,dh \right\}. \tag{3.29}$$

As can be seen from (3.29), unlike (3.25), the kth cumulant does not have a closed-form expression. However, the complexity of obtaining the exact interference PDF from (3.29) is still smaller than that of the characteristic function-based method in Section 3.3.1.

An experiment is done in FIGURE 3.7 to examine the effect of hidden primary receiver on the resulting interference compared to the interference for the case of perfect knowledge of primary receiver location. It can be seen from the figure that the hidden primary receiver problem boosts the interference in terms of increased interference mean and variance. This figure also shows that the log-normal approximation still fits well with both the derived CDF and Monte Carlo simulations.

3.4.2 Contention Control

Under the system model given in FIGURE 3.6 and the contention control scheme proposed in Section 3.2.3, the characteristic function of aggregate interference $\phi_Y(\omega)$ can be expressed as

$$\begin{aligned}
\phi_Y(\omega) &= \lim_{l\to\infty} \exp\left\{ q_{\mathrm{mh}} \lambda \pi D_l \left(E\left(e^{i\omega p g(V) h} \right) - 1 \right) \right\} \\
&= \lim_{l\to\infty} \exp\left\{ q_{\mathrm{mh}} \lambda \pi D_l \left(\int_H f_{\mathrm{h}}(h) \int_0^{2\pi} \frac{1}{2\pi} \int_R^l \exp[i\omega p g(r_{\mathrm{cp}}(r,\theta))h] \frac{2r}{D_l} dr\,d\theta\,dh - 1 \right) \right\} \\
&= \lim_{l\to\infty} \exp\left\{ q_{\mathrm{mh}} \lambda \int_H f_{\mathrm{h}}(h) \int_0^{2\pi} \int_R^l \exp\left[i\omega p g(r_{\mathrm{cp}}(r,\theta))h\right] r - r\,dr\,d\theta\,dh \right\},
\end{aligned} \tag{3.30}$$

with $D_l = l^2 - R^2$.

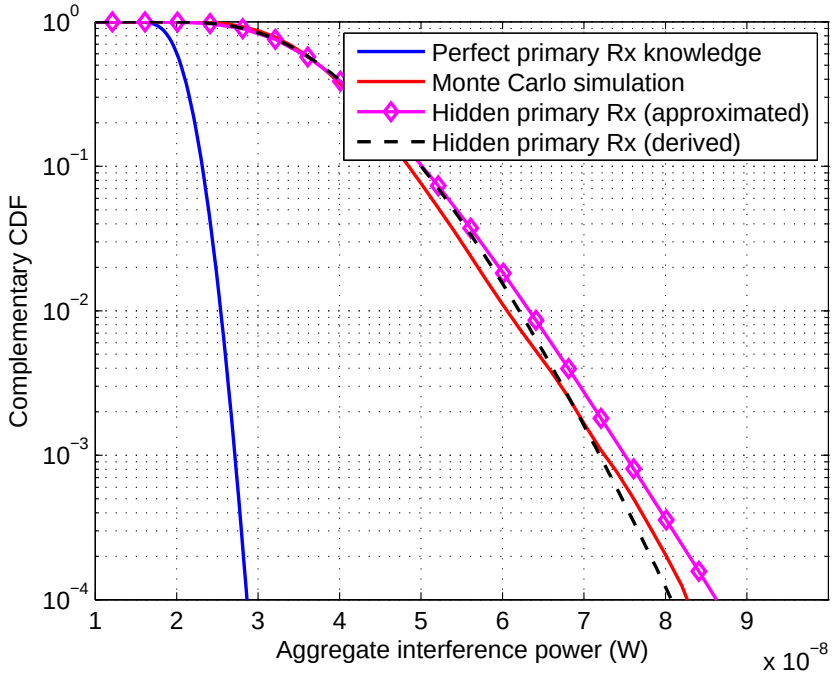

FIGURE 3.7: Log-normal approximation for interference distribution with a hidden primary receiver under power control (R =200 m, λ =3 user/10^4m^2, β =4, $r_{\text{pwc}} = 20$ m, $\alpha = 4$, $P_{\max} = 1$ W and $r_p = 0.5R$).

Using the same log-normal approximation method as in Section 3.3.2, the kth cumulant of interference can be written as

$$k_n = \lim_{l\to\infty} q_{\text{mh}}\lambda \int_H f_{\text{h}}(h) \int_0^{2\pi} \int_R^l [pg(r_{\text{cp}}(r,\theta))h]^n \, r - r dr \, d\theta \, dh. \tag{3.31}$$

The effect of hidden primary receiver under contention control is evaluated in FIGURE 3.8, where a pathloss-only channel is assumed. As we can see from this figure, the uncertainty about the primary receiver location leads to interference with larger mean and variance as compared to that in the case with perfect knowledge of primary receiver location. It can be seen from this figure that the log-normal fitting for the interference tends to be less accurate as the interference increases compared to the power control case shown in FIGURE 3.7.

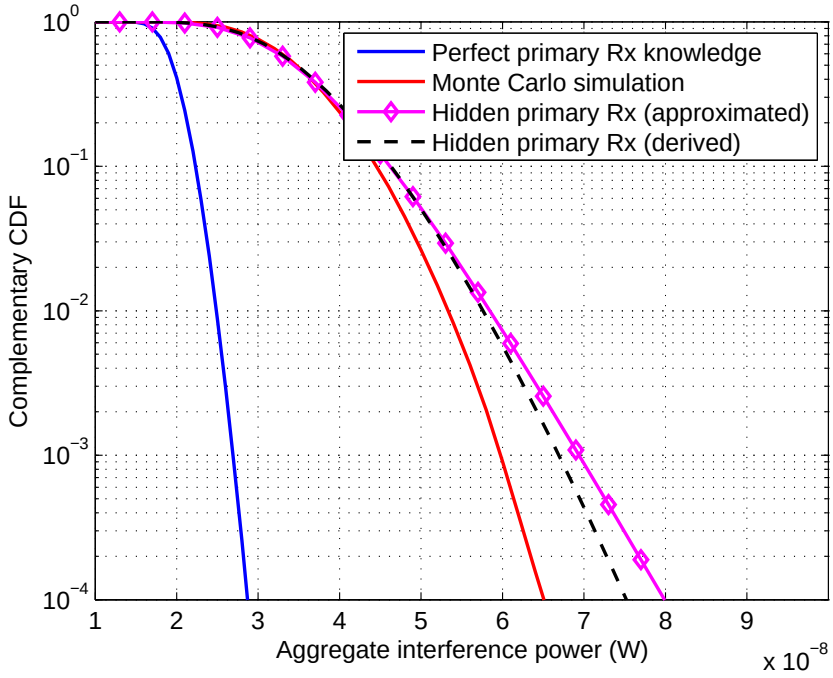

FIGURE 3.8: Log-normal approximation for interference distribution with a hidden primary receiver under contention control (R =200 m, λ =3 user/10^4m^2, β =4, $d_{\min} = 20$ m, $p = 1$ W and $r_p = 0.5R$).

3.4.3 Hybrid Power/Contention Control

For the case of hybrid power/contention control, the effect of hidden primary receiver on the resulting interference distribution is analysed via Monte Carlo simulations as shown in FIGURE 3.9, whose initial setup is the same as the one used in FIGURE 3.8 except that power control range is $r_{\text{hyb}} = 30$ m. It can bee seen from FIGURE 3.9 that the uncertainty about the primary receiver location boosts the interference in terms of increased mean, variance, and heavier tails for the hybrid control scheme as well. As we can see by comparing FIGURES 3.7, 3.8 and 3.9, the hidden primary receiver phenomenon has similar impact on the resulting interference distribution for all the three interference management schemes.

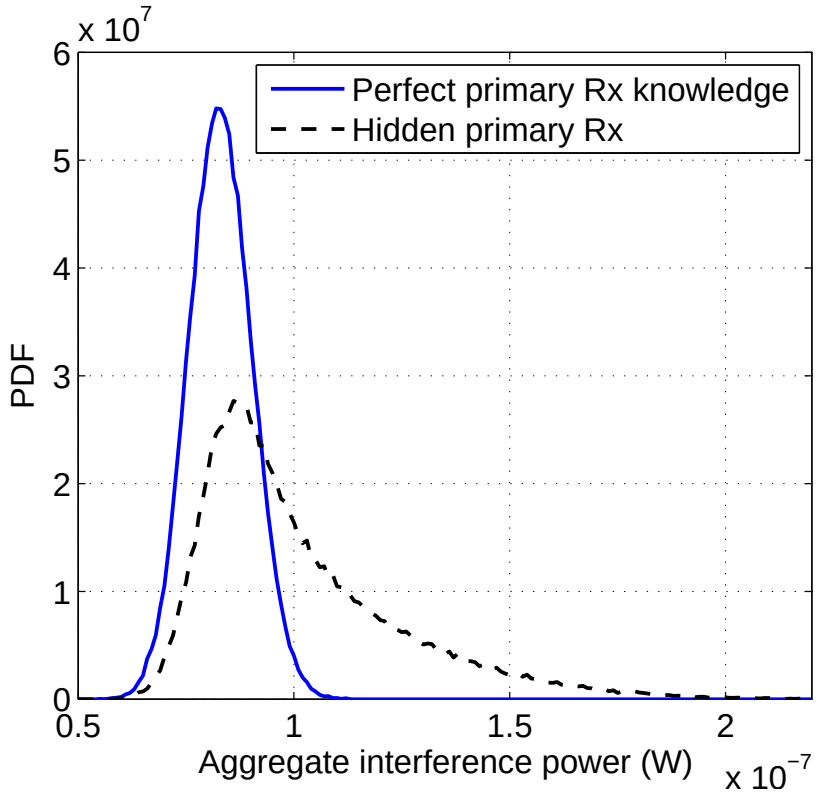

FIGURE 3.9: Impact of hidden primary receiver on interference distribution for CR networks under hybrid power/contention control scheme (R =200 m, λ =3 user/10^4m^2, β =4, $\alpha = 4$, $d_{\min} = 20$, $p = 1$ W, $r_p = 0.5R$ and $r_{\text{hyb}} = 30$ m).

3.5 Numerical Studies and Discussions

The aggregate interference power from CR transmitters employing power control or contention control is investigated numerically in this section. For the power control scheme, FIGURE 3.10 shows the effect of different power control parameters on their resulting aggregate interference. The detailed setup for the initial power control scheme is as follows: the maximum transmission power for each CR transmitter $P_{\max} = 1$ W, the density of CR transmitter $\lambda = 3$ user/10^4m^2, the IR radius $R = 100$ m, the power control range $r_{\text{pwc}} = 20$ m, the pathloss exponent $\beta = 4$ and the power control exponent $\alpha = 4$. From the two rightmost PDFs in this figure, it can seen that introducing power control scheme actually shifts the interference distribution leftwards compared to the distribution without power control. It means that the power control scheme can reduce the interference experienced at the primary receiver in terms of reducing its mean and slightly decreasing its variance. When deploying a CR network under

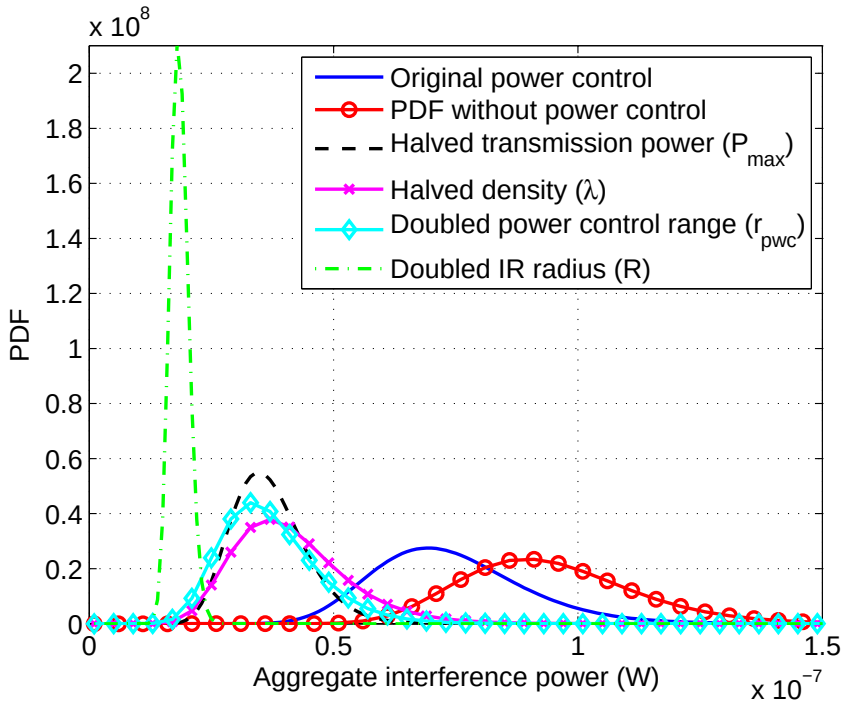

FIGURE 3.10: Impact of various CR deployment parameters on the aggregated interference for CR networks with power control (R =100 m, λ =3 user/10^4m^2, β =4, $r_{\text{pwc}} = 20$ m, $\alpha = 4$ and $P_{\max} = 1$ W).

the power control scheme, its resulting interference can be controlled by manipulating several parameters including $P_{\max}$, r_{pwc}, λ, and R. It can be seen in FIGURE 3.10 that the interference can be reduced by either decreasing the maximum transmission power and/or CR density, or increasing the power control range and/or IR radius. Interestingly, it also suggests that adjusting the IR radius is an effective way to control the interference, since the interference is more sensitive to the IR radius than to any other parameter as demonstrated in FIGURE 3.10. Meanwhile, the interference is least sensitive to the CR user density in the sense that halving λ leads to higher interference compared to doubling r_{pwc}, halving $P_{\max}$ or doubling R.

For the contention control scheme, the impact of contention control parameters on the resulting interference is depicted in FIGURE 3.11, whose initial setup is the same as that of FIGURE 3.10 except that the transmission power for each CR transmitter is $p = 1$ W and the contention control range is $d_{\min} = 20$ m. It can be seen from the two rightmost PDFs in FIGURE 3.11 that the contention control scheme results in an interference distribution with reduced mean like the power control scheme in

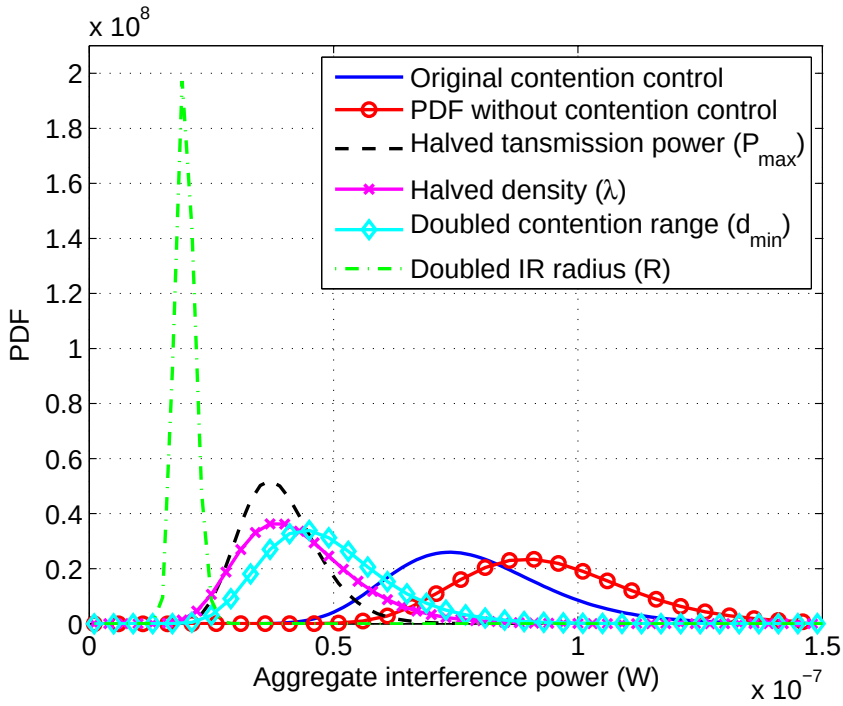

FIGURE 3.11: Impact of various CR deployment parameters on the aggregated interference for CR networks with contention control (R =100 m, λ =3 user/10^4m^2, β =4, $d_{\min}$ =20 m, and $p = 1$ W).

FIGURE 3.10. Meanwhile, the interference can be reduced by decreasing p, λ, and/or increasing R or $d_{\min}$. It can be observed by comparing FIGURE 3.11 with FIGURE 3.10 that (i) increasing the IR radius is an effective approach to reduce the interference for both the power and contention control schemes. However, the power control scheme is more sensitive to the IR radius than the contention control one; (ii) reducing the transmission power and/or CR transmitter density affects the interference in the very similar manner for these two control schemes.

The impact of hybrid control parameters on the resulting interference is also evaluated in FIGURE 3.12. It can be observed that most parameters have similar impact on the interference as those of power or contention schemes. However, the hybrid control scheme is extremely sensitive to the power control range r_{hyb}, which suggests that the power control range should be carefully designed to protect the primary network.

Finally, the impact of shadow fading on the aggregate interference is investigated for different values of the Nakagami shaping factor m under power and contention control schemes, respectively, in FIGURES 3.13 and 3.14. The initial setup in this example is

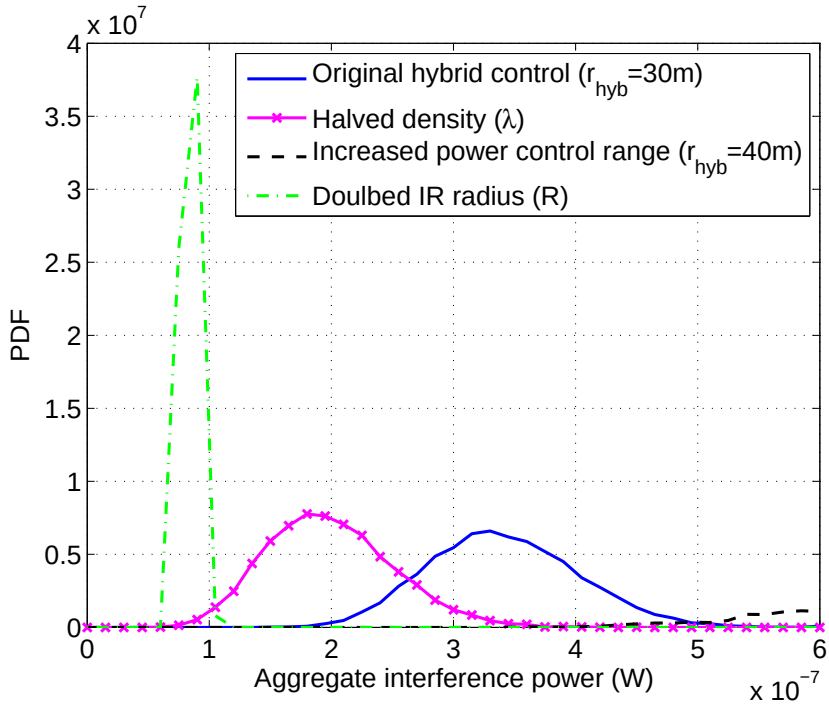

FIGURE 3.12: Impact of CR deployment parameters on the aggregated interference for CR networks with hybrid control scheme (R =100 m, λ =300 user/km^2, β =4, $\alpha = 4$, $p = 1$ W, $d_{\min} = 20$ m and $r_{\text{hyb}} = 30$ m).

the same as the one used for FIGURES 3.10 and 3.11, except that the standard variance is $\sigma_\Omega = 4$ dB. When $m = 1$ the interfering channel becomes a Rayleigh channel, which is dominated by the log-normal shadowing. Whereas, when $m = 100$ the fluctuations of the channel are reduced significantly compared to the Rayleigh fading channel. One fact observed from FIGURES 3.13 and 3.14 is that the interference distributions have larger variance and heavier tails when shadow fading is incorporated for both control schemes. Interestingly, fading tends to make the interference distribution more heavy-tailed than shadowing, i.e., the interference under shadowing has better outage property than that under fading. Moreover, the shadow fading has the similar effect for both control schemes, which agrees with the analysis in Section 3.3.2.

3.6 Chapter Summary

In this chapter, the aggregate interference at a primary receiver caused by multiple CR transmitters with different interference management mechanisms including power

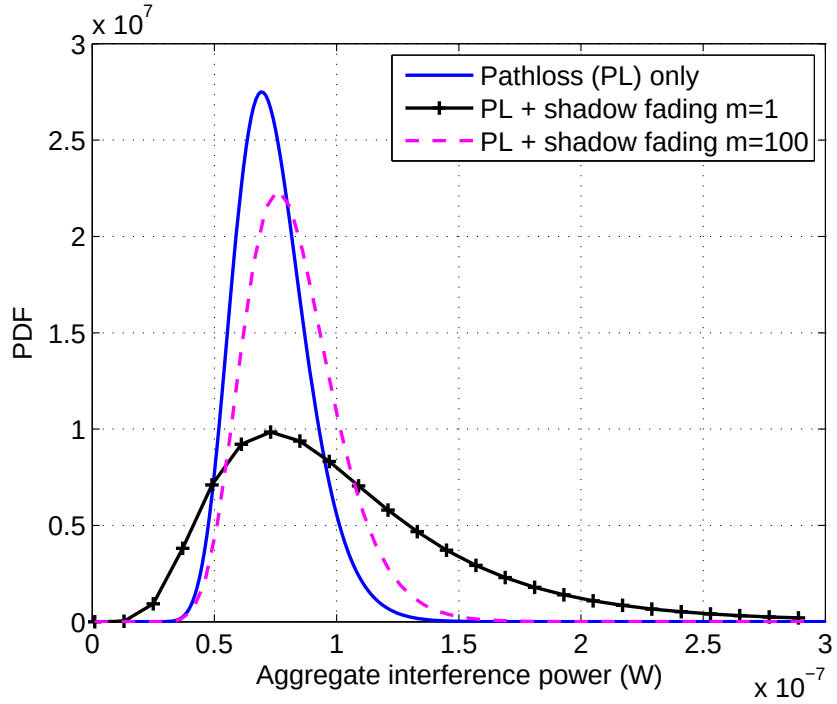

FIGURE 3.13: Impact of shadow fading on the aggregated interference for CR networks with power control (R =100 m, λ =3 user/10^4m^2, β =4, r_{pwc} = 20 m, $\alpha = 4$ and $P_{\max} = 1$ W).

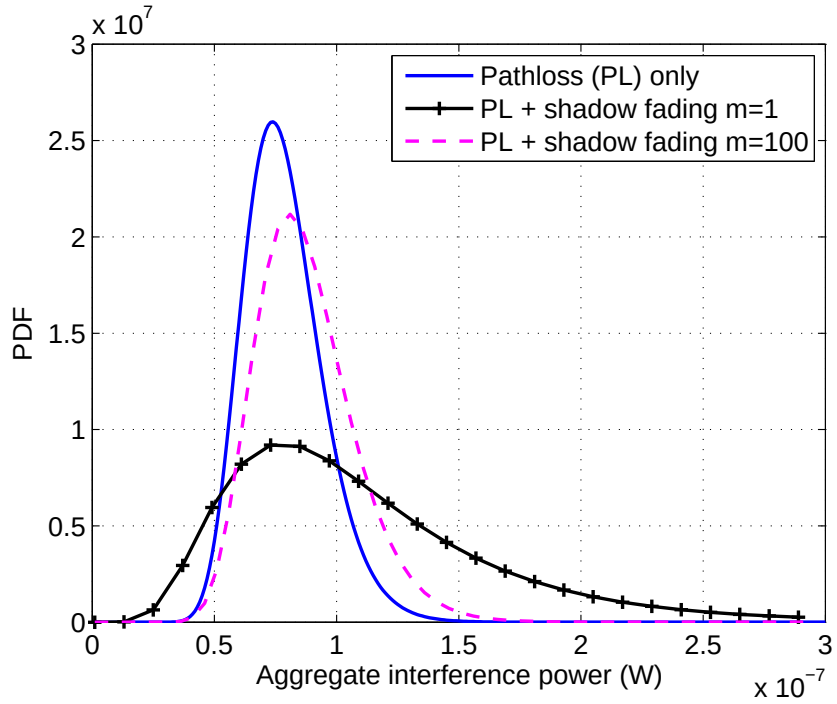

FIGURE 3.14: Impact of shadow fading on the aggregated interference for CR networks with contention control (R =100 m, λ =3 user/10^4m^2, β =4, $d_{\min}$ =20 m and $p = 1$ W).

control, contention control, and hybrid power/contention control schemes has been characterised. The PDFs of the aggregate CR-primary interference for the first two mechanisms have been evaluated analytically while, the interference distribution under the hybrid power/contention control has been studied numerically. Then, the interference distributions for power and contention control schemes have been approximated by log-normal distributions using the cumulant-based approach. We have reached the following conclusions.

- The proposed power control and contention control schemes are two effective approaches to alleviate CR-primary interference. The hybrid control scheme causes higher interference to a primary receiver, but leads to larger CR coverage as compared to either power or contention control schemes.
- There is a fairly good match between the numerically derived PDFs and the approximated counterparts for the aggregate interference. However, the latter approach greatly reduces the computational complexity.

Furthermore, the effect of a hidden primary receiver on the perceived CR-primary interference has also been investigated for the primary receiver. It has been found that the hidden primary receiver problem leads to higher CR-primary interference with increased mean and variance for the interference.

Finally, numerical studies have demonstrated the impact of some CR deployment parameters on the resulting aggregate interference under power and contention control schemes. The following conclusion have been drawn.

- Increasing the IR radius of the primary receiver is an effective way to reduce the CR-primary interference.
- The resulting CR-primary interference under power control scheme is more sensitive to the IR radius than that under the contention control counterpart.
- Shadow fading has similar impact on the aggregate interference for the CR networks adopting the power and contention control schemes.

In summary, the interference models presented in this chapter reveal how CR operation may affect the CR-primary interference, which consequently sheds light on CR deployment to protect primary networks. In the next chapter, we will focus on specific interference mitigation techniques to directly reduce the CR-primary interference and better protect the primary system.

Chapter 4

Interference Mitigation for Cognitive Radio Networks

4.1 Introduction

The impact of CR operation on the resulting CR-primary interference has been analysed in Chapter 3 by examining the interference PDFs for interference-tolerant CR networks. As a natural extension, we investigate how to manage and mitigate the CR-primary interference to protect the primary network in this chapter. Effective interference management is essential to the coexistence of CR and primary networks, since CR networks are not supposed to cause any detrimental interference to the primary system. Interference management mechanisms can be embedded into a CR network in various system design aspects from network planning, radio resource management, MAC, to physical layer signal processing. Our interest in this chapter lies on the MAC and the physical layer signal processing schemes, commonly known as interference mitigation techniques.

In the literature, interference mitigation and interference cancellation are sometimes used interchangeably. To avoid confusion, we clarify several interference management related concepts before proceeding with this chapter. The notion of *Interference cancellation* (IC) was proposed more than 20 years ago. Initially, *it should be interpreted*

to mean the class of techniques that demodulate and/or decode desired information, and then use this information along with channel estimates to cancel received interference from the received signal [51]. That is, IC stands for a set of techniques passively cancelling interference at the receiver side. *Interference suppression* mostly refers to techniques applied at receivers that can suppress interference for the desired signal by exploiting the characteristics of the interfering or desired signal. Unlike the traditional IC which regenerates the interfering signals and subtracts them from the received signal, interference suppression directly suppresses the interference by filtering the received signal according to the characteristics of the interfering or desired signals. *Interference avoidance* (IA) emphasises proactively avoiding interfering with other users. This can be achieved either by system-level approach e.g., static pre-planned frequency reuse scheme for GSM system or the physical layer techniques used at the transmitter side, e.g., transmit beamforming/precoding steering the transmission into the null space of the interference channel. *Interference mitigation* (IM) has broader applicability. It refers to any scheme or technique that can eventually mitigate the interference. Therefore, IM is interchangeable with all the aforementioned notions in wide sense.

The contributions of this chapter lie on:

- A comprehensive review on various physical layer IA techniques applicable to CR transmitters is provided.
- Two precoding-based IA schemes are proposed for CR MIMO systems to avoid interfering with the primary network and to boost the throughput of the CR system.
- To better mitigate the CR-primary interference, we approach the IM from a cross-layer perspective by jointly considering precoding in the physical layer and channel allocation in the MAC layer. Two distributed algorithms are proposed to perform the cross-layer IM.

The rest of this chapter is organised as follows. A variety of IM techniques applicable to CR transmitters are reviewed in Section 4.2. Two precoding-based IM schemes are

proposed in Section 4.3 for CR MIMO systems. The cross-layer IM algorithms are elaborated in Section 4.4. Finally, Section 4.5 concludes this chapter.

4.2 A Review of Interference Avoidance for CR Networks

In the literature, a few papers [23, 51–54] have studied IM techniques in the context of CR networks. In [51], an opportunistic IC schemes was proposed for CR receivers to adaptively cancel the primary signals when they are decodable. In [23, 52–54], active spectrum shaping, transmit beamforming, and transmit precoding techniques were investigated for CR transmitters, respectively. Apart from the aforementioned papers, there exist many other IM techniques [55] that have been proposed and successfully applied to a number of wireless systems to mitigate various types of interference. Widely used IM techniques include the filter-based approach (e.g., Wiener filter), transform-domain approach (e.g., wavelet, chirplet), cyclostationarity-based approach, higher order statistics-based approach, joint detection / multi-user detection (MUD), and spatial processing (e.g., beamforming and precoding). The success of these IM techniques inspires us to study their applications to CR networks.

In this subsection, we consider the IM for inter-network interference from CR transmitters to primary receivers, i.e., IM for CR-primary interference. The IC techniques applicable to CR receivers to mitigate the primary-CR interference are out of the scope of the thesis. Interested readers can refer to [56] for details. The CR transmissions should be well managed to guarantee that the primary services are not harmfully interfered with. It is therefore important for CR transmitters to adopt certain signal processing schemes, referred to as transmitter-side IA techniques, to mitigate both the cochannel interference and adjacent channel interference (i.e., out-of-band interference) caused to primary receivers. A number of applicable schemes will be explained in subsequent section.

Spectrum Shaping

The focus of spectrum shaping, also referred to as pulse shaping, is on generating proper waveforms for secondary signals to minimise the power leakage into the primary bands to be protected. In the literature, spectrum shaping techniques have been well investigated in the context of UWB systems and software defined radios. The goal is to design adaptive pulse waveforms which can dynamically react to the spectral environment and produce desired spectral shapes/notches. Preferably, the signal waveforms should be constructed as the linear combination of a limited number of orthogonal basis functions, also known as the core pulse wavelets. These basis functions should be bandwidth-limited, time-limited, orthogonal to each other, and flexible enough to form any desired shape of the power spectrum. Using orthogonal sinusoid waves as the core pulse wavelets leads to the well-known multicarrier modulation technique. The most popular multicarrier technique is OFDM, which can flexibly mitigate the interference to a particular band by turning off the corresponding subcarriers. However, OFDM wavelets are known to have large side lobes (spectrum leakage), which limit the notch depth to $5-10$ dB. Many techniques have been proposed for side-lobe suppression in OFDM systems. For example, an approach called active interference cancellation was proposed in [53] to improve the notch performance by nullifying some special tones at the edge of the interference band. Another multicarrier technique is the filter bank-based approach [57], which can generate waveforms with smaller side lobes than OFDM. Besides the multicarrier approaches, non-multicarrier pulse-shaping techniques use different orthogonal wavelets, such as the prolate spheroidal wave functions, as the basis functions to construct waveforms with desired spectral properties.

Pulse shaping can be used to reduce both the cochannel interference and adjacent channel interference from CR transmitters to primary networks. Typically, a high suppression gain can be achieved with a medium hardware complexity.

Predistortion Filtering

In practice, one major cause of the adjacent channel interference is the transmission nonlinearity due to cascaded nonlinear components in the RF chain. High linearity is usually required for CR transmitters to ensure minimal interference to primary users. However, high linearity transmitter chains are not only more expensive but also less power efficient. One way to reduce the linearity requirement is to use predistortion techniques. A predistortion module precompensates the signal entering a nonlinear device for anticipated distortion so that the output from the combined pre-distortion module and the nonlinear device is undistorted [55]. Effective predistortion can be achieved through both analogue and digital means. Predistortion filtering is mainly used for suppressing adjacent channel interference. Depending on the degrees of RF signal distortion, it usually provides low to medium suppression gains.

Spread Spectrum

Spread spectrum is a well-known technique that can be used by a CR transmitter to spread the signal energy across a wide bandwidth. The resulting wideband secondary signal would have a low PSD and therefore the interference to a particular narrowband primary system can be reduced. An obvious drawback is that more primary systems operating in the wider band can be interfered with. In the context of CR, spread spectrum reduces the cochannel interference at the expense of increasing the interference in adjacent channels. The hardware complexity is low and high suppression gains (for cochannel interference) are achievable with a large spreading factor.

Transmit Beamforming

Similar to receive beamforming, transmit beamforming [23] and transmit precoding [54] can be applied to CR networks for mitigating interference to primary systems by adaptively choosing weights on the transmit antenna elements to form an emission pattern with nulls towards the directions of primary receivers. It is an effective and

flexible approach to balance between the interference minimisation for primary users and the SINR maximisation for secondary users. Implementations of transmit beamforming are more complicated than receive beamforming since a feedback mechanism is required to inform CR transmitters about the instantaneous channel state information (CSI). Transmit beamforming is effective in suppressing both the cochannel and adjacent channel interference at the expense of high hardware costs.

The aforementioned four transmitter-side IA techniques are summarised and compared in TABLE 4.1 in terms of their capabilities in mitigating cochannel and adjacent channel interference, achievable interference suppression gains, and hardware complexities. In summary, spectrum shaping seems to be the most promising method for transmitter IA. The effectiveness of spectrum shaping, however, may rely on a proper predistortion filter to guarantee that the baseband pulse shapes are not distorted in the RF. Besides, transmit beamforming may be of interest to CR base stations and spread spectrum may be applicable to short-range CR systems operating in a UWB fashion.

TABLE 4.1: Comparison of different interference avoidance techniques applicable for CR transmitters.

	Shaping	**Spread**	**Beamforming**	**Predistortion**
Cochannel interference	Yes	Yes	Yes	No
Adjacent channel interference	Yes	No	Yes	Yes
Suppression gain	High	High	High	Low
Hardware complexity	Medium	Low	High	Low

4.3 Precoding-Based Interference Mitigation for CR MIMO Networks

Among different types of interference involved in CR networks, the CR-primary interference is of great importance, since a CR network have a fundamental premise that it must not impose detrimental interference on the primary network. Therefore, the

CR-primary interference should be carefully managed in order to protect the operation of primary systems. In the rest of this chapter, we confine our attention to IM for CR networks combating the CR-primary interference.

4.3.1 Related Work

Various IA techniques applicable to CR networks have been reported in Section 4.2, including spectrum shaping, predistortion filtering, spread spectrum, etc. As for multiple-antenna CR networks, transmit beamforming (for single-data-stream transmission) [23, 58–61] or precoding (for multiple-data-stream transmission) [62–64] is another effective approach to proactively mitigate interference from CR transmitters to the primary network. On one hand, it steers the CR transmission to avoid interfering with the primary network. On the other hand, it exploits the diversity or the multiplexing gain of the multiple-antenna CR system to enhance the reliability or efficiency of the CR system.

However, in the works [23, 58–64], perfect or partial CSI of CR interference channels to primary network is required at the CR transmitter side to guarantee no/-constrained interference to the primary system. Therefore, extra signalling between primary and CR networks is inevitable to obtain the CSI, which jeopardizes the applicability of these beamforming and precoding schemes. A more practical precoding scheme, which learns the CSI using subspace estimation [65] and does not require a priori CSI has been proposed in [66] and [67]. In the proposed precoding approach, where a CR MIMO transmitter-receiver pair is assumed to coexist with a primary time-division-duplexing (TDD) system, the CR transmitter first senses and estimates the interference channels from the CR to the primary network (CR-primary interference channels), and then nulls the CR transmission to the primary network by projecting the transmission to the estimated null space of the CR-primary interference channels. This approach is termed sensing and projection (SP)-based precoding. However, it does not account for the interference from primary transmitters to the CR receiver, which leads to CR throughput loss. These two works were extended in [68, 69] by removing the primary-CR interference at the CR receiver via null-space

receiver beamforming, which sacrifices the CR throughput as well. Moreover, the CR network in [68, 69] has to work in a TDD mode aligned with the primary system in order to facilitate the null-space receiver beamforming.

In this section, two enhanced SP-based precoding schemes for a CR transmitter, namely, full projection (FP)- and partial projection (PP)-based precoding, are proposed for CR MIMO systems by incorporating the primary-CR interference. As the name suggests, the FP-based scheme nulls the CR transmission by fully projecting the transmission onto the estimated null space of the CR-primary interference channels. Instead of removing the primary-CR interference using null-space receiver beamforming at the CR receiver, the proposed precoding schemes account for the primary-CR interference via sensing. This, on one hand, improves the CR throughput. On the other hand, it introduces more flexibility into the CR deployment, i.e., the CR network does not have to work in a TDD mode as in [68, 69]. The PP-based precoding can further improve the CR throughput by projecting the CR transmission onto a subspace that partially spans the estimated null space of the CR-primary interference channels. As a result, the CR throughput is further improved at the cost of introducing extra interference to the primary network.

The remainder of this section is organised as follows. The system model is given in Section 4.3.2. The principle of the SP-based precoding is introduced in Section 4.3.3. The new precoding schemes are proposed in Section 4.3.4. Finally, the performance of the proposed precoding schemes is evaluated in Section 4.3.5.

Notation: Hereafter in the thesis, vectors are denoted by bold-face lower-case letters, e.g., $\mathbf{x}$, and bold-face upper-case letters are used for matrices, e.g., $\mathbf{X}$. For a matrix $\mathbf{X}$, $\mathtt{tr}[\mathbf{X}]$, $\mathbf{X}^H$ and $\mathbf{X}^\dagger$ denote its trace, Hermitian transpose and pseudoinverse, respectively. $\mathbb{E}[\cdot]$ stands for the statistical expectation operator. $\mathbb{C}^{x\times y}$ denotes the space of $x \times y$ matrices with complex entries.

4.3.2 System Model and Problem Formulation

We consider a CR system as shown in FIGURE 4.1, where a CR transmitter-receiver pair shares the same spectrum with a primary TDD network. Multiple antennas are mounted at the CR nodes and possibly at each of the primary users. The CR transmitter, CR receiver, primary base BS and the kth primary user are equipped with M_t, M_r, M_{bs} and M_k $(k = 1, \cdots, K)$ antennas, respectively. Block-fading channels are assumed for the primary and CR systems, i.e., the variation of the channels is relatively slow compared to the duration of primary uplink and downlink frames. The channels are quasi-static over a block of L symbols.

For a narrowband transmission in the CR link, the received symbol at the CR receiver can be expressed as

$$\mathbf{y} = \mathbf{HFs} + \mathbf{n} + \mathbf{z}, \tag{4.1}$$

where $\mathbf{y} \in \mathbb{C}^{M_r \times 1}$ is the received signal vector at the CR receiver, $\mathbf{s} \in \mathbb{C}^{M_t \times 1}$ and $\mathbf{F} \in \mathbb{C}^{M_t \times M_t}$ are the transmit information vector with $\mathbb{E}[\mathbf{ss}^H] = \mathbf{I}$ and precoding matrix of the CR transmitter, respectively. $\mathbf{H} \in \mathbb{C}^{M_r \times M_t}$ is the channel matrix from

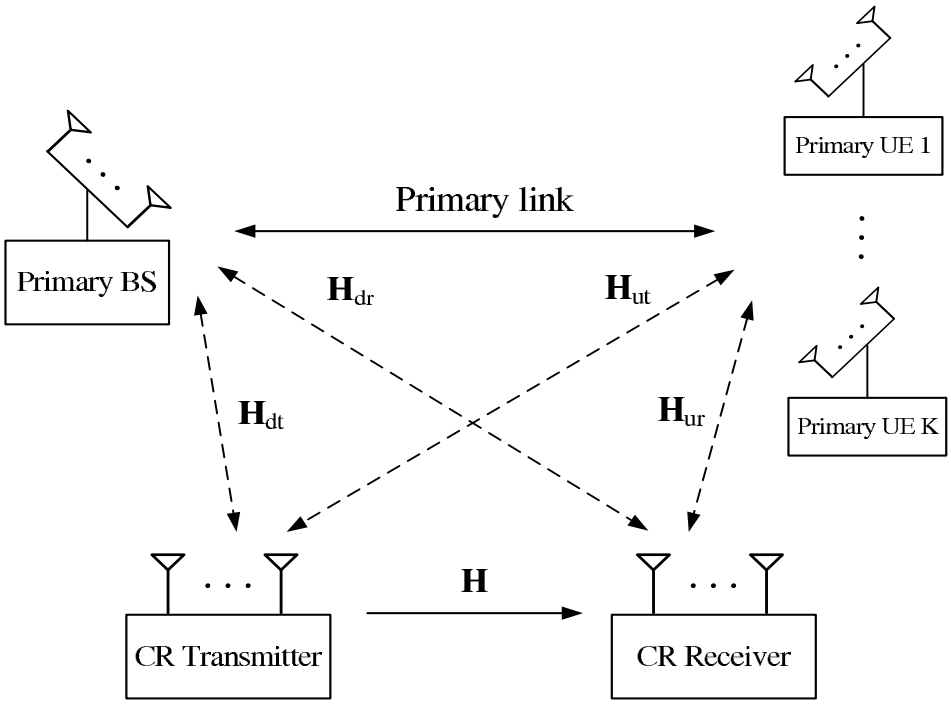

FIGURE 4.1: A CR MIMO transmitter-receiver pair coexists with a primary TDD system.

the CR transmitter to CR receiver, whose elements are independent and identically distributed (i.i.d.) complex Gaussian random variables with zero mean and variance σ_H^2, and $\mathbf{n} \in \mathbb{C}^{M_r \times 1}$ stands for the AWGN vector with zero mean and covariance matrix $\mathbb{E}[\mathbf{n}\mathbf{n}^H] = \sigma_n^2\mathbf{I}$. Moreover, $\mathbf{z} \in \mathbb{C}^{M_r \times 1}$ denotes the interference from the primary network to the CR receiver. It can be written as

$$\mathbf{z} = \begin{cases} \mathbf{H}_{\text{ur}}\mathbf{x}_u, & \text{during primary uplink} \\ \mathbf{H}_{\text{dr}}\mathbf{x}_d, & \text{during primary downlink.} \end{cases} \tag{4.2}$$

The matrices $\mathbf{H}_{\text{ur}} \in \mathbb{C}^{M_r \times \sum_{k=1}^{K} M_k}$ in (4.2) and $\mathbf{H}_{\text{ut}} \in \mathbb{C}^{M_t \times \sum_{k=1}^{K} M_k}$ (see FIGURE 4.1) represent the interference channels from all the K active primary users to the CR receiver and to the CR transmitter, respectively, during primary uplink. Similarly, $\mathbf{H}_{\text{dr}} \in \mathbb{C}^{M_r \times M_{bs}}$ in (4.2) together with $\mathbf{H}_{\text{dt}} \in \mathbb{C}^{M_t \times M_{bs}}$ (see FIGURE 4.1) stand for the interference matrices from the primary BS to the CR receiver and to the CR transmitter during primary downlink. All these interference matrices ($\mathbf{H}_{\text{ur}}$, $\mathbf{H}_{\text{ut}}$, $\mathbf{H}_{\text{dr}}$ and $\mathbf{H}_{\text{dt}}$) have i.i.d. complex Gaussian random elements with zero mean and covariance σ_{ur}^2, σ_{ut}^2, σ_{dr}^2 and σ_{dt}^2, respectively. Moreover, $\mathbf{x}_u \in \mathbb{C}^{\sum_{k=1}^{K} M_k \times 1}$ and $\mathbf{x}_d \in \mathbb{C}^{M_{bs} \times 1}$ are the transmitted signal vectors of all the K primary users and primary BS, respectively. We define the covariance matrix of the interference in (4.2) as $\mathbf{Z} \triangleq \mathbb{E}[\mathbf{z}\mathbf{z}^H]$. The maximum average CR transmission power is P_{cr}. Therefore, the precoding matrix $\mathbf{F}$ needs to satisfy the following constraint $\mathtt{tr}[\mathbb{E}[\mathbf{F}\mathbf{s}\mathbf{s}^H\mathbf{F}^H]] = \mathtt{tr}[\mathbf{F}\mathbf{F}^H] \leq P_{cr}$.

4.3.3 Principle of SP-Based Precoding

The precoding problem for the CR transmitter is modeled as the following optimisation problem [63]

$$\max_{\mathbf{F}} \quad \log_2 \det\left(\mathbf{I} + \frac{\mathbf{H}\mathbf{F}\mathbf{F}^{\text{H}}\mathbf{H}^{\text{H}}}{\sigma_{\text{n}}^2}\right) \tag{4.3}$$

$$\text{subject to} \quad \mathtt{tr}[\mathbf{F}\mathbf{F}^H] \leq P_{cr} \tag{4.4}$$

$$\mathtt{tr}[\mathbf{G}_k\mathbf{F}\mathbf{F}^H\mathbf{G}_k^H] \leq \Gamma_k \quad k = 1, \ldots, L\ . \tag{4.5}$$

In (4.5), $\mathbf{G}_k \in \mathbb{C}^{M_k \times M_t}$ is the channel matrix from the CR transmitter to the kth primary user. Thus, the channel matrix from the CR transmitter to all primary users becomes $\mathbf{H}_{\text{ut}}^H = [\mathbf{G}_1^T, \cdots, \mathbf{G}_K^T]^T$ where channel reciprocity is assumed. The constraints on the CR transmission power and the maximum allowed interference perceived at each primary user are given by (4.4) and (4.5), respectively.

The projected channel singular value decomposition (SVD) or P-SVD precoding has been proposed in [63] as a suboptimal solution for the above optimisation problem. It first projects the CR channel $\mathbf{H}$ onto the null space of $\mathbf{H}_{\text{ut}}^H$. The effective CR channel matrix $\mathbf{H}_\perp$ after projection becomes [63]

$$\mathbf{H}_\perp = \mathbf{H}(\mathbf{I} - \mathbf{U}_G \mathbf{U}_G^H) \tag{4.6}$$

where $\mathbf{U}_G$ comes from the SVD of $\mathbf{H}_{\text{ut}}^H$, i.e., $\mathbf{H}_{\text{ut}}^H = \mathbf{V}_G \mathbf{\Lambda}_G^{1/2} \mathbf{U}_G^H$. Then, the precoding matrix of the CR transmitter for the effective CR channel $\mathbf{H}_\perp$ can be obtained as [63]

$$\mathbf{F} = \mathbf{U}_\perp \left[(\mu \mathbf{I} - \mathbf{\Lambda}_\perp^{-1})^+ \right]^{\frac{1}{2}} \tag{4.7}$$

where $\mathbf{U}_\perp$ and $\mathbf{\Lambda}_\perp$ originate from the SVD of $\mathbf{H}_\perp$, i.e., $\mathbf{H}_\perp = \mathbf{V}_\perp \mathbf{\Lambda}_\perp^{1/2} \mathbf{U}_\perp^H$, $(\cdot)^+ = \texttt{max}(0, \cdot)$ and μ denotes the power level for a water-filling (WF) algorithm such that $\texttt{tr}[(\mu \mathbf{I} - \mathbf{\Lambda}_\perp^{-1})^+] = P_{cr}$. With perfect CSI of $\mathbf{H}_{\text{ut}}^H$, the precoding with $\mathbf{F}$ will completely avoid interference to primary users.

In practice, $\mathbf{H}_{\text{ut}}^H$ has to be estimated. Therefore, the SP precoding is introduced in [66] and [67] to estimate the space $\mathbf{U}_G \mathbf{U}_G^H$ spanned by $\mathbf{H}_{\text{ut}}^H$ via sensing for (4.6). The SP precoding is composed of two phases - uplink sensing and downlink transmission as shown in FIGURE 4.2.

By analogy with the multiple signal classification (MUSIC) technique [65], the signal covariance matrix is decomposed into signal and noise subspaces to estimate $\mathbf{U}_G$ at

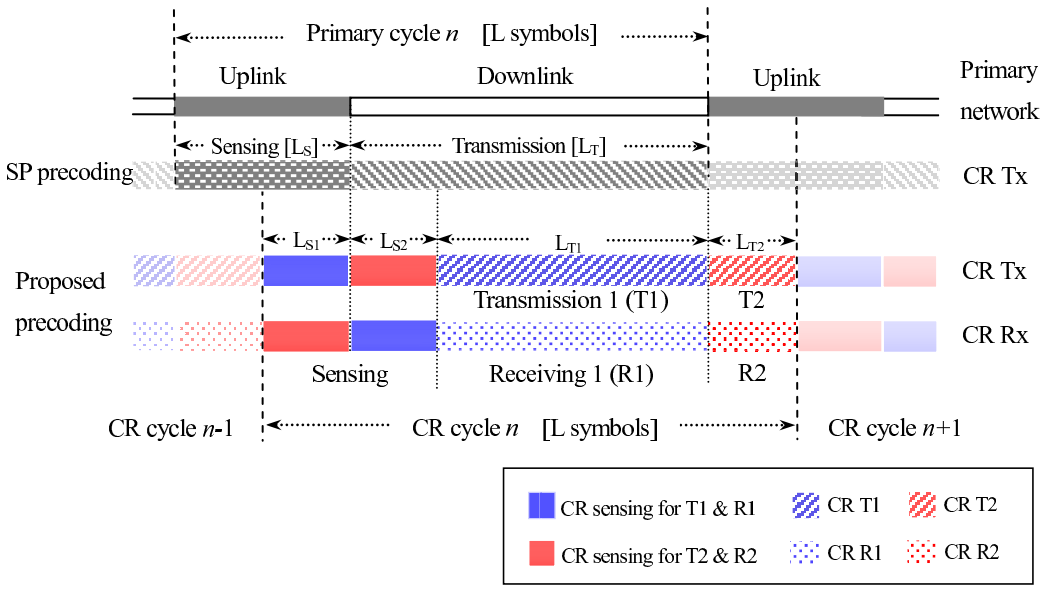

FIGURE 4.2: System diagram for the proposed precoding schemes.

the end of the sensing phase, which can be mathematically expressed as [66]

$$\hat{\mathbf{R}}_{\text{ut}} = \frac{1}{L_S}\sum_{i=1}^{L_S} \mathbf{r}_{\text{ut}}(i)\mathbf{r}_{\text{ut}}^H(i) \tag{4.8}$$

$$= \hat{\mathbf{U}}\hat{\mathbf{\Lambda}}\hat{\mathbf{U}}^H \tag{4.9}$$

$$= \hat{\mathbf{U}}_G\hat{\mathbf{\Lambda}}_G\hat{\mathbf{U}}_G^H + \hat{\mathbf{U}}_n\hat{\mathbf{\Lambda}}_n\hat{\mathbf{U}}_n^H. \tag{4.10}$$

In (4.8), $\mathbf{r}_{\text{ut}}(i) = \mathbf{H}_{\text{ut}}\mathbf{x}_u(i) + \mathbf{n}(i)$ is the ith received symbol at the CR transmitter, and $\hat{\mathbf{R}}_{\text{ut}}$ denotes the average covariance matrix of the received symbols. An eigenvalue decomposition (EVD) is then performed on $\hat{\mathbf{R}}_{\text{ut}}$ in (4.9), where $\hat{\mathbf{\Lambda}} = \text{diag}(\lambda_1, \cdots, \lambda_{\text{M}_\text{t}})$ is a diagonal matrix with descendingly ordered eigenvalues of $\hat{\mathbf{R}}_{\text{ut}}$ and $\hat{\mathbf{U}} \in \mathbb{C}^{M_t \times M_t}$ contains the corresponding eigenvectors. The matrix $\hat{\mathbf{R}}_{\text{ut}}$ is further decomposed into interference and noise components in (4.10) with $\hat{\mathbf{U}}_G$ and $\hat{\mathbf{U}}_n$ being the first $K_p = \texttt{rank}(\mathbf{H}_{\text{ut}})$ and the remaining $(M_t - K_p)$ columns of $\hat{\mathbf{U}}$, respectively, and $\hat{\mathbf{\Lambda}}_G$ and $\hat{\mathbf{\Lambda}}_n$ being their corresponding eigenvalue matrices. A rank estimate for K_p can be carried out by using, e.g., an Akaike information criterion (AIC) or minimum description length (MDL) estimator [70]. The sensing phase is followed by a CR transmission,

where a precoding matrix obtained from (4.7) is applied.

The merit of the SP precoding over the P-SVD approach is that no CSI is required due to the interference space estimation in (4.8)–(4.10). However, both of the precoding algorithms in [66] and [67] do not consider the interference from the primary network to the CR receiver, which eventually leads to rate loss for the CR link.

4.3.4 Proposed Precoding Schemes

In this section, two enhanced precoding schemes are proposed to tackle the problem of CR rate loss of the aforementioned SP precoding. We elaborate the CR precoding during the primary downlink. A similar precoding for the primary uplink can be easily obtained, which is ignored here for brevity.

When incorporating the primary-CR interference, the precoding problem for the CR transmitter during the primary downlink can be modeled as the following optimisation problem

$$\max_{\mathbf{F}} \quad \log_2 \det\left(\mathbf{I} + \frac{\mathbf{H}\mathbf{F}\mathbf{F}^{\mathrm{H}}\mathbf{H}^{\mathrm{H}}}{\mathbf{Z} + \sigma_{\mathrm{n}}^2\mathbf{I}}\right) \tag{4.11}$$

$$\text{subject to} \quad \mathtt{tr}[\mathbf{F}\mathbf{F}^H] \leq P_{cr} \tag{4.12}$$

$$\mathtt{tr}[\mathbf{G}_k\mathbf{F}\mathbf{F}^H\mathbf{G}_k^H] \leq \Gamma_k, \quad k = 1, \ldots, L. \tag{4.13}$$

From (4.11)–(4.13), the precoding matrix for CR transmission during the downlink can be written as [71]

$$\mathbf{F}_d = \mathbf{U}_d \left[(\mu_d\mathbf{I} - \mathbf{\Lambda}_d^{-1})^+\right]^{\frac{1}{2}} \tag{4.14}$$

where μ_d is the power level for the WF algorithm similar to that in (4.7) and $\mathbf{U}_d$ is obtained through the following EVD

$$\begin{aligned}\mathbf{U}_d\mathbf{\Lambda}_d\mathbf{U}_d^H &= \mathbf{H}_\perp^H(\mathbf{Z} + \sigma^2\mathbf{I})^{-1}\mathbf{H}_\perp \\ &= (\mathbf{I} - \mathbf{U}_G\mathbf{U}_G^H)^H\mathbf{H}^H(\mathbf{Z} + \sigma^2\mathbf{I})^{-1}\mathbf{H}(\mathbf{I} - \mathbf{U}_G\mathbf{U}_G^H).\end{aligned} \tag{4.15}$$

It can be seen from (4.14) and (4.15) that in order to obtain the CR precoding matrix, the interference-plus-noise covariance matrix $\mathbf{R}_{\text{ur}} \triangleq \mathbf{Z} + \sigma_n^2\mathbf{I}$ needs to be estimated at the CR receiver, besides the estimation of the interference subspace $\mathbf{U}_G\mathbf{U}_G^H$ at the CR transmitter.

4.3.4.1 Full Projection-Based Precoding

To enable the estimation of $\mathbf{U}_G\mathbf{U}_G^H$ and $\mathbf{R}_{\text{ur}}$, we propose an enhanced precoding scheme. The system diagram for this scheme is demonstrated in FIGURE 4.2. Each CR cycle consists of sensing and transmission phases as shown in FIGURE 4.2. We name the CR transmission during the primary downlink/uplink as the downlink transmission T1/uplink transmission T2. For T1, the space $\mathbf{U}_G\mathbf{U}_G^H$ is estimated at the CR transmitter during the primary uplink according to (4.8)–(4.10) over L_{S1} symbols. The estimation of $\mathbf{R}_{\text{ur}}$ is performed at the CR receiver at the beginning of the primary downlink phase for a batch of L_{S2} symbols via a procedure similar to (4.8). After obtaining these two estimates, the CR transmitter starts transmission T1 using the precoding matrix obtained by (4.14). The uplink transmission session T2 follows immediately after the downlink transmission T1 but right before the sensing phase for the next CR cycle. The CR precoding matrix for T2 can be obtained by another two sensing sessions concurrent with the sensing phase for T1. The downlink and uplink transmissions last for L_{T1} and L_{T2} symbols, respectively. The duration of each CR cycle should not be longer than the channel coherence time due to the block-fading channels. The FP-based channel projection (4.6) is employed in this proposed precoding scheme. Therefore, it is termed as FP precoding.

It can be seen from FIGURE 4.2 that the proposed FP precoding scheme shifts the CR cycle of the SP precoding rightwards in time. By doing this, several benefits are obtained. Firstly, introducing CR receiver sensing phases during both the primary downlink and uplink improves the CR instantaneous throughput by incorporating the interference-plus-noise covariance matrix into precoding, and consequently improves the CR throughput. Secondly, shifting the CR cycle diverts part of the CR transmission from the primary downlink to the uplink which reduces the time that primary

receivers expose themselves to interference from the CR transmitter. This is beneficial to the primary network, since primary users are usually more susceptible to CR interference than the primary BS. It is worth noting that to facilitate the proposed precoding scheme the CR system needs to synchronise the sensing phase with the primary TDD system. However, the CR system can easily achieve this by listening to the primary control channel without intervening the primary operation.

Theoretically, the proposed FP precoding can completely null its transmission towards primary users when the sensing phase is long enough and the channel noise variance is small enough. However, the interference mitigation ability of the proposed FP precoding degrades rapidly when the CR interference-to-noise ratio (INR$\triangleq \sigma_{\text{ut}}^2/\sigma_n^2$) drops below a threshold. This is due to the fact that in (4.10) some components in the noise subspace may swap with those in the interference subspace when the noise amplitude σ_n is relatively larger than the interference channel gain σ_{ut}. This phenomenon is known as a *subspace swap* [72]. The lower bound on the probability of the subspace swap has been investigated in [73] and [74].

For low INR, the interference subspace has a high probability to swap with the noise subspace. When a subspace swap happens, (4.15) can be rewritten as

$$\begin{aligned}\mathbf{U}_d\mathbf{\Lambda}_d\mathbf{U}_d^H &\approx (\mathbf{I}-\hat{\mathbf{U}}_n\hat{\mathbf{U}}_n^H)^H\mathbf{H}^H(\mathbf{Z}+\sigma^2\mathbf{I})^{-1}\mathbf{H}(\mathbf{I}-\hat{\mathbf{U}}_n\hat{\mathbf{U}}_n^H)\\ &= \hat{\mathbf{U}}_G\hat{\mathbf{U}}_G^H\mathbf{H}^H(\mathbf{Z}+\sigma^2\mathbf{I})^{-1}\mathbf{H}\hat{\mathbf{U}}_G\hat{\mathbf{U}}_G^H \end{aligned} \tag{4.16}$$

which means that the precoding matrix $\mathbf{F}_d$ and $\mathbf{H}_{\text{ut}}^H$ span the same space. Therefore, when the CR INR is low the average interference power received at primary users can be expressed as

$$\text{Int}_l^{\text{FP}} = \mathbb{E}[\mathtt{tr}[\mathbf{H}_{\text{ut}}^{\text{H}}\mathbf{F}_{\text{d}}\mathbf{F}_{\text{d}}^{\text{H}}\mathbf{H}_{\text{ut}}]] \propto \text{P}_{\text{cr}}\sigma_{\text{ut}}^2. \tag{4.17}$$

This suggests that the average interference power at primary users is proportional to the channel gain between CR and primary users at low CR INR.

When the CR INR is high, using the similar steps as in [67] the average interference power at primary receivers becomes

$$\begin{aligned}
\mathrm{Int}_h^{\mathrm{FP}} &= \mathbb{E}[\mathtt{tr}[\mathbf{H}_{\mathrm{ut}}^H \hat{\mathbf{U}}_d(\mu_d \mathbf{I} - \mathbf{\Lambda}_d^{-1})^+ \hat{\mathbf{U}}_d^H \mathbf{H}_{\mathrm{ut}}]] && (4.18)\\
&= \mathbb{E}[\mathtt{tr}[\mathbf{H}_{\mathrm{ut}}^H (\hat{\mathbf{U}}_d - \mathbf{U}_d)(\mu_d \mathbf{I} - \mathbf{\Lambda}_d^{-1})^+ (\hat{\mathbf{U}}_d - \mathbf{U}_d)^H \mathbf{H}_{\mathrm{ut}}]] && (4.19)\\
&\approx \mathbb{E}[\mathtt{tr}[\mathbf{H}_{\mathrm{ut}}^H (\mathbf{X}^H \mathbf{H}_{\mathrm{ut}})^\dagger \mathbf{N}^H \mathbf{U}_d (\mu_d \mathbf{I} - \mathbf{\Lambda}_d^{-1})^+ \mathbf{U}_d{}^H \mathbf{N} (\mathbf{H}_{\mathrm{ut}}^H \mathbf{X})^\dagger \mathbf{H}_{\mathrm{ut}}]] && (4.20)\\
&= \sigma_n^2 P_{cr} \mathbb{E}[\mathtt{tr}[\mathbf{H}_{\mathrm{ut}}^H (\mathbf{X}^H \mathbf{H}_{\mathrm{ut}})^\dagger (\mathbf{H}_{\mathrm{ut}}^H \mathbf{X})^\dagger \mathbf{H}_{\mathrm{ut}}]] && (4.21)\\
&= \frac{\sigma_n^2 P_{cr}}{L_{S1}} \mathtt{tr}[\mathbf{Q}_u] && (4.22)
\end{aligned}$$

where (4.19) is due to $\mathbf{H}_{\mathrm{ut}}^H \mathbf{U}_d = \mathbf{0}$; (4.20) is obtained using the fact that $\hat{\mathbf{U}}_d - \mathbf{U}_d \approx -(\mathbf{X}^H \mathbf{H}_{\mathrm{ut}})^\dagger \mathbf{N}^H \mathbf{U}_d$ for high INR [75] with $\mathbf{X} \triangleq [\mathbf{x}_u(1), \mathbf{x}_u(2), \cdots, \mathbf{x}_u(L_{S1})]$, and $\mathbf{N} \triangleq [\mathbf{n}(1), \mathbf{n}(2), \cdots, \mathbf{n}(L_{S1})]$; (4.21) is obtained due to the independence of $\mathbf{X}^H \mathbf{H}_{\mathrm{ut}}$ and $\mathbf{N}$ and $\mathbb{E}[\mathbf{N}^H \mathbf{Y} \mathbf{N}] = \sigma_n^2 \mathtt{tr}[\mathbf{Y}]\mathbf{I}$ for any constant matrix $\mathbf{Y}$; $\mathbf{Q}_u \triangleq \mathbb{E}[\mathbf{x_u} \mathbf{x_u}^H]$ in (4.22) is the transmit covariance matrix for the primary user. An interesting fact is observed from (4.22) that at high CR INR the average received interference at primary users does not depend on the interference channel $\mathbf{H}_{\mathrm{ut}}^H$. The average interference is proportional to the channel noise σ_n^2 and inversely proportional to the sensing length L_{S1}.

4.3.4.2 Partial Projection-Based Precoding

To further improve the throughput of the CR link, the CR transmitter does not need to fully project its transmission to the null space of the entire interference space. Instead, it may null its transmission to a subspace partially spanning the interference space. Based on this analysis we introduce another precoding scheme, namely, the PP precoding.

The PP precoding works in a similar manner to the proposed FP precoding except for the selection of the interference space. For the downlink CR precoding, the CR transmitter first obtains $\hat{\mathbf{\Lambda}}$ and $\hat{\mathbf{U}}$ via EVD in (4.9) during uplink sensing. Then, a subspace $\hat{\mathbf{U}}_m \hat{\mathbf{U}}_m^H$ partially spanning the interference space is obtained by choosing m eigenvectors corresponding to the first m largest eigenvalues of $\hat{\mathbf{\Lambda}}$, where m can be

determined according to various criteria. One candidate criterion is

$$\frac{\sum_{i=m+1}^{M_{\min}} \lambda_i}{\sum_{i=1}^{m} \lambda_i} \leq r_{t/d} \tag{4.23}$$

with $M_{\min} \triangleq \texttt{min}(M_t, \sum_{k=1}^{K} M_k)$. We call $r_{t/d}$ the trivial over dominant interference ratio (TDIR). This selection process chooses m dominant interference subchannels to form an estimate of the interference space and ignores the other $(M_{\min}-m)$ trivial ones. When equal power is assigned to each CR antenna, $r_{t/d}$ stands for the maximum ratio of the resulting and nullified interference to the primary receiver. Finally, substituting the estimated subspace $\hat{\mathbf{U}}_m\hat{\mathbf{U}}_m^H$ for $\hat{\mathbf{U}}_G\hat{\mathbf{U}}_G^H$ in (4.6), the precoding matrix $\mathbf{F}_d$ for the downlink CR transmission is obtained via (4.14). However, we may fail to find a value of m satisfying (4.23). In this case, the proposed FP precoding is used. The uplink CR precoding can be performed in the similar manner as the downlink counterpart.

The joint PDF of the ordered eigenvalues $\lambda \triangleq [\lambda_1, \lambda_2, \cdots, \lambda_{M_{\min}}]$ of $\hat{\mathbf{R}}_{\text{ut}}$, with $\lambda_1 \geq \lambda_2 \geq \cdots \geq \lambda_{M_{\min}} \geq \sigma_n^2$ is [76]

$$f_\lambda(\lambda_1, \lambda_2, \cdots, \lambda_{M_{\min}}) = \frac{1}{{P_p}^{M_{\min}}} f_{\tilde{\lambda}}\left(\frac{\lambda_1-\sigma_n^2}{P_p}, \frac{\lambda_2-\sigma_n^2}{P_p}, \cdots, \frac{\lambda_{M_{\min}}-\sigma_n^2}{P_p}\right) \tag{4.24}$$

where P_p is the transmission power of each primary user antenna and $f_{\tilde{\lambda}}(\tilde{\lambda}_1, \tilde{\lambda}_2, \cdots, \tilde{\lambda}_{M_{\min}})$ with $\tilde{\lambda}_1 \geq \tilde{\lambda}_2 \geq \cdots \geq \tilde{\lambda}_{M_{\min}}$ is given by

$$f_{\tilde{\lambda}}(\tilde{\lambda}_1, \tilde{\lambda}_2, \cdots, \tilde{\lambda}_{M_{\min}}) = \frac{\prod_{i=1}^{M_{\min}} e^{-\tilde{\lambda}_i} \tilde{\lambda}_i^{M_{\max}-M_{\min}} \prod_{i=1}^{M_{\min}-1} \left[\prod_{j=i+1}^{M_{\min}} (\tilde{\lambda}_i - \tilde{\lambda}_j)^2\right]}{\prod_{i=1}^{M_{\min}} (M_{\max}-i)! \prod_{i=1}^{M_{\min}} (M_{\min}-i)!} \tag{4.25}$$

with $M_{\max} \triangleq \texttt{max}(M_t, \sum_{k=1}^{K} M_k)$. Therefore, the probability for the occurrence of (4.23) is

$$p_m = \int_{\mathbf{S}} f_\lambda(\lambda_1, \lambda_2, \cdots, \lambda_{M_{\min}})\, d\lambda_1\, d\lambda_2 \cdots d\lambda_{M_{\min}} \tag{4.26}$$

where $\mathbf{S} \triangleq \{(\lambda_1, \lambda_2, \cdots, \lambda_{M_{\min}}) |\, (4.23) \cap \lambda_1 \geq \lambda_2 \geq \cdots \geq \lambda_{M_{\min}} \geq \sigma_n^2\}$.

In other words, for the PP precoding scheme the probabilities of using the 'real' PP (m satisfying (4.23) exists) and using FP are p_m and $(1-p_m)$, respectively. Therefore, the CR transmitter uses $[(1-p_m)\sum_{k=1}^{K} M_k + p_m m]$ and $\sum_{k=1}^{K} M_k$ degrees of freedom (DoF)

for interference mitigation in the PP and FP precoding schemes. Meanwhile, the DoF for CR transmission for the PP and FP precoding are $[M_t-(1-p_m)\sum_{k=1}^{K}M_k-p_m m]$ and $(M_t-\sum_{k=1}^{K}M_k)$, respectively. This means that compared to the proposed FP precoding the PP precoding scheme transfers $p_m(\sum_{i=1}^{K}M_k-m)$ DoF from interference mitigation to CR transmission, which leads to a higher throughput for the CR link. It can be seen from (4.24)–(4.26) that in the large INR regime, p_m is fixed for a given noise power σ_n^2 and P_p, i.e., the probability of the 'real' PP and FP does not change with the interference channel $\mathbf{H}_{\text{ut}}^H$. Considering the fact from (4.22) that at high INRs the average interference power of FP Int_h^{FP} is fixed and the average interference power resulting from 'real' PP Int^{PP} is proportional to the square of the interference channel gain σ_{ut}^2, the overall average interference of the PP precoding $\text{Int}_h^{\text{PP}}=p_m\text{Int}^{\text{PP}}+(1-p_m)\text{Int}_h^{\text{FP}}$ is linearly proportional to σ_{ut}^2 for large INRs.

4.3.5 Numerical Results and Discussions

In this section, the performance of the proposed precoding schemes is evaluated via simulations. We consider a scenario where a CR MIMO system coexists with a primary TDD system which has one 2-antenna BS and two single-antenna users. Each CR node is equipped with four antennas, i.e., $M_t=M_r=4$, $M_{bs}=2$, $K=2$ and $M_1=M_2=1$. The primary network works as a downlink-broadcast and an uplink multiple-access system. The primary BS uses perfect zero-forcing beamforming at both the primary downlink and uplink. The transmission power of the CR and primary networks is 1. All the results are obtained by averaging over 2000 simulation runs.

First, we evaluated the CR throughput and CR-primary interference of the CR system with the proposed precoding schemes over different values of signal-to-noise ratios, $\text{SNR}\triangleq\sigma_H^2/\sigma_n^2$. In FIGURE 4.3(a), the throughputs (mutual information in (4.11) averaged over a CR cycle) of the two proposed precoding schemes are compared with that of the SP precoding in [66] [67] and the P-SVD precoding with perfect CSI of [63]. The system setup is as follows: $L_{S1}=L_{S2}=L_{T2}=50$, $L_{T1}=350$, $\sigma_H^2=\sigma_{\text{ut}}^2=1$, $P_{cr}=1$, and $r_{t/d}=0.1$. It can be seen that the proposed FP/PP precoding schemes lead to higher CR throughput than the SP precoding, and the throughput

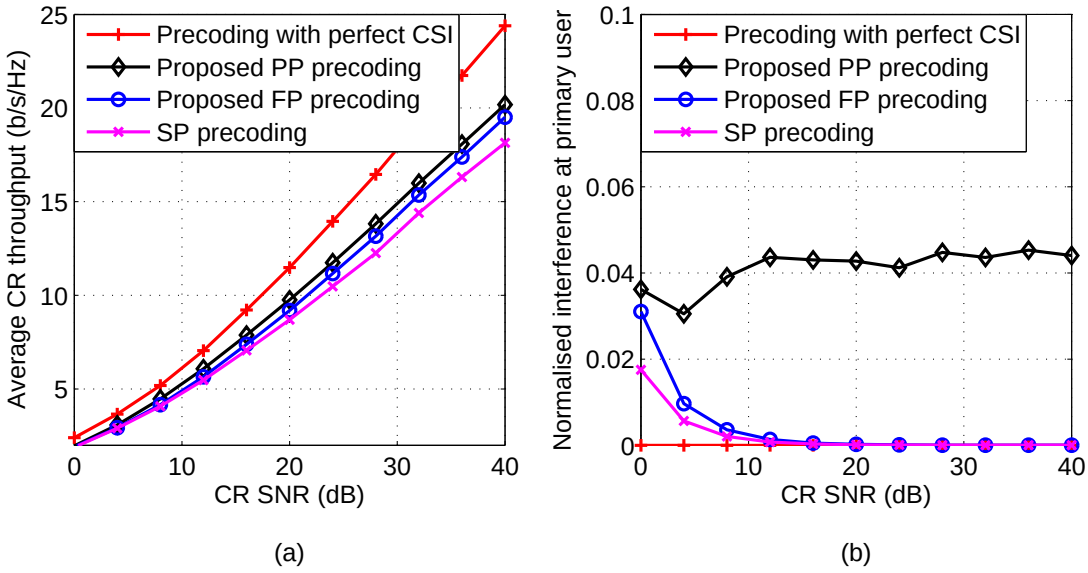

FIGURE 4.3: CR throughput and the resulting interference under different precoding schemes ($M_t = M_r = 4$, $M_{\text{bs}} = 2$, $K = 2$, $M_1 = M_2 = 1$, $L_{S1} = L_{S2} = L_{T2} = 50$, $L_{T1} = 350$, $\sigma_H^2 = \sigma_{\text{ut}}^2 = 1$, $P_{cr} = 1$, and $r_{t/d} = 0.1$).

gain becomes larger as the SNR increases. The resulting CR-primary interference is evaluated in FIGURE 4.3(b), where the interference is normalised by the interference caused by CR transmission with equal power allocation. It can be seen from this figure that the FP precoding scheme leads to similar amount of interference to the primary system as SP and P-SVD schemes in high CR SNR regime. This suggests that when the CR SNR is high the FP precoding outperforms the SP counterpart.

In FIGURE 4.4, we evaluate the impact of CR INR on the CR throughput and the resulting CR-primary interference under different precoding schemes. It has the same setup as that of FIGURE 4.3 with $\sigma_n^2 = 10^{-4}$. By comparing FIGURE 4.4(a) with FIGURE 4.4(b), it can be seen that the proposed FP/PP precoding schemes outperform the SP counterpart at low INRs, since they lead to higher CR throughput without introducing extra interference. At high INRs, both the proposed FP and SP precoding schemes have fixed interference, and there is a fairly good agreement between the derived and simulated interference of the FP precoding. Another phenomenon that can be seen from FIGURE 4.4(b) is that the interference of the SP precoding is slightly smaller than that of the FP precoding, which is due to the fact that the sensing of

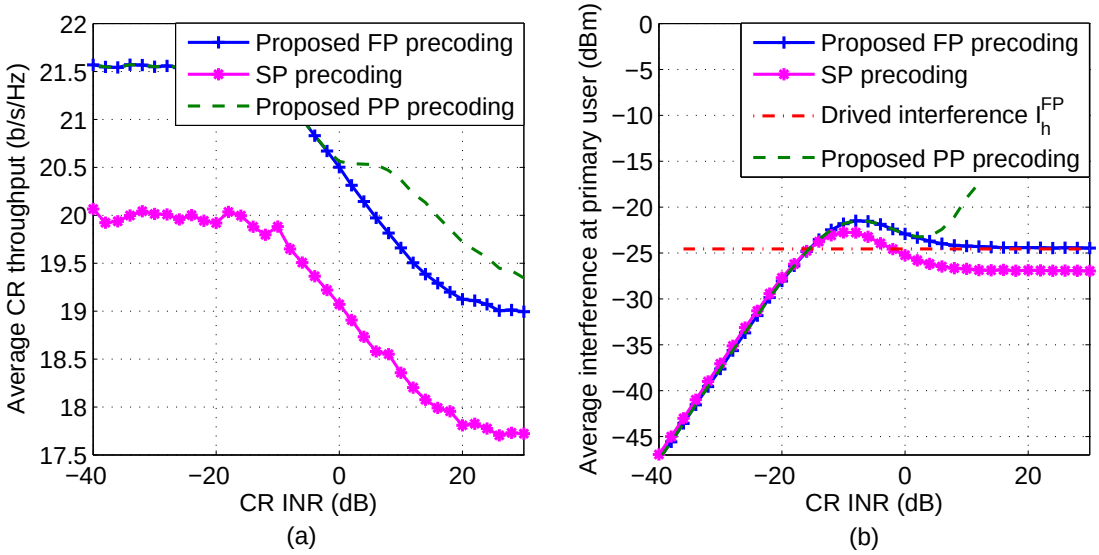

FIGURE 4.4: (a) CR throughput and (b) resulting interference of different precoding schemes ($M_t = M_r = 4$, $M_{\text{bs}} = 2$, $K = 2$, $M_1 = M_2 = 1$,, $L_S = 100$, $L_{S1} = L_{S2} = L_{T2} = 50$, $L_{T1} = 350$, $\sigma_H^2 = 1$, $P_{cr} = 1$, $r_{t/d} = 0.1$, and $\sigma_n^2 = 10^{-4}$).

the SP precoding is longer than the uplink sensing of the FP precoding. Moreover, at high INRs the interference of the proposed PP precoding is linearly proportional to the CR INR, which supports our analysis in Section 4.3.4.2.

4.4 Cross-Layer Interference Mitigation for CR MIMO Networks

The IM for CR MIMO systems has been investigated in Section 4.3 by proposing two precoding schemes in physical layer. In this section, we approach the IM for CR MIMO networks from a cross-layer perspective.

4.4.1 Related Work

Transmit precoding [62–64] is an effective IM approach to proactively mitigate CR-primary interference for CR MIMO systems. The precoding in [62–64] assumes that

the channel information between CR and primary networks is known. But, this information is not always available to the CR network. This problem was tackled in [66, 67, 77] by employing subspace technology to estimate the CR-primary channel information before precoding. In [66] and [67], precoding schemes were proposed with the application of the MUSIC technique to estimate the CR-primary channel information. However, the interference from the primary network was simply ignored in these two works during the CR precoding, which leads to CR throughput loss. In [77], an improved precoding scheme was proposed by estimating the interference from the primary to the CR networks and taking it into account for the CR precoding. Therefore, the throughput of the CR network was boosted.

The aforementioned precoding techniques are prominent examples of IM techniques in the physical layer. When multiple CR nodes share the spectrum with the primary network, channel allocation of the CR network opens another door to the CR-primary IM. Channel allocation has been extensively studied especially for cellular networks [78]. For CR networks, two adaptive channel allocation schemes were presented in [79] based on a game theoretic framework. Therefore, it is desirable to jointly consider the channel allocation in the MAC layer and precoding in the physical layer to mitigate interference from CR to primary network. This idea has already been applied to ad hoc networks in [80] and [81], where a joint iterative channel allocation and beamforming algorithm was proposed for interference avoidance. To the best of the authors' knowledge, no research attempt has been made to mitigate interference from CR to primary networks from this perspective.

In this section, we propose two distributed cross-layer algorithms for CR MIMO systems to minimise the CR-primary interference and maximise the throughput of the CR network. Channel allocation in the MAC layer and a sensing and projection-based precoding scheme presented in [77] in the physical layer are jointly designed in our work. For the case when channel information among CR nodes is available, we present an iterative algorithm to update the channel allocation and precoding matrices iteratively for all CR transmitters to balance between the CR-primary interference and CR throughput. Alternatively, when the channel information among CR nodes

is unknown, a non-iterative algorithm together with a channel estimation scheme are proposed to perform the joint channel allocation and precoding.

The remainder of this section is organised as follows. The system model and problem formulation are given in Section 4.4.2. The cross-layer interference mitigation algorithms are presented in Section 4.4.3. The performance of the proposed cross-layer schemes are evaluated via simulations in Section 4.4.4.

4.4.2 System Model and Problem Formulation

The system model is demonstrated in FIGURE 4.5. Consider K pairs of CR MIMO transmitter and receiver coexisting with a primary TDD system. Each primary and CR node is equipped with M_p and M_c antennas, respectively. The primary system operates over N sub-channels $\{f_1, f_2, \cdots, f_N\}$. Each CR pair resides in one of the N sub-channels. The channel allocation for all active CR transmitters is denoted as $\mathscr{A} = \{A_1, A_2, \cdots, A_K\}$, where $A_k \in \{f_1, f_2, \cdots, f_N\}, k = 1, 2, \cdots, K$.

Block fading channels are assumed for the primary and CR systems. In FIGURE 4.5, $\mathbf{H}_{i,j,A_i}$ stands for the channel matrix from the ith CR transmitter to the jth CR receiver over sub-channel A_i $(i, j = 1, 2, \cdots, K)$. We assume $\mathbf{H}_{i,j,A_i} \sim \mathcal{CN}(0, \sigma^2_{\mathrm{H},i,j,A_i})$, which means that its elements are i.i.d. circular symmetric complex Gaussian random variables with zero mean and covariance $\sigma^2_{\mathrm{H},i,j,A_i}$. Here, $\mathbf{G}_{U,i,A_i} \sim \mathcal{CN}(0, \sigma^2_{\mathrm{U},i,A_i})$ and $\mathbf{G}_{D,j,A_j} \sim \mathcal{CN}(0, \sigma^2_{\mathrm{D},j,A_j})$ $(i, j = 1, 2, \cdots, K)$ represent the interference channel matrices from the primary user to the ith CR transmitter during uplink and from the primary BS to the jth CR receiver during downlink, respectively. Thus, the channel matrix from the ith CR transmitter to the primary user is $\mathbf{G}^H_{U,i,A_i}$ due to uplink/-downlink reciprocity. These channels are quasi-static over a block of L symbols. The channel between each CR pair $\mathbf{H}_{i,i,A_i}$ $(i = 1, 2, \cdots, K)$ is assumed to be known to CR transmitters, but the channels between the primary and CR networks ($\mathbf{G}_{U,i,A_i}$ and $\mathbf{G}_{D,j,A_j}$) are unknown. The source information vector to transmit for the ith CR transmitter is denoted as $\mathbf{s}_i$ $(i = 1, 2, \cdots, K)$ and $\mathbb{E}[\mathbf{s}_i \mathbf{s}_i^H] = \mathbf{I}$ is assumed. The transmitted signal vectors for the primary uplink and downlink are denoted as $\mathbf{x}_u$ and

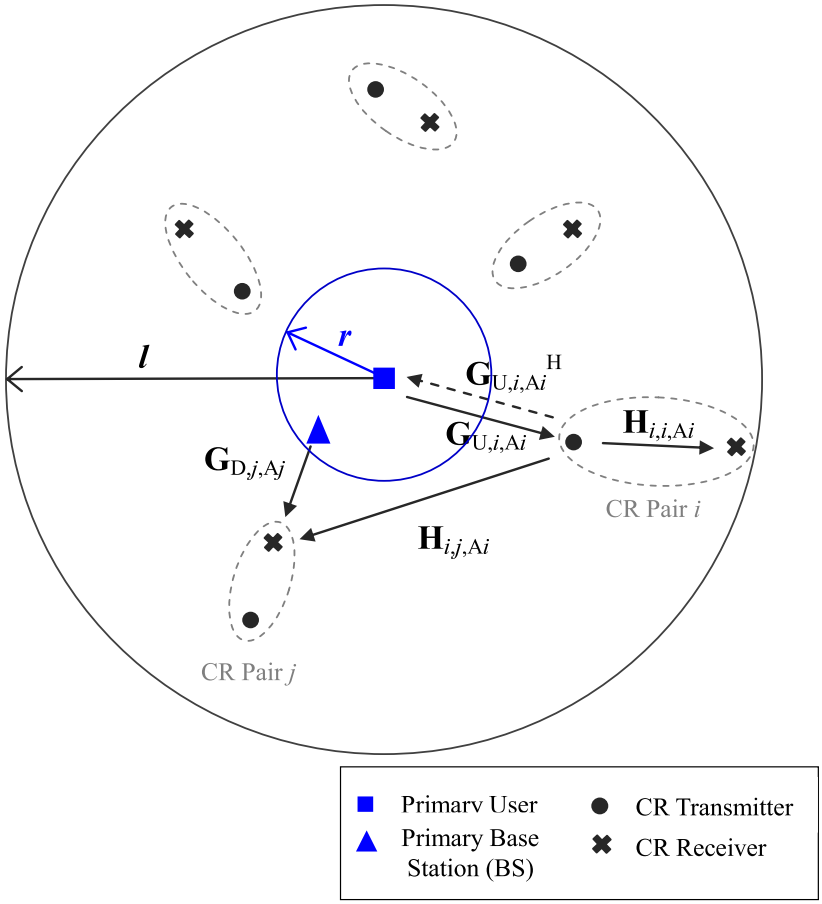

FIGURE 4.5: System model for multiple CR pairs coexisting with a primary system.

$\mathbf{x}_d$, with their transmit covariance matrices being $\mathbf{Q}_u \triangleq \mathbb{E}[\mathbf{x}_u \mathbf{x}_u^H]$ and $\mathbf{Q}_d \triangleq \mathbb{E}[\mathbf{x}_d \mathbf{x}_d^H]$, respectively.

4.4.2.1 Precoding in the Physical Layer

A FP-based precoding proposed in [77] is applied to the CR network to proactively mitigate the cochannel CR-primary interference. The system diagram of the FP precoding is shown in FIGURE 4.2. It is capable of estimating the CR-primary interference channel and projecting the CR transmission into the null space of the CR-primary interference channel. Therefore, the resulting CR-primary interference is minimised.

We denote the precoding strategy for all CR transmitters during downlink as $\mathscr{F} = (\mathbf{F}_{1,A_1}, \mathbf{F}_{2,A_2}, \cdots, \mathbf{F}_{K,A_K})$. The precoding matrix $\mathbf{F}_{i,A_i}$ for the ith CR transmitter

at the sub-channel A_i ($i = 1, 2, \cdots, K,\ \forall A_i \in \{f_1, f_2, \cdots, f_N\}$) during the primary downlink can be written as [77]

$$\mathbf{F}_{i,A_i} = \mathbf{U}_i \left[(\mu \mathbf{I} - \mathbf{\Lambda}_i^{-1})^+\right]^{\frac{1}{2}} \tag{4.27}$$

where $(\cdot)^+ = \mathtt{max}(0, \cdot)$ and μ denotes the water level for the water-filling algorithm. Given the transmission power of each CR transmitter P_{cr}, we have $\mathtt{tr}[(\mu \mathbf{I} - \mathbf{\Lambda}_i^{-1})^+] = P_{cr}$. $\mathbf{U}_i$ and $\mathbf{\Lambda}_i$ are obtained through the following EVD

$$\begin{aligned}\mathbf{U}_i \mathbf{\Lambda}_i \mathbf{U}_i^H =& (\mathbf{I} - \mathbf{U}_{G,i,A_i} \mathbf{U}_{G,i,A_i}^H)^H \mathbf{H}_{i,i,A_i}^H \mathbf{R}_{\mathrm{dr},i,A_i}^{-1} \\ & \times \mathbf{H}_{i,i,A_i} (\mathbf{I} - \mathbf{U}_{G,i,A_i} \mathbf{U}_{G,i,A_i}^H)\end{aligned} \tag{4.28}$$

where $\mathbf{U}_{G,i,A_i}$ is the matrix spanning the space of the interference channel from the ith CR transmitter to the primary user at sub-channel A_i. It is estimated via sensing at the ith CR transmitter during primary uplink. The estimation can be expressed as

$$\mathbf{R}_{\mathrm{ut},i,A_i} = \frac{1}{L_{s1}} \sum_{t=1}^{L_{s1}} \mathbf{r}_{\mathrm{ut},i,A_i}(t) \mathbf{r}_{\mathrm{ut},i,A_i}^H(t) \tag{4.29}$$

$$= \hat{\mathbf{U}}_i \hat{\mathbf{\Lambda}}_i \hat{\mathbf{U}}_i^H \tag{4.30}$$

$$= \mathbf{U}_{G,i,A_i} \mathbf{\Lambda}_{G,i,A_i} \mathbf{U}_{G,i,A_i}^H + \mathbf{U}_{n,i,A_i} \mathbf{\Lambda}_{n,i,A_i} \mathbf{U}_{n,i,A_i}^H \tag{4.31}$$

where $\mathbf{R}_{\mathrm{ut},i,A_i}$ denotes the average covariance matrix of the received symbols at the ith CR transmitter over sub-channel A_i during primary uplink, $\mathbf{r}_{\mathrm{ut},i,A_i}(t) = \mathbf{G}_{U,i,A_i} \mathbf{x}_u(t) + \mathbf{n}(t)$ is the tth received symbol at the ith CR transmitter with $\mathbf{n}(t) \sim \mathcal{CN}(\mathbf{0}, \sigma_n^2 \mathbf{I})$ being the AWGN vector. EVD is then performed on $\mathbf{R}_{\mathrm{ut},i,A_i}$ in (4.30) with $\hat{\mathbf{\Lambda}}_i = \mathtt{diag}(\lambda_1, \lambda_2, \cdots, \lambda_{M_c})$. $\mathbf{U}_{G,i,A_i}$ is obtained by further decomposing (4.30) into interference and noise components as shown in (4.31) where the diagonal matrix $\mathbf{\Lambda}_{G,i,A_i}$ consists of the M_p largest eigenvalues of $\mathbf{R}_{\mathrm{ut},i,A_i}$ and $\mathbf{U}_{G,i,A_i}$ is the corresponding eigenvectors.

Another component that needs to be estimated in (4.28) is $\mathbf{R}_{\mathrm{dr},i,A_i}$ ($i = 1, 2, \cdots, K$) the covariance matrix of the received signal at the ith CR receiver during primary

downlink over sub-channel A_i . Given a channel allocation $\mathscr{A}$, it can be written as

$$\mathbf{R}_{\mathrm{dr},i,A_i} = \sum_{\forall k: A_k = A_i, k \neq i} \mathbf{H}_{k,i,A_i} \mathbf{F}_{k,A_i} \mathbf{F}_{k,A_i}^H \mathbf{H}_{k,i,A_i}^H + \mathbf{Z}_{i,A_i} \tag{4.32}$$

where

$$\mathbf{Z}_{i,A_i} = \mathbf{G}_{D,i,A_i} \mathbf{Q}_d \mathbf{G}_{D,i,A_i}^H + \sigma_n^2 \mathbf{I}, \ \forall i, \forall A_i \in \{f_1, f_2, \cdots, f_N\}. \tag{4.33}$$

It can be seen from (4.32) and (4.33) that $\mathbf{R}_{\mathrm{dr},i,A_i}$ at the ith CR receiver consists of three components. The first component of the right hand side of (4.32) is the interference from cochannel CR transmitters to the ith CR receiver (cochannel CR-CR interference). While, the interference from the primary BS and the noise constitute the second and third components, respectively. Given $\mathscr{A}$ and $\mathscr{F}$, the cochannel CR-CR interference can be evaluated at each CR receiver. $\mathbf{Z}_{i,A_i}$ is estimated at the ith CR receiver during downlink sensing via a step similar to (4.29).

4.4.2.2 Channel Allocation in the MAC Layer

Besides the aforementioned precoding-based interference mitigation scheme in the physical layer, the CR-primary interference can also be managed by carefully selecting the operation channel for each CR node. Therefore, we jointly consider channel allocation in the MAC layer and the FP-based precoding in the physical layer for the CR network to minimise the CR-primary interference and maximise the CR throughput. It can be formulated as the following multiple criteria optimisation (MCO) problem

$$\min_{\mathscr{A},\ \mathscr{F}} \mathrm{Int}_i, \quad i = 1, 2, \cdots, K \tag{4.34}$$

$$\max_{\mathscr{A},\ \mathscr{F}} \mathrm{I}_i, \quad i = 1, 2, \cdots, K \tag{4.35}$$

$$\text{subject to} \ \ \mathtt{tr}[\mathbf{F}_{i,A_i} \mathbf{F}_{i,A_i}^H] \leq P_{cr}, \quad i = 1, 2, \cdots, K \tag{4.36}$$

$$A_i \in \{f_1, f_2, \cdots, f_N\}, \quad i = 1, 2, \cdots, K \tag{4.37}$$

where Int_i and I_i are the average interference caused by the ith CR transmitter to the primary user and the mutual information of the ith CR link during primary downlink,

respectively. They are given by

$$\mathrm{Int}_i = \mathbf{G}_{U,i,A_i}^H \mathbf{F}_{i,A_i} \mathbf{F}_{i,A_i}^H \mathbf{G}_{U,i,A_i} \tag{4.38}$$

$$\mathrm{I}_i = \log_2 \det \left(\mathbf{I} + \frac{\mathbf{H}_{i,i,A_i} \mathbf{F}_{i,A_i} \mathbf{F}_{i,A_i}^H \mathbf{H}_{i,i,A_i}^H}{\mathbf{R}_{\mathrm{dr},i,A_i}} \right). \tag{4.39}$$

In this section, we focus on the joint channel allocation and precoding for CR transmission during the primary downlink. A similar problem for the primary uplink can be formulated by following the similar procedure of the downlink counterpart. However, it is ignored here for brevity.

4.4.3 Joint Channel Allocation and Precoding

Scalarisation of multiple objectives is one of the most commonly used approaches [82] for solving MCO problems. The MCO problem (4.34)–(4.37) can be scalarised into a single objective optimisation problem as follows

$$\min_{\mathscr{A},\ \mathscr{F}} \sum_{i=1}^{K} \mathrm{obj}_i = \sum_{i=1}^{K} \left[\eta \left(\mathrm{Int}_i \right) - \gamma \left(\mathrm{I}_i \right) \right] \tag{4.40}$$

$$\text{subject to } \ \mathtt{tr}[\mathbf{F}_{i,A_i} \mathbf{F}_{i,A_i}^H] \leq P_{cr}, \quad i = 1, 2, \cdots, K \tag{4.41}$$

$$A_i \in \{f_1, f_2, \cdots, f_N\}, \quad i = 1, 2, \cdots, K \tag{4.42}$$

where $\eta(\cdot)$ and $\gamma(\cdot)$ are continuous and monotonically increasing functions. When $\eta(\cdot)$ is convex and $\gamma(\cdot)$ is concave, the problem (4.40)–(4.42) can be transformed into a convex optimisation problem by ignoring the cochannel CR-CR interference when computing the CR throughput I_i in (4.39)[83]. Then, dual optimisation can be employed to solve the convex optimisation problem as in [84].

The cochannel CR-CR interference is not always negligible for the FP-based precoding especially when CR pairs are distributed closely to each other. Moreover, the above optimisation problem requires to be solved in a centralised manner, which is not desirable for CR networks. Next, we propose two distributed cross-layer algorithms

for solving the optimisation problem (4.40)–(4.42) without ignoring the cochannel CR-CR interference.

4.4.3.1 Known CR-CR interference channels

We first propose a joint iterative channel allocation and precoding (JICAP) algorithm when CR-CR interference channels are known to all CR pairs. The proposed JICAP algorithm is depicted in TABLE 4.2. It works in the following manner. Firstly, all the CR pairs carry out sensing at all sub-channels as depicted in FIGURE 4.2. During the primary uplink, $\mathbf{U}_{G,i,A_i}$ is estimated at each CR transmitter from (4.29)–(4.31) over all sub-channels. Each CR receiver estimates $\mathbf{Z}_{i,A_i}$ over all sub-channels during the downlink sensing. Secondly, each CR transmitter obtains the initial precoding matrices from (4.27) and (4.28) for all sub-channels by ignoring the cochannel CR-CR

TABLE 4.2: The JICAP algorithm.

1. Estimate $\mathbf{U}_{G,i,A_i}$ and $\mathbf{Z}_{i,A_i}$ $(\forall i,\ \forall A_i \in \{f_1, f_2, \cdots, f_N\})$
   during uplink and downlink sensing at each CR pair.
2. Obtain initial precoding matrices $\mathbf{F}_{i,A_i}$ by ignoring cochannel
   CR-CR interference for each CR transmitter $(\forall i,\ \forall A_i \in \{f_1, f_2, \cdots, f_N\})$.
3. Start the following iteration
   For $t = 1, 2, \cdots$
      For $i = 1, 2, \cdots, K$
         Select $A_i(t)$ to minimise the obj_i in (4.40).
      Next i
      Update $\mathscr{A} \leftarrow \{A_1(t), A_2(t), \cdots, A_K(t)\}$.

      For $i = 1, 2, \cdots, K$
         Update $\mathbf{R}_{\text{dr},i,A_i}$ according to $\mathscr{A}$.
         Obtain $\mathbf{F}_{i,A_i}(t)$ from (4.27)–(4.33).
      Next i
      Update $\mathscr{F} \leftarrow \{\mathbf{F}_{1,A_1}(t), \mathbf{F}_{2,A_2}(t), \cdots, \mathbf{F}_{K,A_K}(t)\}$.

      Terminate when the channel allocation $\mathscr{A}$ converges or when reaching
      a certain iteration number.
   Next t

interference. Finally, the channel allocation and precoding are performed iteratively. In each iteration, $\mathscr{A}$ is first updated by selecting a sub-channel minimising the objective function obj_i for each CR transmitter. With the updated $\mathscr{A}$, the interference from cochannel CR transmitters is evaluated and the covariance matrix of the received signal $\mathbf{R}_{\text{dr},i,A_i}$ is updated accordingly at each CR receiver. Then, the precoding matrix for each CR transmitter is updated from (4.27) and (4.28). The iteration terminates when the channel allocation $\mathscr{A}$ converges or when reaching a certain iteration number.

The criterion to select a sub-channel for the ith CR pair is to minimise the objective function obj_i in (4.40). Therefore, evaluating the average interference from the ith CR transmitter to the primary user Int_i is indispensable for the channel allocation. However, it is impossible to obtain Int_i directly from (4.38), since the CR-primary channel $\mathbf{G}_{U,i,A_i}^H$ is unknown. The relationship of the average CR-primary interference Int_i with the CR-primary interference channel gain $\sigma_{\text{U},i,A_i}^2$ and noise power σ_n^2 has been given in [77]. As shown in FIGURE 4.6, it is found that Int_i is proportional to $\sigma_{\text{U},i,A_i}^2$ at low CR interference-to-noise ratios (INRs$\triangleq \sigma_{\text{U},i,A_i}^2/\sigma_n^2$). While, in the large INR regime, the average interference can be written as [77]

$$\text{Int}_i = \frac{\sigma_n^2 P_{cr}}{L_{S1}} \texttt{tr}[\mathbf{Q}_u] \tag{4.43}$$

where the noise power σ_n^2 can be estimated from (4.30) using

$$\sigma_n^2 = \frac{\sum_{i=M_p+1}^{M_c} \lambda_i}{M_c - M_p}. \tag{4.44}$$

Similarly, the channel gain from the kth CR transmitter to the primary user $\sigma_{\text{U},i,A_i}^2$ can be estimated from (4.30) via

$$\sigma_{\text{U},i,A_i}^2 = \frac{\sum_{i=1}^{M_p} \lambda_i}{M_p}. \tag{4.45}$$

With these two estimations, the average CR-primary interference Int_i can be evaluated by using the results in [77]. Consequently, the channel allocation can be carried out without priori knowledge of $\mathbf{G}_{U,i,A_i}^H$.

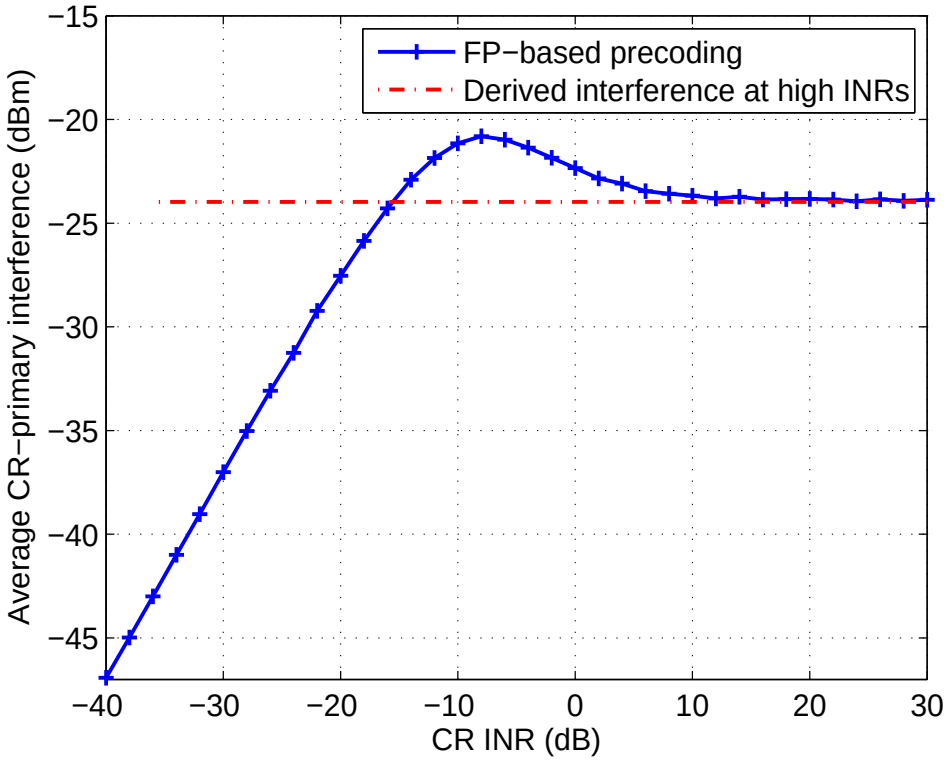

FIGURE 4.6: Relationship between CR INR and the average CR-primary interference ($M_p = 2$, $M_c = 4$, $K = 1$, $L_{S1} = L_{S2} = 50$, $\sigma_H^2 = 1$, $P_{cr} = 1$ Unit, and $\sigma_n^2 = 10^{-4}$).

It can be seen from the proposed JICAP algorithm that there exist two types of interaction across the MAC and physical layers. On one hand, the channel allocation $\mathscr{A}$ from the MAC layer is passed down to the physical layer to update the precoding matrices. On the other hand, the precoding strategy $\mathscr{F}$ from the physical layer is fed up to the MAC layer to evaluate the objective function obj_i for channel selection.

4.4.3.2 Unknown CR-CR interference channels

To facilitate the proposed JICAP algorithm in Section 4.4.3.1, it is obvious that the precoding matrices $\mathbf{F}_{i,A_i}$ together with the associated CR-CR interference channel $\mathbf{H}_{i,j,A_i}$ are needed by the jth CR pair ($i, j = 1, 2, \cdots, K,\ \forall i \neq j$) for both channel allocation and precoding. Hereafter, we name them as effective CR-CR interference channels $\mathbf{H}_{i,j,A_i}\mathbf{F}_{i,A_i}$. However, these information is not always available to the CR

network. Various estimation techniques can be employed to perform channel estimation [85], but it incurs much communication overhead for the proposed JICAP algorithm due to the iterative nature. In this subsection, we apply a novel channel estimation approach to the cross-layer interference mitigation and propose a non-iterative channel allocation and precoding (NICAP) algorithm for the CR MIMO system.

The NICAP works in the same way as the JICAP for the first two steps as shown in Table 4.2. After that, each CR transmitter obtains the initial precoding matrices for all sub-channels without taking into account the cochannel CR-CR interference. Each CR pair then selects an initial sub-channel minimising the objective function obj_i by ignoring the cochannel CR-CR interference. Next, the effective CR-CR interference channels $\mathbf{H}_{i,j,A_i}\mathbf{F}_{i,A_i}$ are estimated by each CR pair using the method below. Finally, the ultimate channel allocation and precoding strategy is determined for CR spectrum sharing.

The effective CR-CR interference channels are estimated in the following way. After the initial channel allocation, CR pairs can be divided into N groups according to their operating sub-channels. Each group consists of CR pairs operating at the same sub-channel, i.e., $S_n = \{i\text{th CR pair}|A_i = f_n,\ i = 1, 2, \cdots, K\}$ $(n = 1, 2, \cdots, N)$. For CR pairs within the same group, they work in the time division multiplexing (TDM) manner. All N CR groups are transmitting simultaneously in this phase. During the transmission of a CR transmitter, all the rest CR receivers in the entire CR network are sensing and estimating the average covariance matrix of the received signal. Suppose that each CR pair is allocated a time slot with duration of L_s symbols. The tth $(t = 1, 2, \cdots, L_s)$ received signal at the jth CR receiver during the time slot of the ith CR pair $(j = 1, 2, \cdots, K, \forall j \neq i)$ is

$$\mathbf{r}_{i,j,A_i}(t) = \mathbf{H}_{i,j,A_i}\mathbf{F}_{i,A_i}\mathbf{s}_i(t) + \mathbf{G}_{D,j,A_i}\mathbf{x}_d(t) + \mathbf{n}(t). \tag{4.46}$$

It can be seen from (4.46) that the received signal consists of three components: the cochannel interference from the ith CR transmitter, the interference from the primary BS during downlink and the AWGN $\mathbf{n}$. Then the average covariance matrix of the

received signal at the jth CR receiver during the ith CR transmission can be expressed as

$$\begin{aligned}\mathbf{R}_{i,j,A_i} &= \sum_{t=1}^{L_s} \mathbf{r}_{i,j,A_i}(t)\mathbf{r}_{i,j,A_i}(t)^H \\ &\overset{(a)}{=} \mathbf{H}_{i,j,A_i}\mathbf{F}_i\mathbf{F}_i^H\mathbf{H}_{i,j,A_i}^H + \mathbf{G}_{D,j,A_i}\mathbf{Q}_d\mathbf{G}_{D,j,A_i}^H + \sigma_n^2\mathbf{I} \\ &\overset{(b)}{=} \mathbf{H}_{i,j,A_i}\mathbf{F}_i\mathbf{F}_i^H\mathbf{H}_{i,j,A_i}^H + \mathbf{Z}_{j,A_i} \end{aligned} \tag{4.47}$$

where in (4.47), (a) is due to the fact that $\mathbb{E}[\mathbf{s}_i\mathbf{s}_i^H] = \mathbf{I}$ and $\mathbb{E}[\mathbf{x}_d\mathbf{x}_d^H] = \mathbf{Q}_d$; substituting (4.33) into (a) yields (b). Therefore, the covariance matrix of the effective CR-CR interference channel from the ith CR transmitter to the jth CR receiver at sub-channel A_i can be expressed as

$$\mathbf{H}_{i,j,A_i}\mathbf{F}_{i,A_i}\mathbf{F}_{i,A_i}^H\mathbf{H}_{i,j,A_i}^H = \mathbf{R}_{i,j,A_i} - \mathbf{Z}_{j,A_i}. \tag{4.48}$$

The above equation suggests that the covariance matrices of the effective CR-CR interference channels needed by the channel allocation and precoding can be obtained via the effective CR-CR channel estimation mentioned above and the primary downlink sensing. It is easy to understand that the average duration for the effective CR-CR interference channel estimation phase is KL_s/N. Moreover, the NICAP algorithm works in a non-iterative manner and the effective CR-CR interference channels are only estimated for one time. Therefore, the cross-layer communication overhead is significantly reduced compared to that of the JICAP.

It is worth noting that compared to non-cross-layer interference mitigation schemes both of the proposed cross-layer approaches are performed at the expense of increased complexity due to the cross-layer consideration. In general, the complexity involved in each proposed approach increases with the increase of CR number. Moreover, the complexity increase of the JICAP algorithm is more obvious than that of the NICAP due to its iterative nature.

4.4.4 Simulation Results

The performance of the proposed JICAP and NICAP algorithms is evaluated via simulations in this section. In our simulations, we consider that $K = 10$ pairs of CR links coexist with a primary system. The primary network operates over $N = 3$ sub-channels. Each primary and CR node is equipped with $M_p = 2$ and $M_c = 4$ antennas, respectively. The primary user locates at the origin of a 2-dimensional plane. As demonstrated in FIGURE 4.5, the primary BS and all the CR pairs are uniformly distributed around the primary user with radii $r = 10$m and $l = 100$m, respectively. Rayleigh fading channels are assumed for the primary and the CR systems. The CR transmission power and the noise power are set as $P_{cr} = 1$ and $\sigma_n^2 = 10^{-4}$. The uplink and downlink sensing for the FP-based precoding both last for 25 symbols. The time slot for each CR pair during the effective CR-CR channel estimation is also set to 25 symbols, i.e., $L_{s1} = L_{s2} = L_s = 25$. The objective function for the JICAP algorithm is designed as $\text{obj}_i = 3 \times 10^5 \text{Int}_i - \text{I}_i$.

With this setup, both the CR sum rate (mutual information) and the overall average resulting interference perceived at the primary user are examined for the two proposed algorithms in FIGURE 4.7. Each point in our simulations is obtained by averaging over 2000 simulation runs. The performance of these two proposed algorithms is compared with that of another two schemes: non-cross-layer and minimum interference approaches. For the former approach, a random channel allocation is performed and then used throughout the whole CR transmission phase. Its channel allocation and precoding are performed separately and no interaction exists between the physical and the MAC layers. Hence, it is termed as the non-cross-layer approach. While, for the latter the channel allocation in each iteration aims at minimising the resulting CR-primary interference, i.e., the second criteria (4.35) for the MCO problem is ignored.

It can be seen from FIGURE 4.7 that compared to the non-cross-layer approach, the proposed JICAP and NICAP algorithms reduce the CR-primary interference and boost the CR throughput at the same time. Therefore, the cross-layer schemes outperform the non-cross-layer counterpart. The minimum interference approach can

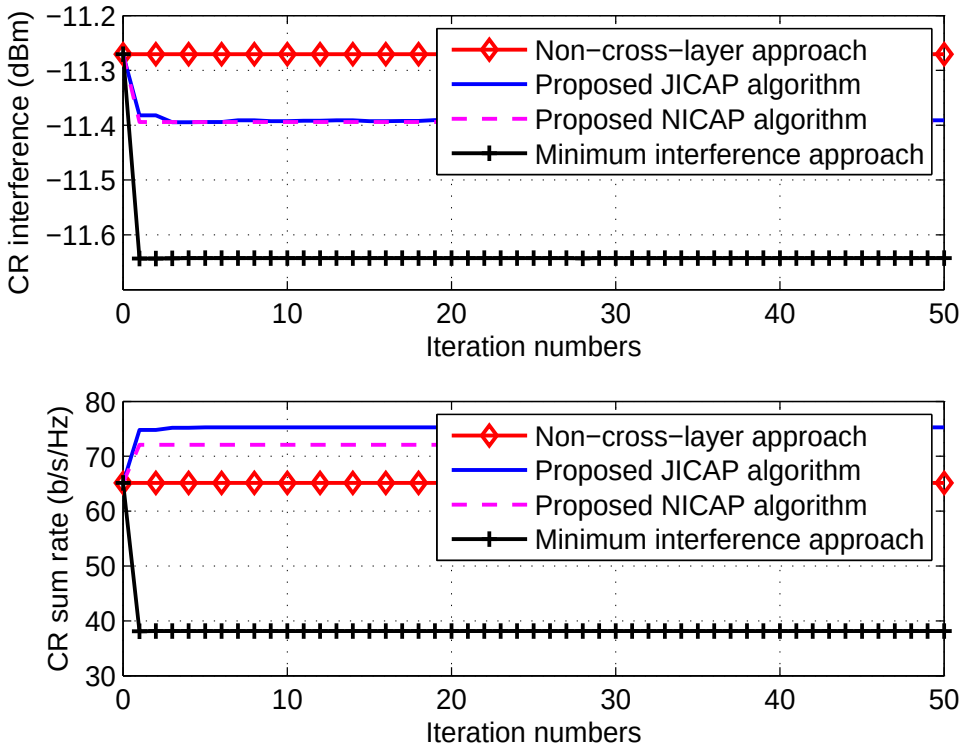

FIGURE 4.7: Performance evaluation of the proposed cross-layer algorithms ($r = 10$m, $l = 100$m, $K = 10$, $N = 3$, $M_p = 2$, $M_c = 4$, $L_{s1} = L_{s2} = L_s = 25$, $P_{cr} = 1$, and $\sigma_n^2 = 10^{-4}$).

further reduce the CR-primary interference by compromising the CR throughput. This suggests that the proposed cross-layer algorithms can effectively balance the interference minimisation and the CR throughput maximisation. Furthermore, it can also been seen from FIGURE 4.7 that the NICAP algorithm together with the proposed estimation scheme for the effective CR-CR interference channels leads to similar performance to that of the JICAP with known CR-CR interference channels.

Finally, the convergence of the proposed JICAP algorithm is evaluated in FIGURE 4.8 for one realisation of the primary and CR systems. We use the same setup as that of FIGURE 4.7. As we can see from FIGURE 4.8, the channel allocation for all 10 CR pairs converges rapidly. Meanwhile, the CR sum rate converges right after the convergence of the channel allocation. This is due to the fact that after the channel allocation is fixed the FP-based precoding does not take long to reach the Nash equilibrium - a

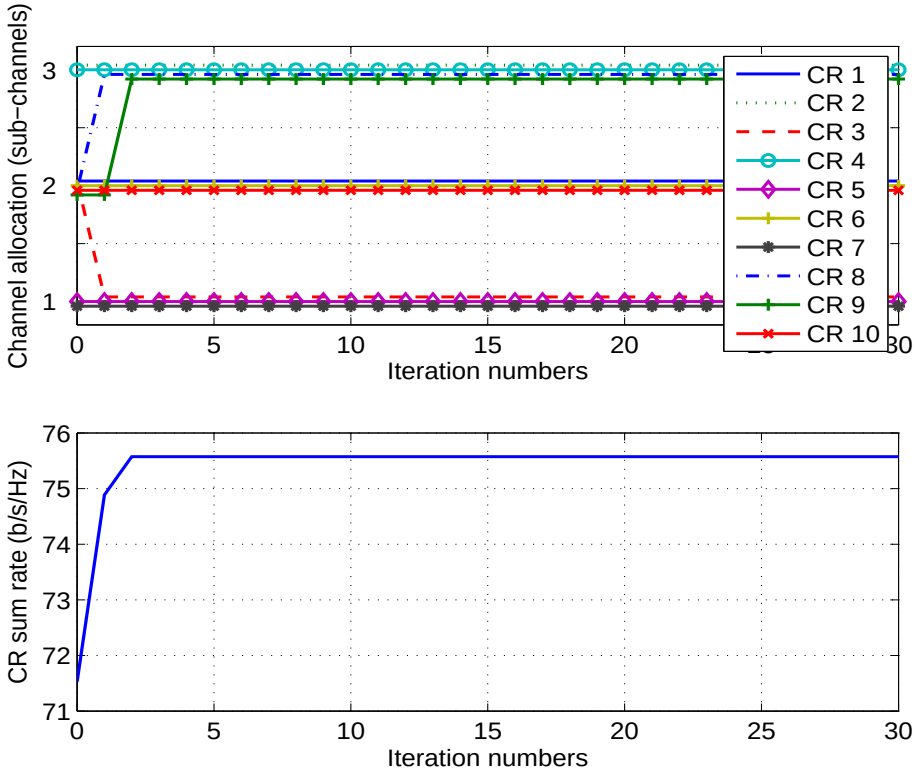

FIGURE 4.8: Convergence of the proposed JICAP algorithm ($r = 10$m, $l = 100$m, $K = 10$, $N = 3$, $M_p = 2$, $M_c = 4$, $L_{s1} = L_{s2} = L_s = 25$, $P_{cr} = 1$, and $\sigma_n^2 = 10^{-4}$).

stable state where no CR links can improve their throughput by unilaterally changing their own precoding matrices.

4.5 Chapter Summary

CR networks could lead to complex and sophisticated interference scenarios. This has inspired our investigation on applying IM techniques to CR networks with a special focus on mitigating the inter-network interference. Various IA techniques have been found to be useful for CR transmitters to rigidly control their emission patterns and thereby mitigate the CR-primary interference.

Then, we confine our attention to the mitigation of CR-primary interference for CR MIMO systems. Two SP precoding-based schemes, namely, FP and PP precoding,

have been proposed for CR MIMO systems to mitigate their interference to the primary network and improve the CR throughput. These two precoding schemes are capable of estimating the CSI of interference channels between primary and CR networks and can account for the interference from the primary system via a novel sensing approach. Therefore, no extra signalling is required between primary and CR systems, which consequently eases the deployment of CR networks. The performance of the proposed precoding schemes has been evaluated and compared with that of the existing precoding approaches. It has been demonstrated that the FP precoding can boost the CR throughput and does not introduce extra interference to the primary system in the low INR regime. The PP precoding can further improve the CR throughput if the primary system can tolerate some extra interference.

Finally, the mitigation of CR-primary interference has been investigated from a cross-layer perspective for CR MIMO systems. A distributed iterative channel allocation and precoding algorithm has been proposed to minimise the CR-primary interference and maximise the CR throughput when interference channels among CR nodes are available. While, for the scenario with unknown CR-CR interference channel information, we have proposed a non-iterative cross-layer algorithm together with an estimation scheme for effective CR-CR interference channels. Simulation results have demonstrated that (i) both of the proposed cross-layer algorithms outperform the non-cross-layer approach in terms of the resulting CR-primary interference and the CR throughput; (ii) the non-iterative algorithm achieves similar performance to the iterative counterpart without incurring much communication overhead.

So far, the CR-primary interference has been investigated from two aspects: interference modelling in Chapter 3 and interference mitigation in Chapter 4. Both of them give insights into CR deployment aiming at reducing the CR-primary interference. In the next chapter, we shift our attention to the study of the other type of interference originating from CR networks, i.e., CR-CR interference.

Chapter 5

Interference Channel Analysis for Spectrum-Sharing Cognitive Radio Networks

5.1 Introduction

Besides the CR-primary interference investigated in Chapters 3 and 4, the other type of interference from CR networks, CR-CR interference, is also worth studying. In this chapter, we analyse the CR-CR interference channel for spectrum-sharing CR nodes when they interfere with each other. We model the rate control in interference systems as an MCO problem, analyse the interference channel by characterising its resulting Pareto rate region and apply game theory to coordinate the interfering users and solve the MCO problem. The results presented in this chapter are primarily related to the spectrum-sharing CR networks as we look for the increase of spectrum utilisation. They are also valid for the long-standing interference channel analysis of other spectrum sharing networks. The underlying CR-CR interference channel can be easily generalised into a general interference channel regardless the working mode of the CR network. For interference-free CR networks, the CR-CR interference channel does not differ from other interference channels apart from the spectrum sensing

prior to the spectrum exploiting. As for interference-tolerant CR networks, the SP precoding schemes delineated in Chapter 4 can be employed by CR MIMO systems. Then, the effective CR-CR interference channels become the projection of CR-CR channels into the null space of the associated CR-primary channels. To this end, we perform the analysis for generalised MIMO interference channels, whose results apply to CR interference systems as well.

We start this chapter by giving some introduction on MCO. The MCO, which is featured by the need to simultaneously optimise multiple noncommensurable or even incompatible objectives, has been widely used in automatic control, telecommunications, economics, and many other fields of engineering and science [86]. An MCO problem usually admits infinite number of *noninferior solutions*, which form a *Pareto boundary* and encompass a *Pareto region* [87]. A noninferior solution in the Pareto boundary is considered to be *Pareto optimal* in the sense that no other solution can improve the performance of some objectives without deteriorating other objective(s). The characteristics of the Pareto region are of particular interest in terms of shedding light on solving the corresponding MCO problem.

Two main processes are involved in solving the MCO problem, namely, computing and decision making [82]. In the former process, a set of noninferior solutions for the MCO problem is obtained, while, in the latter one, a final solution among the noninferior solutions is determined according to certain preferences of the system. Depending on the principle according to which these two processes interact with each other in searching for a compromise solution, the MCO problem can be solved using one of the following three approaches [82]: *priori*, *posteriori* and *progressive* articulation of preferences. As the name suggests, the decision maker expresses its preferences prior to the computing process in the first approach. These preferences are often given in the form of an utility function aggregating all objectives. As for the posteriori case, the preferences of the decision maker are not known before computing. Thus, all the noninferior solutions for the MCO problem should be found before decision making. Unlike the first two approaches, for the progressive articulation of preferences, computing and decision making are performed in an alternating manner.

In each iteration, a population of noninferior solutions is maintained during computing process; then, the decision maker chooses several suitable compromise solutions for the computing process in next iteration to produce a new generation of noninferior solutions. After rounds of iterations, the final solution is obtained. Evolutionary algorithms are usually employed in this approach [88].

Among the three aforementioned approaches for solving the MCO problem, the priori articulation of preferences is most commonly used due to its simplicity and effectiveness. It can be further broken down into three broad classes of methods: *scalarisation of multiple objectives* - the MCO problem is transformed into a single-objective optimisation problem by scalarising the multiple objectives into a single-valued utility function [82]; *prioritisation of multiple objectives* - a certain priority is assigned to each objective and the problem is optimised according to the priority order of its objectives [89]; *goal-value method* - a goal value (usually the minimum attained performance) is assigned to each objective before optimisation to indicate its corresponding desired level of performance [90].

The rate control problem in multi-user interference systems can be formulated as an MCO problem. The convexity of the Pareto rate region of such MCO problem is a desirable feature for interference systems. Various approaches have been applied to convexify a rate region[1] [91], [92]. One widely-used approach is based on the use of a convex hull (see, for example [91]), which corresponds to the so-called time-sharing strategies. However, the time-sharing rate boundary is achievable only in terms of average rate rather than instantaneous rate. Another approach is based on using orthogonal strategies (orthogonal signaling schemes), e.g., TDM and frequency division multiplexing (FDM) [92]. Orthogonal signalling schemes significantly simplify the MCO problem, but they usually lead to smaller achievable rate regions. The corresponding rate loss can be significant when the interference is low [93]. Therefore, it is desirable to analyse the convexity of the true Pareto rate region employing pure strategy.

[1]When referring to rate region/boundary, we mean the Pareto rate region/boundary hereafter, if there is no particular other clarification.

To solve the MCO problem in multi-user interference systems, several methods have been developed in the literature based on the widely-used priori articulation of preferences approach [82]. The most representative one is the sum-rate maximisation (see, for example, the sum-rate maximisation for multi-user MIMO interference systems in [94]). The obvious drawback of this method is the lack of fairness, since the performance of users with bad channel conditions is always sacrificed. The fairness can be improved by weighted sum rate approaches like in [95], but it is not straightforward to determine the weighting coefficients for all users. The preference can also be based on proportional fairness [96], where the fairness of a user is proportional to its channel condition. Recently, game theory has been increasingly used in the rate control and optimisation for communication systems [97]. Particularly, the NB from cooperative game theory has been widely used to solve the MCO problem for multi-user interference systems. Note that NB is an effective scheme to balance the fairness of individual users and the system-level performance[98]. Representative examples in the literature include [92] and [99] for single-input single-output (SISO), [91] and [100] for multiple-input single-output (MISO), and [101] for MIMO interference systems. In [101], a practical suboptimal algorithm for finding the NB solution was designed by exploring the gradient projection method [94]. However, little research has been done to characterise the pure strategy based NB for MIMO interference systems.

In this chapter, we apply MCO to the rate control problem in multi-user interference systems. Specifically, we formulate the cooperative rate control of MIMO interference systems as an MCO problem. The contribution of this chapter can be summarised as follows.

- The Pareto rate region of the MCO problem is characterised. It is proved that the condition that interference-plus-noise covariance matrices approach the identity matrix is a sufficient condition for the convexity of the rate region. Moreover, a significant implication is found that when interference is high, interference mitigation techniques are preferable for convexifying the rate region.

- Various rate region convexification approaches including a multi-stage IC and a FP precoding-based IA scheme are analysed. An achievable rate region based on FP precoding is also given for MIMO interference systems.

- The MCO problem for rate control in multi-user MIMO interference systems is converted to a single-objective Nash-product maximisation problem by scalarising the multiple objectives using NB. The characteristics of the NB over MIMO interference systems such as the uniqueness of the pure-strategy NB solution and the optimality of NB solutions resulting from different convexification approaches are studied.

In a word, this chapter gives clue on how to coordinate the operation of CR users in spectrum-sharing CR networks. The remainder of this chapter is organised as follows. The MCO problem and Nash-product maximisation problem for multi-user MIMO interference systems are formulated in Section 5.2. In Section 5.3, the Pareto rate region is characterised and various rate region convexification approaches for MIMO interference systems are analysed. The characteristics of pure-strategy NB solution and the optimality of NB solutions resulting from different convexification approaches are studied in Section 5.4. The convexity of the rate region, fairness of NB, and the existence of the FP precoding based NB solution for MIMO interference systems are exemplified in Section 5.5 via numerical studies. Finally, conclusions are drawn in Section 5.6.

5.2 Problem Formulation

5.2.1 MCO in MIMO Interference Systems

Consider an M-user MIMO interference system in which all users use the same wireless channel simultaneously. The transmitter and receiver for user i $(i = 1, 2, \cdots, M)$ are equipped with N_i^t and N_i^r antennas, respectively. The $N_i^r \times 1$ complex baseband signal

vector received by user i can be written as [102]

$$\mathbf{y}_i = \mathbf{H}_{ii}\mathbf{x}_i + \sum_{j=1, j\neq i}^{M} \mathbf{H}_{ji}\mathbf{x}_j + \mathbf{n}_i \quad (i = 1, 2, \cdots, M) \tag{5.1}$$

where $\mathbf{x}_i \in \mathbb{C}^{N_i^t \times 1}$ is the transmitted signal vector for user i; $\mathbf{H}_{ii} \in \mathbb{C}^{N_i^r \times N_i^t}$ and $\mathbf{H}_{ji} \in \mathbb{C}^{N_i^r \times N_j^t}$ are channel matrices from transmitter i and transmitter j to receiver i, respectively; we assume $\mathbf{H}_{ii} \sim \mathcal{CN}(0, \rho_i)$ $(i = 1, 2, \cdots, M)$, i.e., the elements are i.i.d. circular symmetric complex Gaussian random variables with zero mean and variance ρ_i; we also have $\mathbf{H}_{ji} \sim \mathcal{CN}(0, \eta_{ji})$ $(j = 1, 2, \cdots, M;\ j \neq i)$; and $\mathbf{n}_i \in \mathbb{C}^{N_i^r \times 1}$ is the AWGN vector of user i with zero mean and covariance matrix $\mathbb{E}[\mathbf{n}_i \mathbf{n}_i^H] = \mathbf{I}$. Here, ρ_i is the normalised SNR for user i and η_{ji} is the normalised INR from transmitter j to receiver i.

We assume that: (i) each transmitter and receiver transmits and receives symbols independently; (ii) the co-channel interference from other users is unknown and treated as noise, i.e., no interference cancellation techniques are employed by receivers; (iii) the channel varies slowly and it is constant during the period of each symbol transmission.

The mutual information for user i can be expressed as [103]

$$I_i(\mathbf{Q}) = \log_2 \det\left(\mathbf{I} + \mathbf{H}_{ii}\mathbf{Q}_i\mathbf{H}_{ii}^H\mathbf{R}_{-i}^{-1}\right), \quad i = 1, 2, \cdots, M \tag{5.2}$$

where $\mathbf{Q}_i = \mathbb{E}[\mathbf{x}_i\mathbf{x}_i^H]$ is the Hermitian positive semi-definite transmit covariance matrix of the input signal vector for user i, i.e., $\mathbf{Q}_i \succeq 0$, and

$$\mathbf{R}_{-i} = \mathbf{I} + \sum_{j=1, j\neq i}^{M} \mathbf{H}_{ji}\mathbf{Q}_j\mathbf{H}_{ji}^H, \quad i = 1, 2, \cdots, M \tag{5.3}$$

is the interference-plus-noise covariance matrix for user i. We define $\mathbf{Q} \triangleq \{\mathbf{Q}_1, \cdots, \mathbf{Q}_M\}$ as a set of transmit covariance matrices. Since the transmission of each user is power limited, the following trace constraint applies to $\mathbf{Q}_i$

$$\mathtt{tr}[\mathbf{Q}_i] \leq p_i, \quad i = 1, 2, \cdots, M. \tag{5.4}$$

We also assume that each transmitter i has the full knowledge of the instantaneous channels and the transmit covariance matrices of all the other transmitters.

The rate control objective in the MIMO interference system is the rate[2] maximisation for all users by optimising their transmit covariance matrices $\mathbf{Q}_i$ $(i = 1, 2, \cdots, M)$ under the trace constraints given by (5.4). Therefore, rate control in the multi-user MIMO interference system can be formulated as the following MCO problem

$$\begin{aligned} \max_{\mathbf{Q}} \; & I_i(\mathbf{Q}) \quad i = 1, 2, \cdots, M \\ \text{subject to} \; & \mathbf{Q}_i \succeq 0, \quad i = 1, 2, \cdots, M \\ & \mathtt{tr}[\mathbf{Q}_i] \leq p_i, \quad i = 1, 2, \cdots, M. \end{aligned} \tag{5.5}$$

5.2.2 Scalarisation of the MCO Using NB

According to game theory, a game consists of three elements: *players*, *strategies* and *utilities* [104]. Players are rational parties involved in the game. Strategies stand for actions or behaviours taken by players. Utilities are usually defined in the form of a certain performance metric for players. The MIMO interference system delineated above can be modelled as a MIMO interference game, whose players are the users in the MIMO system, the rate of each user represents the utility of the corresponding player, and the transmit covariance matrix of each user forms the strategy space of each player.

A game can be classified as either competitive or cooperative according to the cooperation scheme among players. In a competitive game, as the name suggests, all the players compete with each other rationally and selfishly. Players neither communicate nor cooperate with each other. A steady state in competitive games for which each player can not improve its utility by unilaterally changing its own strategy is called the Nash Equilibrium (NE) [104]. For a MIMO interference game, the NE can be

[2]Hereafter, when referring to rate, we mean mutual information (5.2).

mathematically expressed as

$$\forall i = 1, 2, \cdots, M,\ \mathbf{Q}_i \succeq 0,\ \mathtt{tr}[\mathbf{Q}_i] \leq p_i :\ I_i(\mathbf{Q}_i^*, \mathbf{Q}_{-i}^*) \geq I_i(\mathbf{Q}_i, \mathbf{Q}_{-i}^*) \tag{5.6}$$

where $\mathbf{Q}_i^*$ and $\mathbf{Q}_{-i}^*$ denote the transmit covariance matrices of the NE for user i and for all the other users except i, respectively. The transmit covariance matrix of each player leading to the NE can be found via iterative water filling (IWF) as [105]

$$\mathbf{Q}_i^* = \mathbf{U}_i(\mu_i \mathbf{I} - \mathbf{D}_i^{-1})^+ \mathbf{U}_i^H, \quad i = 1, 2, \cdots, M \tag{5.7}$$

where $\mathbf{U}_i \mathbf{D}_i \mathbf{U}_i^H = \mathbf{H}_{ii}^H \mathbf{R}_{-i}^{-1} \mathbf{H}_{ii}$ is the EVD of $\mathbf{H}_{ii}^H \mathbf{R}_{-i}^{-1} \mathbf{H}_{ii}$, $\mathbf{U}_i$ $(i = 1, 2, \cdots, M)$ is the unitary matrix of eigenvectors, $\mathbf{D}_i$ $(i = 1, 2, \cdots, M)$ is a diagonal matrix of eigenvalues, and μ_i denotes the power level given by IWF. It is worth noting that the NE for MIMO interference systems is not necessarily unique [106].

Generally, the NE is not optimal from the system point of view due to its competitive and selfish nature. Whereas, in a cooperative game, all the players negotiate with each other prior to the game, which usually results in utility improvement [107], [108]. There exist many cooperative game-theoretic approaches. In this chapter, we restrict our attention to the NB as one of the most popular approaches to scalarise the multiple objectives of the MCO problem (5.5) [98].

The NB is well defined in a convex rate region [98]. In the context of the MIMO interference game, for the case when the rate region is convex, the bargaining set, i.e., the set of available strategies for user i, can be expressed as

$$S = \{\mathbf{Q}_i | \mathbf{Q}_i \succeq 0,\ \mathtt{tr}[\mathbf{Q}_i] \leq p_i,\ \text{and}\ I_i(\mathbf{Q}) > I_i^{\text{NE}}, i = 1, 2, \cdots, M\} \tag{5.8}$$

where I_i^{NE} is the utility of the NE for user i. It also has a *disagreement point*, which is defined as the state that players resort to when the cooperation fails. Naturally, the NE is taken as the disagreement point in NB. By applying the NB, the multiple objectives in the MCO problem (5.5) can be scalarised. Then, the MCO problem can

be transformed into the following single-objective optimisation problem

$$\begin{aligned} \max_{\mathbf{Q}} & \prod_{i=1}^{M} (I_i(\mathbf{Q}) - I_i^{\mathrm{NE}}) \\ \text{subject to} \quad & \mathbf{Q}_i \succeq 0, \quad i = 1, 2, \cdots, M \\ & \mathtt{tr}[\mathbf{Q}_i] \leq p_i, \quad i = 1, 2, \cdots, M \\ & I_i(\mathbf{Q}) > I_i^{\mathrm{NE}}, \quad i = 1, 2, \cdots, M \ . \end{aligned} \tag{5.9}$$

It is worth noting that the NB corresponds to the so-called *proportional fairness* and the Nash product $\prod_{i=1}^{M}(I_i(\mathbf{Q}) - I_i^{\mathrm{NE}})$ is converted to the rate product of all users when $I_i^{\mathrm{NE}} = 0, \ \forall i$. An intuitive explanation of the above optimisation problem is that the NB introduces a cooperation scheme among all MIMO users and regulates their transmissions by optimising transmit covariance matrices under the power constraints (5.9). On one hand, it guarantees that the utility of each MIMO user is not less than the one given by the NE. On the other hand, it maximises the Nash product of the whole MIMO system. Therefore, it provides a trade off between the fairness requirements to individual users and the overall performance of the whole system.

In the sequel, we first characterise the Pareto rate region of the MIMO interference systems and investigate interference mitigation-based rate region convexification schemes when the rate region is non-convex. An achievable rate region for MIMO interference system is given as well. Then, we study several characteristics of the NB in MIMO interference systems such as the uniqueness of the pure-strategy NB solution and the optimality of different NB solutions.

5.3 Rate Region Characterisation and Convexification

5.3.1 Convexity of Pareto Rate Region

The convexity of the rate region is a desirable feature for multi-user interference systems. Its immediate merit is that it usually yields larger rate region compared to a nonconvex one. More importantly, the convexity of the rate region is a necessary condition to ensure the convexity of rate control/optimisation problem. It simplifies the MCO problem and makes it solvable and practically realisable. In the context of the MIMO interference systems, we first investigate the convexity of the true Pareto rate region using pure strategies, which treat interference as noise and do not employ any other interference management mechanisms. The true Pareto rate region is both achievable in terms of instantaneous rate and usually larger than the orthogonal signaling-based counterpart in low interference cases [93]. We derive the following sufficient condition ensuring the convexity of its rate region.

Proposition 1 : *If the interference-plus-noise covariance matrices* $\mathbf{R}_{-i} \rightarrow \mathbf{I}$ $(i = 1, 2, \cdots, M)$*, the Pareto rate region of the MIMO interference system is convex.*

It is straightforward that the condition that utility functions $I_i(\mathbf{Q})$ $(i = 1, 2, \cdots, M)$ in (5.2) are concave over $\mathbf{Q}$ is sufficient for the convexity of the rate region for MIMO interefrence system. We can prove that the uitility functions are concave under the condition that interference-plus-noise covariance matrices approach $\mathbf{I}$. Thus, this condition is also sufficient for the convexity of the rate region. The detailed proof is provided in Appendix F. It is worth noting that Proposition 1 still holds when considering a CR network with interference temperature constraint like (4.13). This is due to the fact that interference constraint does not change the convexity of the bargaining set S (5.8).

The condition that $\mathbf{R}_{-i} \rightarrow \mathbf{I}$ means that $\sum_{j \neq i} \mathbf{H}_{ji} \mathbf{Y}_j \mathbf{H}_{ji}^H \rightarrow \mathbf{0}$. This corresponds to the condition that INRs η_{ji} $(i, j = 1, 2, \cdots, M,\ j \neq i)$ in (5.1) are sufficiently small.

Hence, the immediate implication of Proposition 1 is that the rate region is convex when the interference is low.

The rate region of interference systems is not always convex. There exist three broad approaches to convexify a non-convex rate region.

- **Convex hull** - the most direct approach for rate region convexification. It stems from the time-sharing signalling of extremity points on the rate boundary, where all users agree to use one set of transmitting strategies for certain fraction of time and to use the other set of strategies during the rest of the time (see, for example [91]). Therefore, the time-sharing signalling fills the 'depressions' of the rate region and make it convex. However, the rate region due to time-sharing signalling is only achievable in terms of the average rate (over time). Thus, the rate region of convex hull is not always achievable in terms of instantaneous rate [91].

- **Orthogonal signalling** - the most commonly used approach to convexify a rate region. In this case, users agree to split the radio resource (time or bandwidth) into several orthogonal parts and each user uses one part only. TDM and FDM are two prominent examples of orthogonal signalling. It worth noting that time sharing is involved in both TDM and convex hull. TDM distinguishes itself from the convex hull in the sense that the former is pure time-sharing signalling among single-user operation points. However, for the latter the time-sharing signalling is only used to fill the 'depressions' of the rate region as shown in FIGURE 5.1. The orthogonal signalling significantly simplifies the MCO problem of rate control, but the associated rate loss may be significant [93]. This is due to the fact that orthogonalisation completely removes interference from interfering users, but it also reduces the radio resource available to each user compared to that of the pure strategy.

- **Interference mitigation**- besides the convex hull and orthogonal signalling, Proposition 1 suggests that reducing interference for each user can also make the rate region convex. Therefore, various interference mitigation techniques are

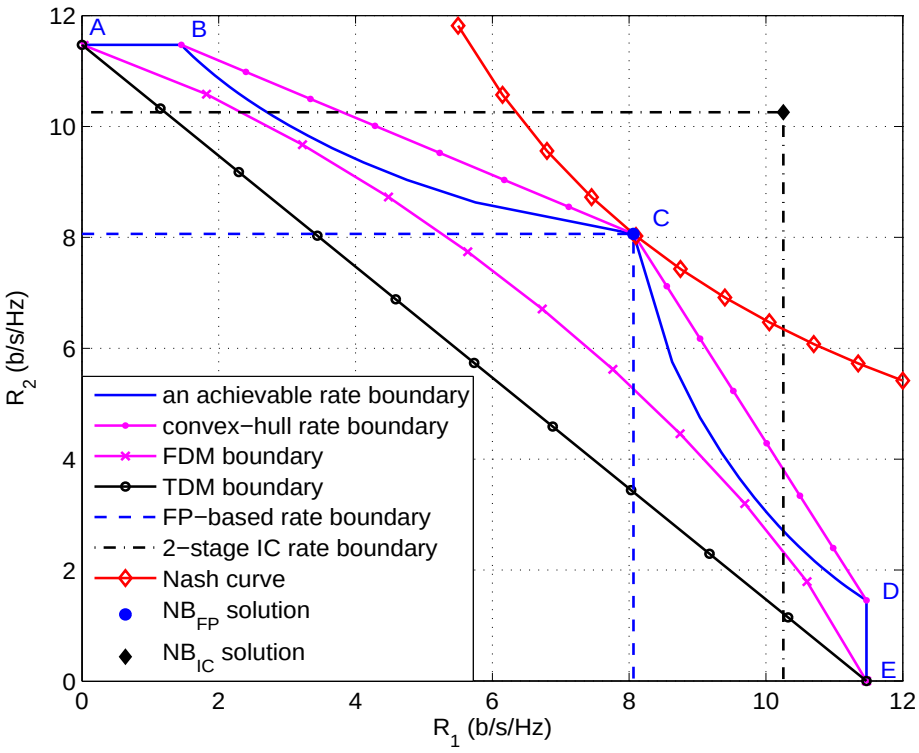

FIGURE 5.1: An example of different signalling schemes and NB solutions of 2-user MIMO interference system.

applicable to convexify the rate region. Interference mitigation can be mainly divided into two categories according to their applicability: (i) interference cancellation at the receiver and (ii) interference avoidance at the transmitter.

5.3.2 Rate Region Convexification Using Interference Cancellation

Various interference cancellation techniques [56] can be used for interference systems. The widely used multi-user detection technique [109], including successive interference cancellation (SIC) and parallel interference cancellation (PIC), is one suitable candidate for interference systems. SIC and PIC first decode the interfering signals and then subtract the reconstructed interfering signals from the received signal.

The following comparison between orthogonal signalling and interference cancellation technique is of interest. Orthogonal signaling is a simple and widely-used method to produce a convex rate region at the cost of rate loss. When the interference is high, applying interference cancellation techniques to an interference system eventually transforms a high-interference system into a low-interference system, which consequently leads to a convex rate region according to the Proposition 1. Moreover, interference cancellation removes the interference perceived at receivers, but unlike orthogonal signaling the radio resource (time, bandwidth) available to each user for interference cancellation remains the same as for pure strategy. Therefore, the following remark about the practical significance of the rate region convexification can be made.

Remark 1: *When the interference is high, interference cancellation techniques outperform orthogonal signalling techniques for convexifying a rate region in the sense that they lead to a convex rate region of a larger size.*

We can obtain the immediate conclusion from Remark 1 that interference cancellation ensures the uniqueness of NB solution, meanwhile, the interference cancellation based NB (NB_{IC}) solution has larger user rates than the orthogonal signaling based NB solution.

As a special case, we propose a multi-stage interference cancellation technique for a 2-user MIMO interference systems. The generalisation to the multi-user case is straightforward and it is omitted here for brevity. It is worth noting that our objective is to demonstrate the advantages of the interference cancellation over orthogonal signalling for the multicriteria optimisation via NB rather than considering practically appealing interference cancellation designs.

To design our interference cancellation technique, it is required that both receivers cooperate with each other and perform multi-stage interference cancellation as follows. First, the receivers of users 1 and 2 decode their signals of interest and pass them to the receivers of users 2 and 1, respectively. Using (5.1), the decoded signals from receivers of users 1 and 2 in the first stage of interference cancellation can be written

as:

$$\hat{\mathbf{x}}_1^{(1)} = \mathbf{H}_{11}^{-1}\mathbf{y}_1 \tag{5.10}$$

$$\hat{\mathbf{x}}_2^{(1)} = \mathbf{H}_{22}^{-1}\mathbf{y}_2 \tag{5.11}$$

where $\hat{\mathbf{x}}_i^{(1)}$ $(i = 1, 2)$ are the decoded signals at the receivers of users 1 and 2 in the first stage of the interference cancellation procedure. Second, after receiving the decoded signals from another user, the receivers of users 1 and 2 reconstruct the interference signals from the decoded signals, which can be expressed as $\mathbf{H}_{21}\hat{\mathbf{x}}_2^{(1)}$ and $\mathbf{H}_{12}\hat{\mathbf{x}}_1^{(1)}$ for users 1 and 2, respectively. Then, each receiver subtracts the reconstructed interfering signal from its originally received signal so to obtain the following signals used in the second stage of the interference cancellation procedure

$$\begin{aligned}\mathbf{y}_1^{(2)} &= \mathbf{y}_1 - \mathbf{H}_{21}\hat{\mathbf{x}}_2^{(1)} \\ &= \left(\mathbf{H}_{11} - \mathbf{H}_{21}\mathbf{H}_{22}^{-1}\mathbf{H}_{12}\right)\mathbf{x}_1 + \mathbf{n}_1 - \mathbf{H}_{21}\mathbf{H}_{22}^{-1}\mathbf{n}_2 \qquad (5.12)\\ \mathbf{y}_2^{(2)} &= \mathbf{y}_2 - \mathbf{H}_{12}\hat{\mathbf{x}}_1^{(1)} \\ &= \left(\mathbf{H}_{22} - \mathbf{H}_{12}\mathbf{H}_{11}^{-1}\mathbf{H}_{21}\right)\mathbf{x}_2 + \mathbf{n}_2 - \mathbf{H}_{12}\mathbf{H}_{11}^{-1}\mathbf{n}_1 \qquad (5.13)\end{aligned}$$

where $\mathbf{y}_i^{(2)}$ $(i = 1, 2)$ are the input signals at the second stage of interference cancellation. The matrix inverse operator in (5.10) – (5.13) should be changed to pseudo inverse when the channel matrices are not square.

The decoding, reconstruction, and subtraction procedure is repeated stage after stage and terminated after a certain stage or after a stopping criteria on the value of the remaining error is satisfied. Note that it is guaranteed that at each stage the new estimate of a signal is at least not worse than the estimate in the previous stage [110]. An example of a 2-stage interference cancellation is demonstrated in FIGURE 5.1 for a 2-user MIMO interference system.

5.3.3 Rate Region Convexification Using Interference Avoidance

Interference avoidance refers to proactive approaches employed at the transmitter side to avoid interfering unintended receivers. In the context of MIMO interference systems, null space projection-based precoding is one of the most widely-used interference avoidance schemes. It steers the transmission of each MIMO transmitter into the null space of interfering channel from the MIMO transmitter to its unintended receivers. There exist two null space projection-based precoding schemes, namely, FP- and PP-based precoding [77]. The FP/PP precoding fully/partially projects the MIMO transmission into the null space of the interfering channel. FP precoding is capable of completely avoiding interfering unintended receivers and transforming the MIMO interference system into an interference-free system. Therefore, it can be used to convexify the rate region of MIMO interference system.

To facilitate the FP precoding, the number of transmit antennas of each user must be larger than the total number of receive antennas of all unintended receivers, i.e.,

$$N_i^t > \sum_{j \neq i} N_j^r \quad (i, j = 1, 2, ..., M). \tag{5.14}$$

For user i, its transmit covariance matrix using FP precoding with transmission power p_i can be written as [77]

$$\mathbf{Q}_{\perp i}(p_i) = \mathbf{U}_{\perp i}(\mu_i \mathbf{I} - \mathbf{\Lambda}_{\perp i}^{-1})^{+} \mathbf{U}_{\perp i}^H \quad (i = 1, 2, \ldots, M) \tag{5.15}$$

with μ_i being the power level obtained from the water filling and $\mathtt{tr}[(\mu_i \mathbf{I} - \mathbf{\Lambda}_{\perp i}^{-1})^{+}] = p_i$. In (5.15), $\mathbf{U}_{\perp i}$ and $\mathbf{\Lambda}_{\perp i}$ are obtained from the EVD $\mathbf{U}_{\perp i}\Lambda_{\perp i}\mathbf{U}_{\perp i}^H = (\mathbf{I} - \mathbf{U}_{gi}\mathbf{U}_{gi}^H)^H \mathbf{H}_{ii}^H \mathbf{H}_{ii}$ $(\mathbf{I} - \mathbf{U}_{gi}\mathbf{U}_{gi}^H)$, and $\mathbf{U}_{gi}$ is the matrix consisting of the first $\sum_{j \neq i} N_j^r$ columns of the unitary matrix $\mathbf{U}_G$ stemming from another EVD $\mathbf{U}_G \mathbf{\Lambda}_G^{\frac{1}{2}} \mathbf{V}_G^H = \mathbf{H}_{-i}^H$, where

$$\mathbf{H}_{-i} = [\mathbf{H}_{i1}; \ldots; \mathbf{H}_{i\,i-1}; \mathbf{H}_{i\,i+1}; \ldots; \mathbf{H}_{iM}] \tag{5.16}$$

denotes the vertically concatenated interference channels from user i to all its unintended users j $(j \neq i)$.

The rate region of FP precoding for a 2-user MIMO interference system is also shown in FIGURE 5.1. As it can be seen from this figure, the FP precoding based rate region is rectangular, which is obvious convex. It can also be seen from FIGURE 5.1 that the FP precoding based rate region is smaller than that of the proposed multi-stage IC scheme.

The performance of the aforementioned rate region convexification schemes is summarised in TABLE 5.1, where their requirements on CSI and receiver (Rx) cooperation, implementation complexity and the size of resultant rate region are compared.

TABLE 5.1: Comparison of various rate region convexification schemes

	CSI	Rx cooperation	Complexity	Rate region size
TDM	not required	not required	low	small
FDM	not required	not required	low	medium
Multi-stage IC	required	required	high	large
FP-based IA	required	not required	medium	medium

5.3.4 Rate Region Characterisation

In what follows, we characterise the rate region for MIMO interference systems satisfying (5.14) by giving an achievable rate region. We start with a 2-user MIMO system. Its rate boundary can be obtained by finding the rate tuple $(R_1, \max_{\mathbf{Q}}(\mathrm{I}_2))$. Given a rate R_1 for user 1, the corresponding rate for user 2 R_2 on the rate boundary is the maximum rate which can be achieved by user 2. This can be expressed as the following optimisation problem

$$\begin{aligned} \max_{\mathbf{Q}} \;\; & R_2 = I_2(\mathbf{Q}) \\ \text{subject to} \;\; & I_1(\mathbf{Q}) = R_1, \\ & \mathbf{Q}_i \succeq 0, \quad i = 1, 2 \\ & \mathtt{tr}[\mathbf{Q}_i] \leq p_i, \quad i = 1, 2. \end{aligned} \tag{5.17}$$

The largest R_2 on the whole rate boundary can be achieved when (i) there is no interference from user 1 to user 2, i.e., user 1 adopts the FP precoding with transmit covariance matrix $\mathbf{Q}_{\perp 1}$, and (ii) user 2 employs the maximum rate precoding with the following transmit covariance matrix and full-power transmission

$$\mathbf{Q}_{\mathrm{MR}_2}(p_2) = \mathbf{U}_{\mathrm{MR}_2}(\mu_2\mathbf{I} - \mathbf{\Lambda}_{\mathrm{MR}_2}^{-1})^{+}\mathbf{U}_{\mathrm{MR}_2}^{H} \tag{5.18}$$

where $\mathbf{U}_{\mathrm{MR}_2}$ and $\mathbf{\Lambda}_{\mathrm{MR}_2}$ come from the EVD $\mathbf{U}_{\mathrm{MR}_2}\mathbf{\Lambda}_{\mathrm{MR}_2}\mathbf{U}_{\mathrm{MR}_2}^{H} = \mathbf{H}_{22}^{H}\mathbf{H}_{22}$. Therefore, an achievable rate boundary can be obtained as follows.

- For $I_1(\mathbf{Q}_{\perp_1}(0),\mathbf{Q}_{\mathrm{MR}_2}(p_2)) \le R_1 \le I_1(\mathbf{Q}_{\perp_1}(p_1), \mathbf{Q}_{\mathrm{MR}_2}(p_2))$, where $I_i(\mathbf{Q}_1(p_1), \mathbf{Q}_2(p_2))$ denotes the rate of user i when users 1 and 2 adopt the transmit covariance matrices $\mathbf{Q}_1$ and $\mathbf{Q}_2$ with transmission power p_1 and p_2, R_2 can achieve its largest rate. We denote this part of rate boundary as $\mathbb{R}_1$. Then, we have

$$\begin{aligned} &\mathbb{R}_1 : 0 \le R_1 \le I_1(\mathbf{Q}_{\perp_1}(p_1), \mathbf{Q}_{\mathrm{MR}_2}(p_2)) \\ &\qquad R_2 = \log_2 \det\left(\mathbf{I} + \mathbf{H}_{22}\mathbf{Q}_{\mathrm{MR}_2}(p_2)\mathbf{H}_{22}^{H}\right) = \sum_k \left(\log_2(p_2\lambda_k^{\mathrm{MR}_2})\right)^{+}. \end{aligned} \tag{5.19}$$

  The second equality for R_2 in (5.19) is obtained according to [111], $\lambda_n^{\mathrm{MR_i}}$ ($i = 1, 2, \ldots, M$; $n = 1, 2, \ldots, \mathtt{min}(N_i^t, N_i^r)$) is the nth diagonal element of the eigenvalue matrix $\mathbf{\Lambda}_{\mathrm{MR_i}}$, and the operator $\sum_k (x_k)^{+}$ stands for the sum of x_k with $k \in \{n | p_i - 1/\lambda_n^{\mathrm{MR_i}} > 0\}$. It is easy to understand that $\mathbb{R}_1$ coincides with the boundary of the Pareto rate region. In FIGURE 5.1, the the line AB corresponds to $\mathbb{R}_1$ where user 1 uses the FP precoding and sweeps its transmission power form 0 to p_1, and user 2 adopts the maximum rate precoding with full-power transmission.

- At point B in FIGURE 5.1, R_1 cannot be further improved along the line of AB since user 1 is transmitting at full power. However, if user 2 splits some of the transmission power for FP precoding, the interference perceived at receiver 1 caused by user 2 will reduce. Consequently, R_1 can be further improved. Then,

we have the second part of the achievable rate boundary

$$\begin{aligned}\mathbb{R}_2 : R_1 &= \log_2 \det \left\{ \mathbf{I} + \frac{\mathbf{H}_{11}\mathbf{Q}_{\perp_1}(p_1)\mathbf{H}_{11}^H}{\mathbf{H}_{21}\left[\tau\mathbf{Q}_{\perp_2}(p_2) + (1-\tau)\mathbf{Q}_{\mathrm{MR}_2}(p_2)\right]\mathbf{H}_{21}^H} \right\} \\ R_2 &= \log_2 \det \left\{ \mathbf{I} + \mathbf{H}_{22}\left[\tau\mathbf{Q}_{\perp_2}(p_2) + (1-\tau)\mathbf{Q}_{\mathrm{MR}_2}(p_2)\right]\mathbf{H}_{22}^H \right\} \ (0 \le \tau \le 1).\end{aligned} \tag{5.20}$$

It worth noting that $\mathbb{R}_2$ is one of the achievable rate boundaries, which is not necessarily the Pareto rate boundary. In FIGURE 5.1, the curve BC depicts $\mathbb{R}_2$ where user 1 still uses FP precoding with full power and the transmit covariance matrix for user 2 is the convex combination of FP precoding and maximum rate precoding.

- Using the symmetry of the previous results, the other two parts of the achievable rate boundary $\mathbb{R}_3$ and $\mathbb{R}_4$, which are respectively symmetric to $\mathbb{R}_2$ and $\mathbb{R}_1$, can be written as

$$\begin{aligned}\mathbb{R}_3 : R_1 &= \log_2 \det \left\{ \mathbf{I} + \mathbf{H}_{11}\left[(1-\tau)\mathbf{Q}_{\perp_1}(p_1) + \tau\mathbf{Q}_{\mathrm{MR}_1}(p_1)\right]\mathbf{H}_{11}^H \right\} \\ R_2 &= \log_2 \det \left\{ \mathbf{I} + \frac{\mathbf{H}_{22}\mathbf{Q}_{\perp_2}(p_2)\mathbf{H}_{22}^H}{\mathbf{H}_{12}\left[(1-\tau)\mathbf{Q}_{\perp_1}(p_1) + \tau\mathbf{Q}_{\mathrm{MR}_1}(p_1)\right]\mathbf{H}_{12}^H} \right\} \ (0 \le \tau \le 1). \\ \mathbb{R}_4 : R_1 &= \log_2 \det \left(\mathbf{I} + \mathbf{H}_{11}\mathbf{Q}_{\mathrm{MR}_1}(p_1)\mathbf{H}_{11}^H \right) = \sum_k \left(\log_2(p_1 \lambda_k^{\mathrm{MR}_1}) \right)^+ \\ & I_2(\mathbf{Q}_{\mathrm{MR}_1}(p_1); \mathbf{Q}_{\perp_2}(p_2)) \ge R_2 \ge 0.\end{aligned} \tag{5.21}$$

Note that the achievable rate boundaries $\mathbb{R}_3$ and $\mathbb{R}_4$ are obtained by interchanging the index of the transmit covariance matrices from $\mathbb{R}_2$ and $\mathbb{R}_1$. In FIGURE 5.1, the curve CD and line DE correspond to $\mathbb{R}_3$ and $\mathbb{R}_4$, respectively. Therefore, the achievable rate boundary for the 2-user MIMO interference system satisfying (5.14) is $\mathbb{R} = \mathbb{R}_1 \cup \mathbb{R}_2 \cup \mathbb{R}_3 \cup \mathbb{R}_4$.

An achievable rate region for the case of 3-user is illustrated in FIGURE 5.2. The FDM based rate region is also plotted in this figure for comparison. The achievable rate boundary consists of the following two types of 2-dimensional hypersurfaces:

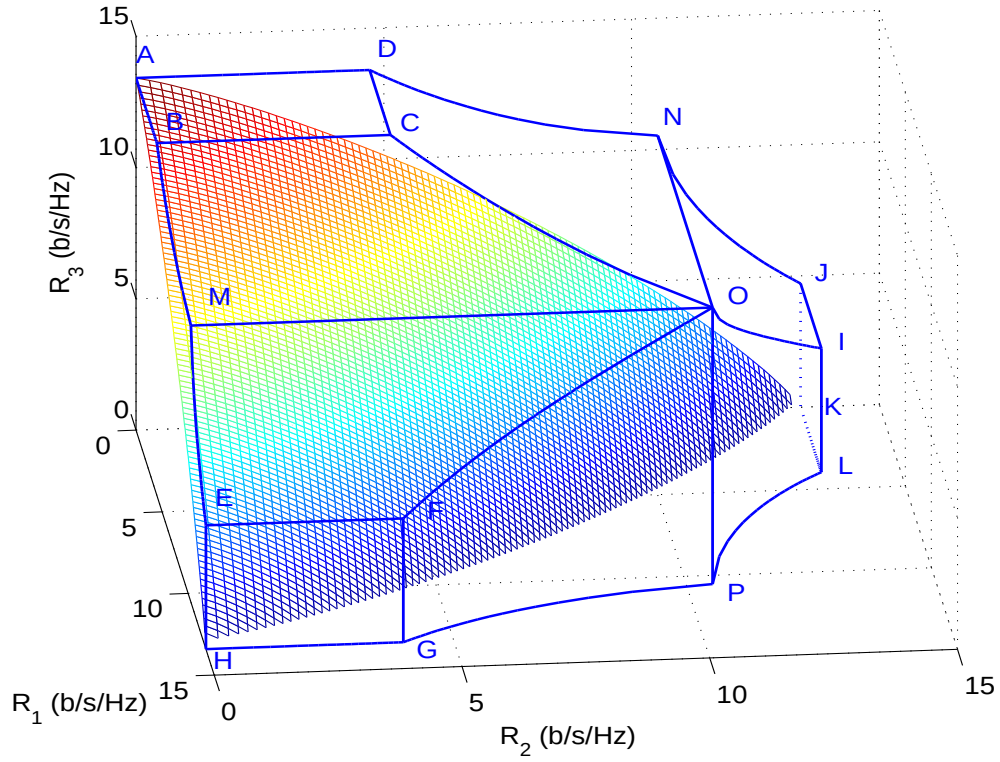

FIGURE 5.2: An achievable rate region for a 3-user MIMO interference system.

- The plane ABCD is obtained when user 1 adopts the full-power maximum rate precoding $\mathbf{Q}_{\mathrm{MR}_1}(p_1)$ and the other two users employ the FP precoding and sweep their transmission power from 0 to p_i, i.e., $\mathbf{Q}_{\perp_i}(\tau_i p_i)$ $(i = 2, 3;\ \tau_i \in [0, 1])$. We can get another two planes EFGH and IJKL by the symmetry of interchanging the index of $\mathbf{Q}_1$, $\mathbf{Q}_2$ and $\mathbf{Q}_3$ of the plane ABCD.

- The surface BCOM corresponds to the operation strategy set of $\{\mathbf{Q}_{\perp_1}(p_1), \mathbf{Q}_{\perp_2}(\tau_2 p_2), \tau\mathbf{Q}_{\mathrm{MR}_3}(p_3) + (1-\tau)\mathbf{Q}_{\perp_3}(p_3)\}$ $(\tau, \tau_2 \in [0, 1])$. Another five similar surfaces (DCON, EFOM, GFOP, LIOP, and JION) can be obtained by interchanging the index of the transmit covariance matrices of the surface BCOM.

By induction, an achievable rate boundary for n-user can be generalised as follows. For an n-user MIMO interference channel satisfying (5.14), one of the achievable rate boundaries can be characterised by the following two types of hypersurfaces of $n-1$ dimensions.

- One user (C_n^1) uses full-power maximum rate precoding $\mathbf{Q}_{\mathrm{MR}_i}(p_i)$ $(i = 1, 2, \cdots, n)$. All the other users adopt varying-power FP precoding, i.e., $\mathbf{Q}_{\perp_j}$ $(\tau_j p_j)(j \neq i, \tau_j \in [0, 1])$.

- One user (C_n^1) uses the convex combinational precoding strategy $\tau\mathbf{Q}_{\mathrm{MR}_i}(p_i) + (1-\tau)\mathbf{Q}_{\perp_i}(p_i)\}$ $(\tau \in [0, 1],\ i = 1, 2, \cdots, n)$. Another user among the remaining $n-1$ users (C_{n-1}^1) adopts the full-power FP precoding $\mathbf{Q}_{\perp_j}$ $(p_j)(j \neq i)$. All the rest users employ varying-power FP precoding $\mathbf{Q}_{\perp_k}$ $(\tau_k p_k)(k \neq i, k \neq j, \tau_k \in [0, 1])$. Thus, the total number of hypersurfaces of these two types aggregate to $\mathrm{C}_n^1 + \mathrm{C}_n^1\mathrm{C}_{n-1}^1 = n + n(n-1) = n^2$.

5.4 Characterisation of Different NB Solutions

5.4.1 Uniqueness of Pure-Strategy NB Solution

It is straightforward to see that the optimisation problem given by (5.9) is identical to

$$\max_{\mathbf{Q}} \ \ln\left(\ln^M 2 \prod_{i=1}^{M} \left(I_i(\mathbf{Q}) - I_i^{\mathrm{NE}}\right)\right)$$

$$\begin{aligned} \text{subject to} \quad & \mathbf{Q}_i \succeq 0, \quad i = 1, 2, \cdots, M \\ & \mathtt{tr}[\mathbf{Q}_i] - p_i \leq 0, \quad i = 1, 2, \cdots, M \\ & I_i^{\mathrm{NE}} - I_i(\mathbf{Q}) < 0, \quad i = 1, 2, \cdots, M\ . \end{aligned} \tag{5.22}$$

Note that (5.22) is a convex optimisation problem if and only if its objective function is concave and its constraint set is convex [83].

Proposition 2 : *When the interference-plus-noise covariance matrices* $\mathbf{R}_{-i} \to \mathbf{I}$ $(i = 1, 2, \cdots, M)$ *, the optimisation problem* (5.22) *is a convex problem.*

This proposition has been proved in Appendix G by showning that the condition that the interference-plus-noise covariance matrices $\mathbf{R}_{-i}$ approach $\mathbf{I}$ is sufficient for both

the concavity of the objective function in (5.22) and the convexity of its constraint set.

From Proposition 2, the following corollary can be obtained.

Corollary 1: *When the NE is not in the Pareto rate boundary, the condition that the interference-plus-noise covariance matrices* $\mathbf{R}_{-i}$ *approach* $\mathbf{I}$*, is the sufficient condition for the uniqueness of the pure-strategy NB solution of MIMO interference systems.*

Proof. The interference-plus-noise covariance matrices $\mathbf{R}_{-i}$ approaching $\mathbf{I}$ can ensure the convexity of the rate region (see Proposition 1) on which the NB is defined. Interestingly, it also guarantees the uniqueness of the NE in MIMO interference systems (see Proposition 1 in [106]), i.e., it guarantees the IWF convergences. Proposition 2 states that if the interference-plus-noise covariance matrices $\mathbf{R}_{-i}$ approach $\mathbf{I}$, then (5.22) is a convex optimisation problem, i.e., there exists at most one solution maximising the objective function of (5.22) [83]. Moreover, the NE not being in the Pareto boundary is necessary for the existence of the NB solution. Applying Propositions 1 and 2 in this chapter and Proposition 1 in [106], we complete the proof. □

For proportional fairness, where the Nash product corresponds to the rate product, it is easy to infer from (5.22) that the interference-plus-noise covariance matrices $\mathbf{R}_{-i}$ approaching $\mathbf{I}$ is also the sufficient condition for the concavity of $\ln(\ln^M 2 \prod_{i=1}^{M} I_i(\mathbf{Q}))$, which is equivalent to the concavity of the rate product logarithm for MIMO interference systems.

5.4.2 Optimality of NB Solutions

Various rate region convexification schemes have been investigated in Section 5.3. Their resultant convex rate regions lead to different NB solutions. It can be observed from FIGURE 5.1 that the TDM and multi-state interference cancellation scheme have the smallest and largest rate regions, respectively. Hence, they lead to the NB solutions with the smallest and largest user rates, respectively. Moreover, the FDM-based NB (NB_{FDM}) solution is optimal over the TDM-based NB (NB_{TDM}) solution

due to the fact that the FDM-based rate region is strictly convex while the TDM-base rate region is not. Next, we analyse the optimality between NB_{FDM} and FP precoding-based NB (NB_{FP}) solutions.

The NB_{FP} solution for user i can be expressed as

$$\begin{aligned} R_i^{\text{NB}_{\text{FP}}} &= \log_2 \det \left(\mathbf{I} + \mathbf{H}_{ii}\mathbf{Q}_{\perp_i}(p_i)\mathbf{H}_{ii}^H\right) \\ &= \max_{\mathbf{Q}_i} \ \log_2 \det \left\{\mathbf{I} + \mathbf{H}_{ii}\left[\mathbf{I} - \mathbf{H}_{-i}^H(\mathbf{H}_{-i}\mathbf{H}_{-i}^H)^{-1}\mathbf{H}_{-i}\right]\mathbf{Q}_i \right. \\ &\qquad \left. \times \left[\mathbf{I} - \mathbf{H}_{-i}^H(\mathbf{H}_{-i}\mathbf{H}_{-i}^H)^{-1}\mathbf{H}_{-i}\right]^H \mathbf{H}_{ii}^H\right\} \\ &= \sum_{k=1}^{N_i^t - \sum_{j\neq i} N_i^r} \left(\log_2(p_i\lambda_k^{\perp})\right)^+, \end{aligned} \tag{5.23}$$

where $\lambda_k^{\perp}(k = 1, 2, \cdots, N_i^t - \sum_{j\neq i} N_i^r)$ are the eigenvalues of the user i's effective channel matrix after projection $\mathbf{H}_{ii}\left[\mathbf{I} - \mathbf{H}_{-i}^H(\mathbf{H}_{-i}\mathbf{H}_{-i}^H)^{-1}\mathbf{H}_{-i}\right]\left[\mathbf{I} - \mathbf{H}_{-i}^H(\mathbf{H}_{-i}\mathbf{H}_{-i}^H)^{-1}\mathbf{H}_{-i}\right]^H\mathbf{H}_{ii}^H$. The second equality in (5.23) is obtained by interpreting the FP precoding as an optimal precoding of the effective channel matrix after null-space projection.

The rate of user i employing FDM when using $t_i(t_i \in [0, 1])$ fraction of the spectrum can be written as

$$\begin{aligned} R_i^{\text{FDM}}(t_i) &= t_i \log_2 \det \left(\mathbf{I} + \frac{\mathbf{H}_{ii}\mathbf{Q}_{\text{MR}_i}(p_i)\mathbf{H}_{ii}^H}{t_i\mathbf{I}}\right) \\ &= t_i \sum_{k=1}^{N_i^r} \left(\log_2(p_i\frac{\lambda_i^{\text{MR}}}{t_i})\right)^+. \end{aligned} \tag{5.24}$$

Let $t_i \sum_{k=1}^{N_i^r} \left(\log_2(p_i\frac{\lambda_i^{\text{MR}}}{t_i})\right)^+ = R_i^{\text{NB}_{\text{FP}}}$, we can use the following criteria to determine the optimality of NB_{FP} and NB_{FDM} solutions:

- when $\sum_{i=1}^{M} t_i > 1$ the NB_{FP} solution outperforms the FDM-based counterpart;
- when $\sum_{i=1}^{M} t_i < 1$ the NB_{FDM} solution is optimal over the NB_{FP} solution.

5.5 Numerical Studies

5.5.1 Convexity of the Rate Region

Proposition 1 in Section 5.3 provides the sufficient condition which guarantees the convexity of the rate region for MIMO interference systems. Unlike Proposition 1 where the interference-plus-noise covariance matrices and then INRs are interpreted in a qualitative manner, in this subsection we investigate the impact of the INRs on the convexity of the rate region quantitatively via numerical studies. Consider a 2-user Rayleigh fading MIMO interference system with parameters $\sigma = 1$ and $N_i^t = N_i^r = 2$ $(i = 1, 2)$. We examine the probability that the rate region is convex for different values of signal-to-interference ratio (SIR). It can be seen from FIGURE 5.3 that when the SNR is -10, 0 and 10 dB, the SIR should be at least 10, 15 and 20 dB, respectively, to ensure that the rate region is convex. Two trends can be observed from FIGURE 5.3: (i) as the SIR increases, i.e., as the INR decreases while the SNR is fixed, the probability that the rate region is convex increases; (ii) as the SNR increases, the SIR needs to increase as well to retain the probability that the rate region is convex.

5.5.2 Fairness of the NB

NB is a bargaining approach which balances the individual fairness and system-level efficiency. The fairness of the NB is guaranteed by the fact that its resultant utility for each user is not less than that of the NE, which is considered as a relatively fair approach due to its selfish and competitive nature. In this subsection, we study the fairness of the NB solution and compare it with other bargaining approaches. The following bargaining solutions from [112] are taken as the benchmark for comparison:

- Egalitarian solution: It is an absolutely fair solution with identical rate for each user.
- Kalai-Smorodinsky (K-S) solution: It results in utilities proportional to their maximal achievable rates.

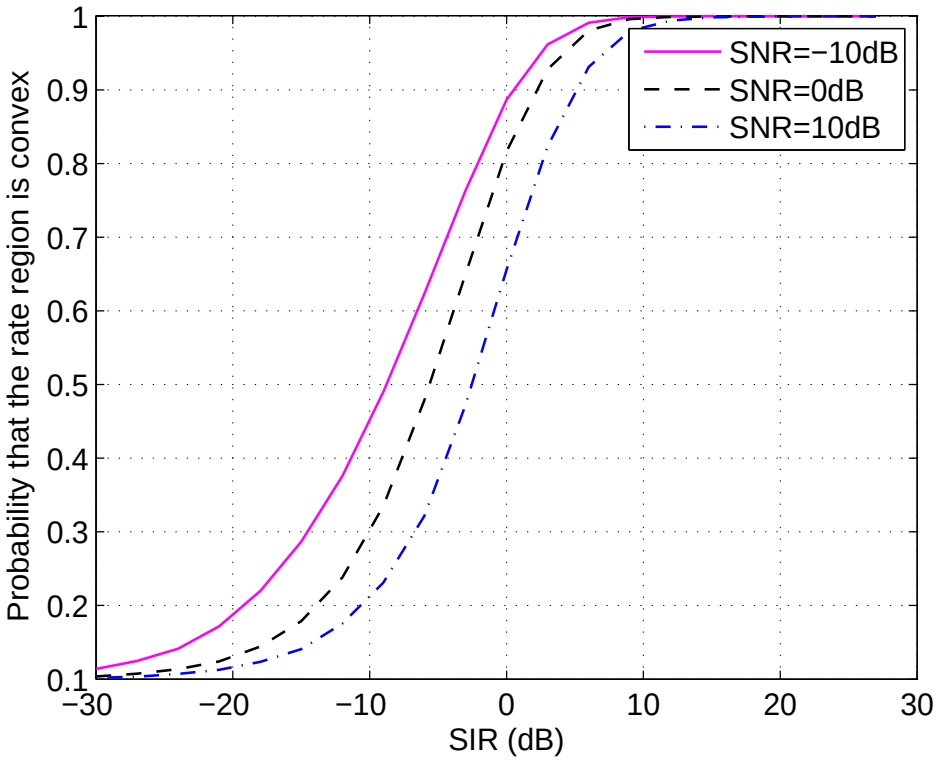

FIGURE 5.3: Probability of convex rate region over different values of SIR.

- Utilitarian solution: This solution maximizes the sum rate of all users.
- Proportional solution: It maximizes the rate product of all users.

We compare the fairness of these bargaining solutions with the NB solution in terms of Jain's fairness index (JFI) [113] having the Egalitarian solution as the absolutely fair solution. Recently, the JFI has been also used to compare difference scheduling algorithms in MIMO broadcast channels [114]. JFI, denoted as J, for the n-user system is [113]

$$J = \frac{(\sum_{i=1}^{n} x_i)^2}{n \sum_{i=1}^{n} x_i^2} \tag{5.25}$$

where $x_i = U_i/U_i^*$, $\{U_1,\ U_2, \cdots, U_n\}$ and $\{U_1^*,\ U_2^*, \cdots, U_n^*\}$ are the measured and optimal utility vectors for the n-user system, respectively. It rates the fairness of the system and ranges from $1/n$ (worst case) to 1 (best case).

To compare the fairness of the NB solution with that of the above mentioned bargaining solutions, we consider a 2-user MIMO interference system with $N_i^t = N_i^r =$

2 $(i = 1, 2)$, $\mathbf{H}_{11} = \text{diag}(8.05, 4.47)$, $\mathbf{H}_{22} = \text{diag}(2.24, 2.68)$, $\mathbf{H}_{21} = \text{diag}(3.74, 3.74)$, $\mathbf{H}_{12} = \text{diag}(1.12, 1.12)$ and $p_1 = p_2 = 1$. FIGURE 5.4 shows the pure-strategy rate boundary, time-sharing rate boundary and different bargaining solutions for this MIMO interference system. These bargaining solutions are demonstrated graphically and geometrically in FIGURE 5.4. For example, the NB solution can be interpreted as the intersection of the rate boundary and the Nash curve. Similarly, the Egalitarian solution, K-S solution, Utilitarian solution and Proportional solution are the intersections of the rate boundary and the following curves $y = x$, $y/x = \max(I_2)/\max(I_1)$, $y + x = \max(I_1 + I_2)$, $yx = \max(I_1 \cdot I_2)$, respectively. JFIs obtained from (5.25) for the NE, NB solution, K-S solution, Utilitarian solution and Proportional solution are 0.9925, 0.9685, 0.8853, 0.8960 and 0.8960, respectively. Note that in this example, the Utilitarian solution is identical to the Proportional solution. It can be seen that the JFI of the NB solution is only slightly smaller than that of the NE but much larger than all the other solutions. Compared with the NE, the NB improves the sum rate of this MIMO system by 18% at the price of only compromising its JFI by

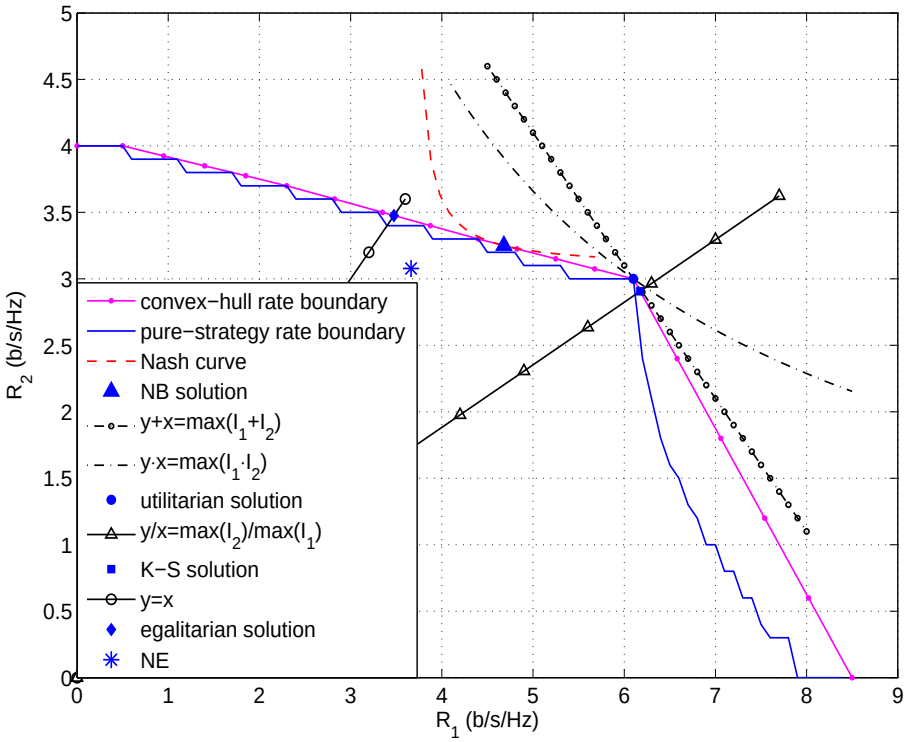

FIGURE 5.4: Various bargaining solutions for a MIMO interference system.

0.9925-0.9685=0.024. These results confirm that the NB is an effective approach well balancing the individual fairness and system performance of interference systems.

5.5.3 Existence of the NB_{FP} Solution

According to the definition of NB, the $\mathrm{NB}_{\mathrm{FP}}$ solution exists only when the resultant rates of FP precoding are larger than those of NE for all users. In FIGURE 5.5, we evaluate the probability for the existence of the $\mathrm{NB}_{\mathrm{FP}}$ solution. It can also be interpreted as the probability that cooperation (using FP precoding) is strictly optimal over competition among users in terms of resultant rates. As we can see from FIGURE 5.5, the probability for the existence of $\mathrm{NB}_{\mathrm{FP}}$ solution increases with the increase of INR, which infers that the FP precoding becomes more favourable than the NE as the INR increases. This is because the rates of the $\mathrm{NB}_{\mathrm{FP}}$ solution do not change against INRs, but the rates of the NE decrease as the INR increases due to the rising interference. Another interesting phenomenon that can be observed from FIGURE 5.5 is that the probability for the existence of the $\mathrm{NB}_{\mathrm{FP}}$ solution is not sensitive to SNR. However, at large INR this probability increases slightly with the increase of SNR. This is due to the fact that given a transmission power for FP precoding the number of effective transmission streams tends to increase as the SNR increases. Meanwhile, the number of effective transmission streams almost does not change over SNRs for the precoding of NE, since at large INR the effective transmission streams of NE for each user are mainly determined by its interfering channel rather than the desired channel, i.e., the SNR has little impact on the number of effective transmission streams.

5.6 Chapter Summary

In this chapter, the rate control problem in multi-user MIMO interference systems has been formulated as an MCO problem. The convexity of the Pareto rate region of this MCO problem has been studied. It has been found that the INR covariance matrices approaching the identity matrix is a sufficient condition guaranteeing the the convexity

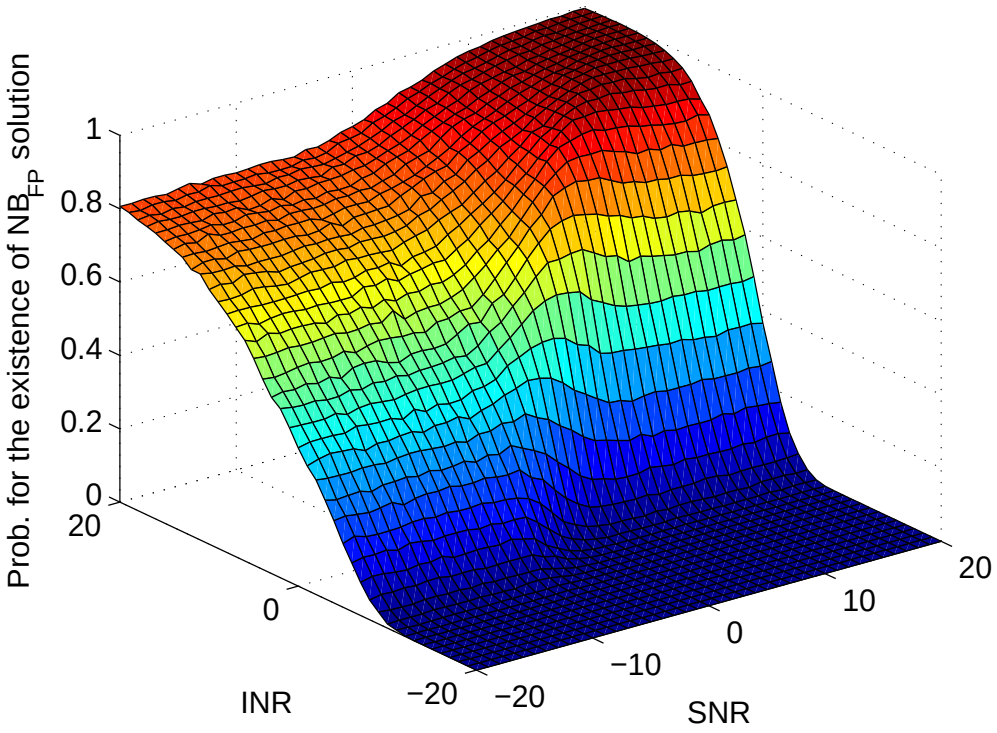

FIGURE 5.5: Existence of the FP-based NB solution for different SNRs and INRs.

of the rate region. Inspired by this finding, we have analysed a family of interference management schemes to convexify the rate region of the MIMO interference system, including orthogonal signalling, a proposed multi-state interference cancellation at receivers and an FP precoding-based interference avoidance scheme at transmitters. It is argued that the interference mitigation techniques are preferable for convexifying the Pareto rate region over other existing techniques in terms of resultant user rates. An achievable rate region has been given for the MIMO interference system as well.

Then, the MCO problem has been transformed into a single-objective optimisation problem by using NB. A variety of characteristics for NB in MIMO interference systems, such as the uniqueness of the pure-strategy NB solution and the optimality of different NB solutions, have been investigated. It has been found that the INR covariance matrices approaching the identity matrix is also a sufficient condition ensuring the uniqueness of the pure-strategy NB solution. A method to determine the optimality between FP- and TDM-based NB solutions has been presented as well. Finally, the convexity of the rate region, the fairness of the NB solution, the impact

of the SNR and INR on the existence of the FP-based NB solution have also been demonstrated via numerical studies.

Chapter 6

Conclusions and Future Work

CR networks could lead to complex and sophisticated interference scenarios. With the introduction of CR networks, two novel types of interference originating from CR networks are introduced, including the CR-primary and CR-CR interference. Both of these interferences deserve careful study in order to protect the primary operation and improve the CR performance. This thesis presents a wealth of comprehensive research on interference modelling and management for CR networks, ranging from CR-primary interference modeling and mitigation to CR-CR interference coordination. In this concluding chapter, we summarise all the key findings from different chapters and suggest several interesting future research directions.

6.1 Summary of Results

Chapter 3 has modelled the aggregate interference at a primary receiver caused by multiple CR transmitters by deriving the interference PDFs. Three different interference management mechanisms power control, contention control, and hybrid power/-contention control schemes have been considered for CR networks. It has been found that the proposed power control and contention control schemes are two effective approaches to alleviate the CR-primary interference, while the hybrid control scheme causes higher interference to a primary receiver, but leads to larger CR coverage as

compared to the other two schemes. Furthermore, the effect of a hidden primary receiver on the perceived CR-primary interference has also been investigated for the primary receiver. It has been shown that the hidden primary receiver problem leads to higher CR-primary interference with increased mean and variance. Finally, numerical studies have demonstrated that increasing the IR radius of the primary receiver is an effective way to reduce the CR-primary interference. More interestingly, the power control scheme is more sensitive to the IR radius than the contention control counterpart.

Chapter 4 has proposed and investigated several IM schemes aiming at mitigating the inter-network interference for CR networks. Firstly, we have reviewed a family of IM techniques for CR networks. We have found that various IA techniques can be applied to a CR transmitter to effectively combat the CR-primary interference. Then, we confine our attention to the mitigation of CR-primary interference for CR MIMO systems. Two practical SP precoding-based schemes, namely, FP and PP precoding, have been proposed for CR MIMO systems to mitigate their interference to the primary network and improve the CR throughput. These two precoding schemes are capable of estimating the CSI of CR-primary interference channels and accounting for the primary-CR interference into precoding via a novel sensing approach. Therefore, no extra signalling is required between primary and CR systems, which consequently eases the deployment of CR networks. To better mitigate the CR-primary interference for CR MIMO systems, we have proposed two cross-layer algorithms by jointly considering the precoding in the physical layer and channel allocation in the MAC layer. Simulation results have demonstrated that both of the proposed cross-layer algorithms outperform the non-cross-layer approach in terms of the resulting CR-primary interference and the CR throughput.

Chapter 5 has analysed the CR-CR interference channels and coordination of the spectrum-sharing CR MIMO users. We have characterised the Pareto rate region for a multi-user MIMO interference system. It has been found that the INR covariance matrices approaching the identity matrix is a sufficient condition guaranteeing the convexity of the rate region. Inspired by this finding, we have analysed a family of

interference management schemes to convexify the rate region of the MIMO interference system, including orthogonal signalling, a proposed multi-state IC at receivers and null space projection precoding-based IA at transmitters. It is argued that the interference mitigation techniques are preferable for convexifying the Pareto rate region in terms of resulting user rates compared with orthogonal signalling-based approaches. Then, we have investigated the coordination of mutually interfering CR users by using NB. A variety of characteristics for NB in MIMO interference systems, such as the uniqueness of the pure-strategy NB solution and the optimality of different NB solutions, have been examined. It has been found that the INR covariance matrices approaching the identity matrix is also a sufficient condition ensuring the uniqueness of the pure-strategy NB solution. A method to determine the optimality between FP- and TDM-based NB solutions has been given as well.

Overall, the studies presented in Chapters 3 to 5 have demonstrated how the CR operation may interfere with the primary network, how to mitigate the CR-primary interference and how to coordinate the mutually interfering CR users. Capable of casting light on the future deployment of CR networks, the research conducted in this thesis are of great practical significance.

6.2 Future Research Topics

For CR-primary interference modelling, the IR has been adopted to protect the primary receiver in this thesis. There are two main types of techniques to identify the IR for a primary network: geo-location technique and spectrum sensing. We have only focused on the geo-location-based approach, which leads to a circular IR. It is also worth considering the scenario of irregular IR due to spectrum sensing in future work. Besides, we have taken PDFs as the metric to model the CR-primary interference. Other metrics like outage probability of a primary receiver can be used to evaluate the CR-primary interference as well. Moreover, joint interference modelling by considering multiple CR receivers can also be done in future.

For CR-primary interference mitigation, the proposed precoding schemes are based on null-space projection. It actually tightens the CR-primary interference constraint by reducing the interference temperature limit to zero. This is suboptimal in terms of the resulting CR throughput when the primary network is interference tolerant. Therefore, it is desirable to investigate other better precoding schemes without tightening the CR-primary interference constraint. As for cross-layer interference mitigation, it is worthwhile to take other interference management mechanisms like power or contention control of CR networks into the cross-layer optimisation.

For the analysis of CR-CR interference channels, we have derived sufficient conditions that guarantee the convexity of the rate region and the uniqueness of the pure-strategy NB solution. The corresponding necessary and sufficient condition is desirable and can be given in future work. Moreover, for the coordination of mutually interfering CR users, interference alignment could be a candidate technique besides orthogonal signalling and interference mitigation to convexify the rate region. It is worth applying interference alignment to spectrum sharing CR networks and compare its performance with other approaches.

Last but not least, the CR-primary and CR-CR interference could also be jointly optimised and mitigated in future work.

Appendix A

Derivation of (3.16)

Substituting (3.9) and (3.10) into (3.15), we have

$$\begin{aligned}
\phi_{\mathrm{Y}}(\omega) = \exp\Bigg\{ & \lambda\pi \int_H f_{\mathrm{h}}(h) \int_{r_{\mathrm{cc}}} f_{\mathrm{cc}}(r) \Big[R^2 \left(1 - e^{i\omega g(R) p(r) h}\right) \\
& + i\omega p_{\mathrm{pwc}}(r_{\mathrm{cc}}) h \int_0^{g(R)} \left(g^{-1}(t)\right)^2 e^{i\omega t p(r) h} dt \Big] \, dr \, dh \Bigg\} \\
= \exp\Bigg\{ & \lambda\pi \int_H f_{\mathrm{h}}(h) \int_0^{r_{\mathrm{pwc}}} f_{\mathrm{cc}}(r) \Big[R^2 \Big(1 - e^{i\omega (\frac{r}{r_{\mathrm{pwc}}})^{\alpha} P_{\max} g(R) h}\Big) \\
& + \frac{i\omega r^{\alpha} P_{\max} h}{r_{\mathrm{pwc}}^{\alpha}} \int_0^{g(R)} \left(g^{-1}(t)\right)^2 e^{i\omega t (\frac{r}{r_{\mathrm{pwc}}})^{\alpha} P_{\max} h} dt \Big] dr dh \\
& + \lambda\pi \int_H f_{\mathrm{h}}(h) \int_{r_{\mathrm{pwc}}}^{\infty} f_{\mathrm{cc}}(r) \Big[R^2 \left(1 - e^{i\omega g(R) P_{\max} h}\right) \\
& + i\omega P_{\max} h \int_0^{g(R)} \left(g^{-1}(t)\right)^2 e^{i\omega t P_{\max} h} dt \Big] \, dr \, dh \Bigg\}.
\end{aligned} \tag{A.1}$$

Using (3.1) and (A.1), the characteristic function (3.16) is obtained.

Appendix B

Derivation of (3.19)

$$
\begin{aligned}
K &= \int_H f_{\mathrm{h}}(h) \int_P f_{\mathrm{p}}(p) \sqrt{hp}\; dp\, dh \\
&= \int_H f_{\mathrm{h}}(h) \sqrt{h}\; dh \int_P f_{\mathrm{p}}(p) \sqrt{p}\; dp \\
&= \sqrt{P_{\max}} \int_H f_{\mathrm{h}}(h) \sqrt{h}\; dh \left(\int_0^c 2\pi r \lambda e^{-\lambda \pi r^2} \left(\frac{r}{c}\right)^{\frac{\alpha}{2}} dr + \int_c^\infty 2\pi \lambda r e^{-\lambda \pi r^2}\; dr \right) \\
&= \sqrt{P_{\max}} \int_H f_{\mathrm{h}}(h) \sqrt{h}\; dh \left(\int_0^c 2\pi r \lambda e^{-\lambda \pi r^2} \left(\frac{r}{c}\right)^{\frac{\alpha}{2}} dr + e^{-\lambda \pi c^2} \right), \qquad \text{(B.1)}
\end{aligned}
$$

where the first equality of (B.1) holds according to [41]. The equation (3.19) is obtained immediately from (B.1).

Appendix C

Derivation of (3.20)

Following similar steps as in [5], the characteristic function of the aggregate interference can be expressed as

$$\phi_{\mathrm{Y}}(\omega) = \lim_{l\to\infty} e^{\lambda\pi(l^2-R^2)(Q-1)} \tag{C.1}$$

where

$$\begin{aligned} Q &= E\left(e^{i\omega P g(V) H}\right) \\ &= \int_H f_{\mathrm{h}}(h) \int_R^l E\left[e^{i\omega P g(r) h}\right] \frac{2r}{l^2-R^2}\, dr\, dh \\ &= \int_H f_{\mathrm{h}}(h) \int_R^l \left[(1-q_{\mathrm{mh}}) + q_{\mathrm{mh}} e^{i\omega p g(r) h}\right] \frac{2r}{l^2-R^2}\, dr\, dh \\ &= 1 - q_{\mathrm{mh}} + q_{\mathrm{mh}} \int_H f_{\mathrm{h}}(h) \int_R^l e^{i\omega p g(r) h} \frac{2r}{l^2-R^2}\, dr\, dh. \end{aligned} \tag{C.2}$$

The integral in the last equality of (C.2) can be written as

$$\lim_{l\to\infty} \int_H f_{\mathrm{h}}(h) \int_R^l e^{i\omega p g(r) h} \frac{2r}{l^2-R^2}\, dr\, dh = 1 + \frac{1}{l^2-R^2} \int_H f_{\mathrm{h}}(h) T(\omega p h) dh \tag{C.3}$$

where $T(\omega p h)$ is given in (3.13). Substituting (C.2) and (C.3) into (C.1), we obtain (3.20).

Appendix D

Derivation of (3.25)

From (3.16) and (3.24), we have

$$
\begin{aligned}
k_n=&\frac{\lambda\pi}{i^n}\int_H f_{\mathrm{h}}(h)\int_0^{r_{\mathrm{pwc}}} f_{\mathrm{cc}}(r)\left[-R^2\left(\frac{ir^{\alpha}P_{\max}g(R)h}{{r_{\mathrm{pwc}}}^{\alpha}}\right)^n+\frac{n\left(ir^{\alpha}P_{\max}h\right)^n}{{r_{\mathrm{pwc}}}^{n\alpha}}\int_0^{g(R)}t^{n-1-\frac{2}{\beta}}dt\right]dr\,dh\\
&+\frac{\lambda\pi}{i^n}\int_H f_{\mathrm{h}}(h)\int_{r_{\mathrm{pwc}}}^{\infty} f_{\mathrm{cc}}(r)\left[-R^2\left(iP_{\max}g(R)h\right)^n+n\left(iP_{\max}h\right)^n\int_0^{g(R)}t^{n-1-\frac{2}{\beta}}dt\right]dr\,dh\\
=&\lambda\pi\int_H f_{\mathrm{h}}(h)h^n dh\left(\frac{n}{n-\frac{2}{\beta}}g^{n-\frac{2}{\beta}}(R)-R^2g^n(R)\right)\left[\int_0^{r_{\mathrm{pwc}}} f_{\mathrm{cc}}(r)\frac{\left(r^{\alpha}P_{\max}\right)^n}{{r_{\mathrm{pwc}}}^{n\alpha}}dr\right.\\
&\left.+\int_{r_{\mathrm{pwc}}}^{\infty} f_{\mathrm{cc}}(r)P_{\max}^n dr\right]\\
=&\frac{2\lambda\pi P_{\max}^n}{(n\beta-2)R^{n\beta-2}}\int_H f_{\mathrm{h}}(h)h^n dh\left(\int_0^{r_{\mathrm{pwc}}}\frac{f_{\mathrm{cc}}(r)r^{n\alpha}}{{r_{\mathrm{pwc}}}^{n\alpha}}dr+\int_{r_{\mathrm{pwc}}}^{\infty} f_{\mathrm{cc}}(r)dr\right).
\end{aligned}
\tag{D.1}
$$

The first equality of (D.1) is obtained based on the following fact

$$
\left[\frac{\partial^n}{\partial\omega^n}\right]_{\omega=0}e^{a\omega}=\left[\frac{\partial^n}{\partial\omega^n}\right]_{\omega=0}\sum_{i=0}^{\infty}\frac{(a\omega)^n}{n!}=a^n. \tag{D.2}
$$

In the last equality of (D.1), the first integral can be expressed as [115]

$$
\int_H f_{\mathrm{h}}(h)h^n dh=e^{n\mu+\frac{n^2\sigma^2}{2}} \tag{D.3}
$$

with μ and σ^2 given in (3.3) and (3.4), respectively. Also, the sum of the last two integrals in (D.1) can be simplified as

$$\int_0^{r_{\text{pwc}}} \frac{f_{\text{cc}}(r) r^{n\alpha}}{{r_{\text{pwc}}}^{n\alpha}} dr + \int_{r_{\text{pwc}}}^{\infty} f_{\text{cc}}(r) dr$$
$$= \frac{n\alpha(n\alpha-2)\cdots 2}{{r_{\text{pwc}}}^{n\alpha}(2\pi\lambda)^{\frac{n\alpha}{2}}} \left(1 - e^{-\lambda\pi {r_{\text{pwc}}}^2}\right) - \sum_{i=1}^{\frac{n\alpha}{2}-1} \frac{n\alpha(n\alpha-2)\cdots(n\alpha-2i+2)}{(2\pi\lambda {r_{\text{pwc}}}^2)^i} {r_{\text{pwc}}}^{n\alpha-2i} e^{-\lambda\pi {r_{\text{pwc}}}^2}. \tag{D.4}$$

Substituting (D.3) and (D.4) into (D.1) yields (3.25).

Appendix E

Derivation of (3.28)

$$
\begin{aligned}
\phi_{\mathrm{Y}}(\omega) &= \lim_{l\to\infty} \exp\left\{\lambda\pi D_l \left(E\left(e^{i\omega p_{\mathrm{pwc}} g(V)h}\right)-1\right)\right\} \\
&= \lim_{l\to\infty} \exp\left\{\lambda\pi D_l\left[\int_H f_{\mathrm{h}}(h)\int_0^\infty f_{\mathrm{cc}}(x)\int_0^{2\pi}\frac{1}{2\pi}\int_R^l \exp\left[i\omega p_{\mathrm{pwc}}(x) g(r_{\mathrm{cp}}(r,\theta))h\right]\frac{2r}{D_l} dr\, d\theta\, dx\, dh - 1\right]\right\} \\
&= \lim_{l\to\infty} \exp\left\{\lambda\int_H f_{\mathrm{h}}(h)\int_0^\infty f_{\mathrm{cc}}(x)\int_0^{2\pi}\int_R^l \exp\left[i\omega p_{\mathrm{pwc}}(x) g(r_{\mathrm{cp}}(r,\theta))h\right] r - r dr\, d\theta\, dx\, dh\right\}
\end{aligned}
\tag{E.1}
$$

with $D_l = l^2 - R^2$. The first equality in (E.1) is obtained in the same way as (C.1) and (C.2). Equation (3.28) can be obtained immediately from (E.1).

Appendix F

Proof of Proposition 1

Proof. Note that a function $g(x)$ is concave if and only if (i) $f(t) = g(tx_1 + (1-t)x_2)$, $0 \leq t \leq 1$ is a concave function of t for any feasible x_1 and x_2, which is equivalent to $f''(t) = d^2 f(t)/dt^2 \leq 0$; and (ii) the domain of $g(x)$ is convex [83].

We consider the following convex combination of two different sets of transmit covariance matrices: $(\mathbf{X}_1, \cdots, \mathbf{X}_L)$ and $(\mathbf{Z}_1, \cdots, \mathbf{Z}_L)$, that is

$$\begin{aligned} \mathbf{Q}(t) &= (1-t)(\mathbf{X}_1, \cdots, \mathbf{X}_M) + t(\mathbf{Z}_1, \cdots, \mathbf{Z}_M) \\ &= (\mathbf{X}_1, \cdots, \mathbf{X}_M) + t(\mathbf{Z}_1 - \mathbf{X}_1, \cdots, \mathbf{Z}_M - \mathbf{X}_M) \\ &= (\mathbf{X}_1, \cdots, \mathbf{X}_M) + t(\mathbf{Y}_1, \cdots, \mathbf{Y}_M) \end{aligned} \tag{F.1}$$

where $0 \leq t \leq 1$ and $\mathbf{Y}_i = \mathbf{Z}_i - \mathbf{X}_i$ $(i = 1, 2, \cdots, M)$. We can expand the utility function (5.2) as

$$\begin{aligned} f_i(t) &= I_i(\mathbf{Q}(t)) \\ &= \log_2 \det\left(\mathbf{I} + \mathbf{H}_{ii}\mathbf{Q}_i\mathbf{H}_{ii}^H\mathbf{R}_{-i}^{-1}\right) \\ &= \frac{1}{\ln 2} \ln \frac{\det(\mathbf{R}_{-i} + \mathbf{H}_{ii}\mathbf{Q}_i\mathbf{H}_{ii}^H)}{\det(\mathbf{R}_{-i})}, \quad i = 1, \cdots, M. \end{aligned} \tag{F.2}$$

Applying the well known property of matrix differential calculus [116], i.e.,

$$\frac{d}{dx}\ln\det\left(\mathbf{A}(x)\right)=\mathtt{tr}\left(\mathbf{A}(x)^{-1}\frac{d\mathbf{A}(x)}{dx}\right), \tag{F.3}$$

we can obtain the first derivative of $f_i(t)$ as

$$\begin{aligned} f_i^{'}(t)&=\frac{1}{\ln 2}\left[\frac{d}{dt}\ln\det(\mathbf{R}_{-i}+\mathbf{H}_{ii}\mathbf{Q}_i\mathbf{H}_{ii}^H)-\frac{d}{dt}\ln\det(\mathbf{R}_{-i})\right]\\ &=\frac{1}{\ln 2}\left[\mathtt{tr}\left(\left(\mathbf{R}_{-i}+\mathbf{H}_{ii}\mathbf{Q}_i\mathbf{H}_{ii}^H\right)^{-1}\left(\frac{d\mathbf{R}_{-i}}{dt}+\mathbf{H}_{ii}\mathbf{Y}_i\mathbf{H}_{ii}^H\right)\right)-\mathtt{tr}\left(\mathbf{R}_{-i}^{-1}\frac{d\mathbf{R}_{-i}}{dt}\right)\right]. \end{aligned} \tag{F.4}$$

In (F.3), $\mathbf{A}(x)$ is a matrix function of scalar parameter x. Using (F.4) and applying two other properties of matrix differential calculus [116], i.e.,

$$\frac{d}{dx}\mathtt{tr}\left(\mathbf{A}(x)\right)=\mathtt{tr}\left(\frac{d\mathbf{A}(x)}{dx}\right) \tag{F.5}$$

$$\frac{d}{dx}\mathbf{A}(x)^{-1}=-\mathbf{A}(x)^{-1}\frac{d\mathbf{A}(x)}{dx}\mathbf{A}(x)^{-1}, \tag{F.6}$$

the second derivative of $f_i(t)$ can be expressed as

$$\begin{aligned} f_i^{''}(t) \;=\; \frac{1}{\ln 2}\Bigg[&\mathtt{tr}\left(-\left(\mathbf{R}_{-i}+\mathbf{M}_i\right)^{-1}\left(\frac{d\mathbf{R}_{-i}}{dt}+\mathbf{N}_i\right)\left(\mathbf{R}_{-i}+\mathbf{M}_i\right)^{-1}\left(\frac{d\mathbf{R}_{-i}}{dt}+\mathbf{N}_i\right)\right)\\ &+\mathtt{tr}\left(\mathbf{R}_{-i}^{-1}\frac{d\mathbf{R}_{-i}}{dt}\mathbf{R}_{-i}^{-1}\frac{d\mathbf{R}_{-i}}{dt}\right)\Bigg] \end{aligned} \tag{F.7}$$

where $\mathbf{M}_i=\mathbf{H}_{ii}\mathbf{Q}_i\mathbf{H}_{ii}^H$ and $\mathbf{N}_i=\mathbf{H}_{ii}\mathbf{Y}_i\mathbf{H}_{ii}^H$.

Let $\mathbf{A}_i=\left(\mathbf{R}_{-i}+\mathbf{M}_i\right)^{-1}$ and $\mathbf{B}_i=d\mathbf{R}_{-i}/dt+\mathbf{N}_i$. Since $\mathbf{A}_i\succeq 0$, there exists a matrix $\mathbf{C}_i$ such that $\mathbf{A}_i=\mathbf{C}_i\mathbf{C}_i^H$. Thus, the first trace in the right hand side of (F.7) can be written as

$$\begin{aligned} \mathtt{tr}\left(-\mathbf{A}_i\mathbf{B}_i\mathbf{A}_i\mathbf{B}_i\right) \;&=\; -\mathtt{tr}\left(\mathbf{C}_i\mathbf{C}_i^H\mathbf{B}_i\mathbf{C}_i\mathbf{C}_i^H\mathbf{B}_i\right)\\ &=\; -\mathtt{tr}\left(\mathbf{C}_i^H\mathbf{B}_i\mathbf{C}_i\mathbf{C}_i^H\mathbf{B}_i\mathbf{C}_i\right)\\ &=\; -\mathtt{tr}\left(\left(\mathbf{C}_i^H\mathbf{B}_i\mathbf{C}_i\right)\left(\mathbf{C}_i^H\mathbf{B}_i\mathbf{C}_i\right)^H\right)\leq 0 \end{aligned} \tag{F.8}$$

The last equality in (F.8) is obtained using the fact that $\mathbf{B}_i$ is Hermitian. The inequality in (F.8) holds due to the fact that $\left(\mathbf{C}_i^H \mathbf{B}_i \mathbf{C}_i\right)\left(\mathbf{C}_i^H \mathbf{B}_i \mathbf{C}_i\right)^H \succeq 0$.

When $\mathbf{R}_{-i} \to \mathbf{I}$, in the right hand side of (F.7), $d\mathbf{R}_{-i}/dt = \sum_{j \neq i} \mathbf{H}_{ji} \mathbf{Y}_j \mathbf{H}_{ji}^H$ approaches $\mathbf{0}$. Then, in the first trace of (F.7), $(\mathbf{R}_{-i}+\mathbf{M}_i)^{-1}$ and $(d\mathbf{R}_{-i}/dt + \mathbf{N}_i)$ are dominated by $(\mathbf{I} + \mathbf{M}_i)^{-1}$ and $\mathbf{N}_i$, respectively. Note also that the second trace can be ignored as compared to the first one. Therefore, when $\mathbf{R}_{-i} \to \mathbf{I}$, $f_i''(t) \leq 0$.

The domain of the utility function $I_i(\mathbf{Q})$ for the MIMO interference system is $\{\mathbf{Q}_i | \mathbf{Q}_i \succeq 0,\ \mathtt{tr}(\mathbf{Q}_i) - p_i \leq 0,\ i = 1, 2, \cdots, M\}$, which is clearly convex. Therefore, the utility function $I_i(\mathbf{Q})$ is concave and consequently the rate region is convex when $\mathbf{R}_{-i} \to \mathbf{I}$. □

Appendix G

Proof of Proposition 2

Proof. First, by using the same methodology as the one used to prove Proposition 1, let us show that the objective function in (5.22) is concave under the condition that the interference-plus-noise covariance matrices $\mathbf{R}_{-i}$ approach $\mathbf{I}$, $\forall i$. Considering the convex combination in (F.1), the objective function of (5.22) can be expanded using (5.2) as

$$f(t) = \ln\left(\ln^L 2 \prod_{i=1}^{M} (I_i(\mathbf{Q}(t)) - I_i^{\mathrm{NE}})\right)$$

$$= \sum_{i=1}^{L} \ln\left(\ln \frac{\det(\mathbf{R}_{-i} + \mathbf{H}_{ii}\mathbf{Q}_i\mathbf{H}_{ii}^H)}{\det(\mathbf{R}_{-i})} - \ln 2 I_i^{\mathrm{NE}}\right). \tag{G.1}$$

Let us define

$$T_i = \ln \frac{\det(\mathbf{R}_{-i} + \mathbf{H}_{ii}\mathbf{Q}_i\mathbf{H}_{ii}^H)}{\det(\mathbf{R}_{-i})} - \ln 2 I_i^{\mathrm{NE}}. \tag{G.2}$$

Using (F.3), (F.5) and (F.6), we obtain the second derivative of $f(t)$ as

$$f''(t) = \sum_{i=1}^{M} \alpha + \beta + \gamma \tag{G.3}$$

where

$$\alpha = \frac{\mathtt{tr}\left(-\left(\mathbf{R}_{-i}+\mathbf{M}_i\right)^{-1}\left(\frac{d\mathbf{R}_{-i}}{dt}+\mathbf{N}_i\right)\left(\mathbf{R}_{-i}+\mathbf{M}_i\right)^{-1}\left(\frac{d\mathbf{R}_{-i}}{dt}+\mathbf{N}_i\right)\right)}{T_i} \tag{G.4}$$

$$\beta = \frac{\mathtt{tr}\left(\mathbf{R}_{-i}^{-1}\frac{d\mathbf{R}_{-i}}{dt}\mathbf{R}_{-i}^{-1}\frac{d\mathbf{R}_{-i}}{dt}\right)}{T_i} \tag{G.5}$$

$$\gamma = -\frac{\left[\mathtt{tr}\left(\left(\mathbf{R}_{-i}+\mathbf{M}_i\right)^{-1}\left(\frac{d\mathbf{R}_{-i}}{dt}+\mathbf{N}_i\right)\right)-\mathtt{tr}\left(\mathbf{R}_{-i}^{-1}\frac{d\mathbf{R}_{-i}}{dt}\right)\right]^2}{T_i^2}. \tag{G.6}$$

Similar to (F.8), the numerator of α in (G.4) is not positive. If the bargaining set S is not empty, then $T_i > 0$. Thus, α is not positive. Similarly, β in (G.5) can be ignored as compared to α when the interference-plus-noise covariance matrices approach $\mathbf{I}$. One can also see that γ in (G.6) is not positive. Therefore, when the interference-plus-noise covariance matrices $\mathbf{R}_{-i}$ approach $\mathbf{I}$, $f^{''}(t) \leq 0$.

The domain of the objective function in (5.22) is $\{\mathbf{Q}_i | \mathbf{Q}_i \succeq 0,\ \mathtt{tr}(\mathbf{Q}_i) - p_i \leq 0,\ i = 1, 2, \cdots, M\}$, which is obviously convex. Therefore, the objective function in (5.22) is concave.

As a next step, let us prove the convexity of the constraint set. The constraint set of (5.22) is identical to the bargain set (5.8). Specifically, it can be rewritten as

$$\begin{aligned} S = &\{\mathbf{Q}_i \,|\, \mathbf{Q}_i \succeq 0,\, \mathtt{tr}(\mathbf{Q}_i) - p_i \leq 0,\, i = 1, 2, \cdots, M\} \cap \\ &\{\mathbf{Q}_i \,|\, -I_i(\mathbf{Q}) + I_i^{\mathrm{NE}} \leq 0,\, i = 1, 2, \cdots, M\} \\ = &\, S_1 \cap S_2. \end{aligned} \tag{G.7}$$

It is easy to establish the convexity of the subset S_1 in (G.7), but the convexity of the subset S_2 is not obvious. Let us define $h(t) = -I_i(\mathbf{Q}(t)) + I_i^{\mathrm{NE}}$. Adopting the same methodology as the proof for the concavity of the utility function $I_i(\mathbf{Q})$, we have

$$\begin{aligned} h^{''}(t) = \mathtt{tr}\Bigg(&\left(\mathbf{R}_{-i}+\mathbf{M}_i\right)^{-1}\left(\frac{d\mathbf{R}_{-i}}{dt}+\mathbf{N}_i\right)\left(\mathbf{R}_{-i}+\mathbf{M}_i\right)^{-1}\left(\frac{d\mathbf{R}_{-i}}{dt}+\mathbf{N}_i\right) \\ &-\mathbf{R}_{-i}^{-1}\frac{d\mathbf{R}_{-i}}{dt}\mathbf{R}_{-i}^{-1}\frac{d\mathbf{R}_{-i}}{dt}\Bigg). \end{aligned} \tag{G.8}$$

A similar result can be obtained that when the interference-plus-noise covariance matrices $\mathbf{R}_{-i}$ approach $\mathbf{I}$, the second term inside the trace operator in (G.8) can be

ignored when compared to the first one. Thus, similar to (F.8), if the interference-plus-noise covariance matrices $\mathbf{R}_{-i}$ approach $\mathbf{I}$, (G.8) can be rewritten as

$$\begin{aligned} h^{''}(t) &\approx \mathtt{tr}\left(\left(\mathbf{R}_{-i}+\mathbf{M}_i\right)^{-1} \left(\frac{d\mathbf{R}_{-i}}{dt}+\mathbf{N}_i\right) \left(\mathbf{R}_{-i}+\mathbf{M}_i\right)^{-1} \left(\frac{d\mathbf{R}_{-i}}{dt}+\mathbf{N}_i\right)\right) \\ &= \mathtt{tr}\left(\left(\mathbf{C}_i^H\mathbf{B}_i\mathbf{C}_i\right) \left(\mathbf{C}_i^H\mathbf{B}_i\mathbf{C}_i\right)^H \right) \geq 0 \end{aligned} \tag{G.9}$$

which implies that when the interference-plus-noise covariance matrices $\mathbf{R}_{-i}$ approach $\mathbf{I}$, $h(t)$ is convex [83], i.e., the subset S_2 in (G.7) is convex. Consequently, the constraint set S in (G.7) is convex as well.

As we can see, the condition that the interference-plus-noise covariance matrices $\mathbf{R}_{-i}$ approach $\mathbf{I}$ is sufficient for both the concavity of the objective function in (5.22) and the convexity of its constraint set. Therefore, the Proposition 2 is proved. □

Bibliography

[1] U.S. Department of Commerce, National Telecommunications and Information Administration, Office of Spectrum Management, "United States frequency allocations," Oct. 2003, [Online]. Available: http://www.ntia.doc.gov/osmhome/allochrt.pdf.

[2] Ofcom UK, "Capture of spectrum utilisation information using moving vehicles," Report No.: 32/2008, Mar. 2009, [Online]. Available: http://stakeholders.ofcom.org.uk/binaries/research/technology-research/vehicles.pdf.

[3] Q. Zhao and B. M. Sadler, "A survey of dynamic spectrum access," *IEEE Signal Process. Mag.,* vol. 24, no. 3, pp. 79–89, May 2007.

[4] S. Haykin, "Cognitive radio: brain-empowered wireless communications," *IEEE J. Selected Areas Commun.*, vol. 23, no. 2, pp. 201–220, Feb. 2005.

[5] X. Hong, C.-X. Wang, and J. S. Thompson, "Interference modeling of cognitive radio networks," in *Proc. IEEE VTC'08-Spring*, Singapore, May 2008, pp. 1851–1855.

[6] FCC, "Facilitating opportunities for flexible, efficient, and reliable spectrum use employing cognitive radio technologies," Comments of the National Telecommunications and Information Administration on FCC ET Docket No. 03-108, Feb. 2005.

[7] FCC Spectrum Policy Task Force, "Report of the spectrum efficiency working group," Nov. 2002. [Online]. Available: http://www.fcc.gov/sptf/reports.html.

[8] Radio spectrum. (n.d.). In *Wikipedia*. Retrieved Mar. 2, 2011, from http://en.wikipedia.org/wiki/Radio_spectrum.

[9] B. Allen, M. Dohler, E. E. Okon, W. Q. Malik, A. K. Brown, and D. J. Edwards, *Ultra-Wideband Antennas and Propagation for Communications, Radar and Imaging*, West Sussex: John Wiley & Sons, 2007.

[10] J. Mitola, III, "Cognitive radio," Licentiate thesis, Royal Institute of Technology, Stockholm, Sweden, 1999.

[11] J. Mitola III and G. Q. Maguire Jr., "Cognitive radio: making software radios more personal," *IEEE Pers. Commun. Mag.*, vol. 6, no. 4, pp. 13–18, Aug. 1999.

[12] I. F. Akyildiz, W. Y. Lee, M. C. Vuran, and S. Mohanty, "NeXt generation/dynamic spectrum access/cognitive radio wireless networks: A survey," *Computer Networks*, vol. 50, no. 13, pp. 2127–2159, Sept. 2006.

[13] R. Qingchun and L. Qilian, "Performance analysis of energy detection for cognitive radio wireless networks," in *Proc. the 2nd International Conference on Wireless Algorithms, Systems and Applications (WASA '07)*, pp. 139-146, Chicago, Ill, USA, Aug. 2007.

[14] S. Haykin, D. J. Thomson, and J. H. Reed, "Spectrum sensing for cognitive radio," *Proc. IEEE*, vol. 97, no. 5, pp. 849-877, May 2009.

[15] G. Taricco, "Optimization of linear cooperative spectrum sensing for cognitive radio networks," *IEEE J. Sel. Topics Signal Process.*, vol. 5, no. 1, pp. 77–86, Feb. 2011.

[16] S. A. Jafar and S. Srinivasa, "Capacity limits of cognitive radio with distributed and dynamic spectral activity," in *Proc. IEEE ICC06*, Istanbul, Turkey, June 2006, pp. 5742-5747.

[17] D. Ugarte and A. B. McDonald, "On the capacity of dynamic spectrum access enable networks," in *Proc. IEEE DySPAN05*, Baltimore, USA, Nov. 2005, pp. 630-633.

[18] C. Cordeiro, K. Challapali, D. Birru, Sai Shankar, "IEEE 802.22: the first worldwide wireless standard based on cognitive radios", *IEEE DySPAN 2005*, pp. 328–337.

[19] IEEE P802.22, "Functional requirements for the 802.22 WRAN standard," IEEE 802.22-05/0007r48, 29 Nov. 2006.

[20] M. Gastpar, "On capacity under received-signal constraints," in *Proc. 42th Annual Allerton Conf. on Commun., Control, and Computing*, Oct. 2004, pp. 1322-1331.

[21] M. Gastpar, "On capacity under receive and spatial spectrum-sharing constraints," *IEEE Trans. Inform. Theory*, vol. 53, no. 2, pp. 471-487, Feb. 2007.

[22] A. Ghasemi and E. S. Sousa, "Capacity of fading channels under spectrum-sharing constraints," in *Proc. IEEE ICC06*, Istanbul, Turkey, June 2006, pp. 4373-4378.

[23] T. K. Phan, S. A. Vorobyov, N. D. Sidiropoulos, and C. Tellambura, "Spectrum sharing in wireless networks via QoS-aware secondary multicast beamforming," *IEEE Trans. Sig. Process.*, vol. 57, no. 6, pp. 2323–2335, June 2009.

[24] T. X. Brown, "An analysis of unlicensed device operation in licensed broadcast service bands," in *Proc. IEEE DySPAN'05*, Baltimore, USA, Nov. 2005, pp. 11–29.

[25] Z. Chen, C.-X. Wang, X. Hong, J. Thompson, S. A. Vorobyov and X. Ge, "Interference modeling for cognitive radio networks with power or contention control," in *Proc. IEEE WCNC 2010*, Sydney, Australia, Apr. 2010.

[26] X. Hong, C.-X. Wang, H.-H. Chen, and Y. Zhang, "Secondary spectrum access networks: recent development on the spatial models," *IEEE Veh. Technol. Mag.*, vol. 4, no. 2, pp. 36–43, June 2009.

[27] X. Hong, C.-X. Wang, J. Thompson, and Y. Zhang, "Demystifying white spaces," in *Proc. IEEE ICCCAS'08*, Xiamen, China, May 2008, pp. 350–354.

[28] T. Kamakaris, D. Kivanc-Tureli, and U. Tureli, "Interference model for cognitive coexistence in cellular systems," in *Proc. IEEE GLOBECOM'07*, Washington, DC, USA, Nov. 2007, pp. 4175–4179.

[29] R. S. Dhillon and T. X. Brown, "Models for analyzing cognitive radio interference to wireless microphones in TV bands," in *Proc. IEEE DySPAN'08*, Chicago, USA, Oct. 2008, pp. 1–10.

[30] G. L. Stuber, S. Almalfouh, and D. Sale, "Interference analysis of TV band whitespace," in *Proc. IEEE*, vol. 97, no. 4, pp. 741–754, Apr. 2009.

[31] N. Hoven and A. Sahai, "Power scaling for cognitive radio," in *Proc. IEEE WNCMC'05*, Hawaii, USA, June 2005, pp. 250–255.

[32] R. Menon, R. M. Buehrer and J. Reed, "Outage probability based comparison of underlay and overlay spectrum sharing techniques," in *Proc. IEEE DySPAN'05*, Baltimore, USA, Nov. 2005, pp. 101–109.

[33] M. Timmers, S. Pollin, A. Dejonghe, A. Bahai, L. Van der Perre, and F. Catthoor, "Accumulative interference modeling for cognitive radios with distributed channel access," in *Proc. IEEE CrownCom'08*, Singapore, May 2008.

[34] R. Menon, R. Buehrer, and J. Reed, "On the impact of dynamic spectrum sharing techniques on legacy radio systems," *IEEE Trans. Wireless Commun.*, vol. 7, no. 11, pp. 4198–4207, Nov. 2008.

[35] Federal Communications Commission, "Second Report and Order and Memorandum Opinion and Order, in the matter of unlicensed operation in the TV broadcast bands (ET Docket No. 04-186) and additional spectrum for unlicensed devices below 900 MHz and in the 3 GHz band (ET Docket No. 02-380), FCC 08-260," Nov. 2008.

[36] G. L. Stuber, *Principles of Mobile Communication*, 2nd Edition, Boston: Kluwer Academic Publishers, 2001.

[37] A. Goldsmith, *Wireless Communications*, Cambridge: Cambridge University Press, 2005.

[38] D. Stoyan, W. S. Kendall, and J. Mecke, *Stochastic Geometry and Its Applications*, Chichester: John Wiley & Sons, 1986.

[39] B. Matern, *Spatial Variation*, Vol. 36 of *Lecture Notes in Statistics,* 2 edn, Springer, New York, 1986.

[40] H. Q. Nguyen, F. Baccelli and D. Kofman, "A stochastic geometry analysis of dense IEEE 802.11 networks," in *Proc. IEEE INFOCOM'07*, Anchorage, USA, May 2007, pp. 1199–1207.

[41] E. S. Sousa and J. A. Silvester, "Optimum transmission range in a direct-sequence spread-spectrum multihop pack radio network," *IEEE J. Sel. Areas Commun.*, vol. 8, no. 5, pp. 762–771, June 1990.

[42] X. Yang and A. P. Pertropulu, "Co-channel interference modeling and analysis in a Poisson field of interferers in wireless communications," *IEEE Trans. Signal Process.*, vol. 51, no. 1, pp. 63–76, Jan. 2003.

[43] P. C. Pinto and M. Z. Win, "Communication in a poisson field of interferers," in *Proc. IEEE 40th Annual Conf. Inform. Sciences and Systems*, Princeton, USA, Mar. 2006, pp. 432–437.

[44] J. E. Paloheimo, "On a theory of search," *Biometrika*, vol. 58, no. 1, pp. 61–75, Apr. 1971.

[45] D. Stoyan, "On estimators of the nearest neighbour distance distribution function for stationary point processes," *Metrika*, vol. 64, no. 2, pp. 139-150, Feb. 2006.

[46] J. Salo, L. Vuokko, H. M. El-Sallabi, and P. Vainikainen, "An additive model as a physical basis for shadow fading," *IEEE Trans. Veh. Technol.*, vol. 56, no. 1, pp. 13–26, Jan. 2007.

[47] M. Pratesi, F. Santucci, and F. Graziosi, "Generalized moment matching for the linear combination of log-normal RVs: application to outage analysis in wireless systems," *IEEE Trans. Wireless Commun.*, vol. 5, no. 5, pp. 1122–1132, May 2006.

[48] C. C. Chan and S. V. Hanly, "Calculating the outage probability in a CDMA network with spatial poisson traffic," *IEEE Trans. Veh. Technol.*, vol. 50, no. 1, pp. 183–204, Jan. 2001.

[49] R. Menon, R. M. Buehrer, and J. H. Reed, "Impact of exclusion region and spreading in spectrum-sharing ad hoc networks," in *Proc. 1st Int. Workshop on Technology and Policy for Accessing Spectrum, TAPAS06*, Aug. 2006.

[50] B. Wild and K. Ramchandran, "Detecting primary receivers for cognitive radio applications," in *Proc. IEEE DySPAN 2005*, Nov. 2005, pp. 124–130.

[51] J. Andrews, "Interference cancellation for cellular systems: a contemporary overview," *IEEE Wireless Comm.*, vol. 12, no. 2, pp. 19–29, Apr. 2005.

[52] P. Popovski, H. Yomo, K. Nishimori, R. D. Taranto, and R. Prasad, "Opportunistic interference cancellation in cognitive radio systems," in *Proc. IEEE DySPAN'07*, Dublin, Ireland, Apr. 2007, pp. 472–475.

[53] H. Yamaguchi, "Active interference cancellation technique for MB-OFDM cognitive radio," in *Proc. 34th European Microwave Conf.*, Amsterdam, Netherland, Oct. 2004, pp. 1105–1108.

[54] J. Zhou and J. S. Thompson; "MISO aided linear interference mitigation for cognitive radio," in *Proc. IET Seminar on Smart Antennas and Cooperative Communications*, London, UK, Oct. 2007.

[55] Ofcom UK, "A study into the application of interference cancellation techniques," Report No.: 72/06/R/037/U, Apr. 2006, [Online]. Available: http://www.ofcom.org.uk/research/technology/research/emer_tech/intcx/summary.pdf.

[56] X. Hong, Z. Chen, C.-X. Wang, and S. A. Vorobyov, "Cognitive radio networks: interference cancellation and management techniques," *IEEE Veh. Technol. Mag.*, vol. 4, no. 4, pp. 76–84, Dec. 2009.

[57] B. F. Boroujeny and R. Kempter, "Multicarrier communication techniques for spectrum sensing and communication in cognitive radios," *IEEE Commun. Mag.*, vol. 46, no. 4, pp. 80–85, Apr. 2008.

[58] J. Zhou and J. S. Thompson, "Linear precoding for the downlink of multiple input single output coexisting wireless systems," *IET Commun.*, vol. 2, no. 6, pp. 742–752, July 2008.

[59] G. Zheng, K.-K. Wong, and B. Ottersten, "Robust cognitive beamforming with bounded channel uncertainties," *IEEE Trans. Sig. Process.*, vol. 57, no. 12, pp. 4871–4881, Dec. 2009.

[60] L. Zhang, Y.-C. Liang, Y. Xin, and H. V. Poor, "Robust cognitive beamforming with partial channel state information," *IEEE Trans. Wireless Commun.*, vol. 8, no. 8, pp. 4143–4153, Aug. 2009.

[61] G. Zheng, S. Ma, K.-K. Wong, and T.-S. Ng, "Robust beamforming in cognitive radio," *IEEE Trans. Wireless Commun.*, vol. 9, no. 2, pp. 570–576, Feb. 2010.

[62] L. Bixio, G. Oliveri, M. Ottonello, M. Raffetto, and C. S. Regazzoni, "Cognitive radios with multiple antennas exploiting spatial opportunities," *IEEE Trans. Sig. Process.*, vol.58, no. 8, pp. 4453–4459, Aug. 2010.

[63] R. Zhang and Y.-C. Liang, "Exploiting multi-antennas for opportunistic spectrum sharing in cognitive radio networks," *IEEE J. Sel. Topics Sig. Process.*, vol. 2, no. 1, pp. 88–102, Feb. 2008.

[64] G. Scutari, D. P. Palomar, and S. Barbarossa, "Cognitive MIMO radio: competitive optimality design based on subspace projections," *IEEE Sig. Process. Mag.*, vol. 25, no. 6, pp. 46–59, Nov. 2008.

[65] R. Roy, T. Kailath, "ESPRIT-estimation of signal parameters via rotational invariance techniques," *IEEE Trans. on ASSP,* vol. 37, no. 7, pp. 984–995, Jul. 1989.

[66] H. Yi, H. Hu, Y. Rui, K. Guo, and J. Zhang, "Null space-based precoding scheme for secondary transmission in a cognitive radio MIMO system using second-order statistics," in *Proc. IEEE ICC'09,* Dresden, Germany, June 2009.

[67] R. Zhang, F. Gao, and Y.-C. Liang, "Cognitive beamforming made practical: Effective interference channel and learning-throughput tradeoff," *IEEE Trans. Commun.,* vol. 58, no. 2, pp. 706–718, Feb. 2010.

[68] H. Yi, "Nullspace-based secondary joint transceiver scheme for cognitive radio MIMO networks using second-order statistics," in *Proc IEEE ICC'11*, Cape Town, South Africa, May 2010.

[69] F. Gao, R. Zhang, Y.C. Liang, and X. Wang, "Design of learning-based MIMO cognitive radio systems," *IEEE Trans. Veh. Technol.*, vol. 59, no. 4, pp. 1707–1720, Apr. 2010.

[70] O. Somekh, O. Simeone, Y. Bar-Ness, and W. Su, "Detecting the number of transmit antennas with unauthorized or cognitive receivers in MIMO systems," in *Proc. IEEE MILCOM'07,* Orlando, USA, Oct. 2007.

[71] Z. Chen, S. A. Vorobyov, C.-X. Wang, and J. S. Thompson, "Nash bargaining over MIMO interference systems," in *Proc. IEEE ICC'09*, Dresden, Germany, June 2009.

[72] D. W. Tufts, A. C. Kot, and R. J. Vaccaro, "The analysis of threshold behavior of SVD-based algorithms", in *Proc. XXIst Annu. Asilomar Conf. Signals. Syst. Comput.,* Monterey, USA, Nov. 1987, pp. 2416–2419.

[73] J. Thomas, L. Scharf, and D. Tufts, "The probability of a subspace swap in the SVD," *IEEE Trans. on Sig. Process.,* vol. 43, no. 3, pp. 730–736, Mar. 1995.

[74] M. Hawkes, A. Nehorai, and P. Stoica, "Performance breakdown of subspace-based methods: prediction and cure," in *Proc. IEEE ICASSP'01*, Salt Lake City, USA, May 2001, pp. 4005–4008.

[75] F. Li, H. Liu, and R. J. Vaccaro, "Performance analysis for DOA estimation algorithm: unification, simplification and observations," *IEEE Trans. Aerospace and Elec. Sys.,* vol. 29, no. 4, pp. 1170–1184, Apr. 1993.

[76] M. Chiani, M. Z. Win, A. Zanella, R. K. Mallik, and J. H. Winters, "Bounds and approximations for optimum combining of signals in the presence of multiple co-channel interferers and thermal noise," *IEEE Trans. Commun.,* vol. 51, no. 2, pp. 296–307, Feb. 2003.

[77] Z. Chen, C.-X. Wang, X. Hong, J. Thompson, S. A. Vorobyov, F. Zhao, H. Xiao, and X. Ge, "Interference mitigation for cognitive radio MIMO systems based on practical precoding," submitted to *IEEE Trans. Wireless Commun.*, 2011.

[78] I. Katzela and M. Naghshineh, "Channel assignment schemes for cellular mobile telecommunication systems: a comprehensive survey," *IEEE Pers. Commun.,* vol.3, no.3, pp. 10–31, June 1996.

[79] N. Nie and C. Comaniciu, "Adaptive channel allocation spectrum etiquette for cognitive radio networks," in *Proc. IEEE DySPAN'05*, Baltimore, USA, Nov. 2005, pp. 269–278.

[80] E. Zeydan, D. Kivanc-Tureli, and U. Tureli, "Joint iterative channel allocation and beamforming algorithm for interference avoidance in multiple-antenna Ad Hoc networks," in *Proc. IEEE MILCOM'07*, Orlando, USA. Oct. 2007, pp. 1–7.

[81] E. Zeydan, D. Kivanc-Tureli, and U. Tureli, "Cross layer interference mitigation using a convergent two-stage game for ad hoc networks," in *Proc. IEEE CISS'08*, Princeton, USA, Mar. 2008, pp. 671–675.

[82] C.-L. Hwang and A. S. M. Masud, *Multiple Objective Decision Making-Methods and Applications*, vol. 164 of *Lecture Notes in Economics and Mathematical Systems*. Berlin, Germany: Springer-Verlag, 1979.

[83] S. Boyd and L. Vandenberghe, *Convex Optimization*. Cambridge: Cambridge University Press, 2004.

[84] R. Wang, V. K. N. Lau, L. Lv, and B. Chen, "Joint cross-layer scheduling and spectrum sensing for OFDMA cognitive radio systems," *IEEE Trans. Wireless Commun.*, vol. 8, no. 5, pp. 2410–2416, May 2009.

[85] H. Liu, G. Xu, L. Tong, and T. Kailath, "Recent developments in blind channel equalization: From cyclostationarity to subspaces," *Signal Process.,* vol. 50, pp. 83-99, Jan. 1996.

[86] R. M. Beeson and W. S. Meisel, "The optimisation of complex systems with respect to multiple criteria," in *IEEE Systems, Man and Cybernetics Group Annual Symposium*, Anaheim, Calif., Oct. 1971, pp. 144–149.

[87] L. Zadeh, "Optimality and non-scalar-valued performance criteria," *IEEE Trans. Automat. Contr.*, vol. 8, no. 1, pp. 59–60, Jan. 1963.

[88] C. M. Fonseca and P. J. Fleming, "Multiobjective optimisation and multiple constraint handling with evolutionary algorithms-Part I: A unified formulation," *IEEE Trans. Syst., Man, Cybern.*, vol. 28, no. 1, pp. 26–37, Jan. 1998.

[89] A. Ben-Tal, "Characterization of Pareto and lexicographic optimal solutions," in *Multiple Criteria Decision Making Theory and Application*, G. Fandel and T. Gal, Eds., vol. 177 of *Lecture Notes in Economics and Mathematical Systems*. Berlin, Germany: Springer-Verlag, 1980, pp. 1–11.

[90] W. Dinkelbach, "Multicriteria decision models with specified goal levels," in *Multiple Criteria Decision Making Theory and Application*, vol. 177 of *Lecture Notes in Economics and Mathematical Systems*, G. Fandel and T. Gal, Eds. Berlin, Germany: Springer-Verlag, 1980, pp. 52–59.

[91] E. Larsson and E. Jorswieck, "Competition versus collaboration on the MISO interference channel", *IEEE J. Sel. Areas Commun.*, vol. 26, no. 7, pp. 1059–1069, Sept. 2008.

[92] A. Leshem and E. Zehavi, "Bargaining over the interference channel," in *Proc. IEEE ISIT*, Seattle, USA, Jul. 2006, pp. 2225–2229.

[93] O. Mehanna, J. Marcos, and N. Jindal, "On achievable rates of the two-user symmetric Gaussian interference channel," in *Proc. 2010 48th Annual Allerton Conference on Communication, Control, and Computing*, Monticello, IL, Sep. 2010, pp.1273–1279.

[94] S. Ye and R. S. Blum, "Optimized signaling for MIMO interference systems with feedback," *IEEE Trans. Signal Process.*, vol. 51, no. 11, pp. 2839–2848, Nov. 2003.

[95] L. Zhang, Y. Xin and Y.-C. Liang, "Weighted sum rate optimization for cognitive radio MIMO broadcast channels," *IEEE Trans. Wireless Commun.*, vol. 8, no. 6, pp. 2950–2959, Jun. 2009.

[96] Y. Ma, "Rate maximization for downlink OFDMA with proportional fairness," *IEEE Trans. Veh. Technol.*, vol. 57, no. 5, pp. 3267–3274, Sep. 2008.

[97] E. AHman and Z. Altman, "S-modular games and power control in wireless networks," *IEEE Trans. Autom. Control*, vol. 48, pp. 839–842, May 2003.

[98] J. F. Nash, "The bargaining problem," *Econometrica*, vol. 18, no. 2, pp. 155–162, Apr. 1950.

[99] A. Leshem and E. Zehavi, "Cooperative game theory and the Gaussian interference channel," *IEEE J. Sel. Areas Commun.*, vol. 26, no. 7, pp. 1078–1088, Sept. 2008.

[100] J. Gao, S.A. Vorobyov, and H. Jiang, "Cooperative resource allocation games under spectral mask and total power constraints," *IEEE Trans. Signal Process.*, vol. 58, no. 8, pp. 4379–4395, Aug. 2010.

[101] M. Nokleby, A. L. Swindlehurst, R. Yue, and Y. Hua, "Cooperative power scheduling for wireless MIMO networks," in *Proc. IEEE GLOBECOM'07*, Washington DC, USA, Nov. 2007, pp. 2982–2986.

[102] G. Arslan, M. F. Demirkol, and Y. Song, "Equilibrium efficiency improvement in MIMO interference systems: a decentralized stream control approach," *IEEE Trans. Wireless Commun.*, vol. 6, no. 8, pp. 2984–2993, Aug. 2007.

[103] F. R. Farrokhi, G. J. Foschini, A. Lozano and R. A. Valenzuela, "Link-optimal space-time processing with multiple transmit and receive antennas," *IEEE Commun. Lett.* vol. 5, no. 3, pp. 85–87, Mar. 2001.

[104] M. J. Osborne and A. Rubinstein, *A Course in Game Theory*, Cambridge, MA: MIT Press, 1994.

[105] W. Wu, W. Rhee, S. Boyd, and J. M. Cioffi, "Iterative water-filling for Gaussian vector multiple-access channels," *IEEE Trans. Inf. Theory*, vol. 50, no. 1, pp.145–152, Jan. 2004.

[106] G. Scutari, D. P. Palomar, and S. Barbarossa, "Optimal linear precoding strategies for wideband noncooperative systems based on game theory–Part I: Nash equilibria," *IEEE Trans. Signal Process.*, vol. 56, no. 3, pp. 1230–1249, Mar. 2008.

[107] J. Nash, "Two-person cooperative games," *Econometrica*, vol. 21, no. 1, pp. 128–140, Jan. 1953.

[108] J. P. Aubin, *Mathematical Method for Game and Economic Theory*, Amsterdam: Elsevier, 1980.

[109] S. Verdu, *Multiuser Detection*, Cambridge: Cambridge University Press, 1998.

[110] G. Xue, J. Weng, T. Le-Ngoc, and S. Tahar, "Adaptive multistage parallel interference cancellation for CDMA," *IEEE J. Sel. Areas Commun.*, vol. 17, no. 10, pp. 18151827, Oct. 1999.

[111] E. Telatar, "Capacity of multiantenna Gaussian channels," *AT&T Bell Laboratories*, Tech. Memo., Jun. 1995.

[112] W. Thomson, "Cooperative models of bargaining," *Handbook of Game Theory*, vol. 2, no. 35, Elsevier Science, 1994.

[113] R. Jain, A. Durresi, and G. Babic, "Throughput fairness index: an explanation," *ATM Forum*, ATM Forum/990045, Feb. 1999.

[114] E. Jorswieck, A. Sezgin, and X. Zhang, "Throughput versus fairness: channel-aware scheduling in multiple antenna downlink," *EURASIP Journal on Wireless Communications and Networking, special issue: Fairness in Radio Resource Management for Wireless Networks*, vol. 2009 (2009), Article ID 271540, 13 pages, doi:10.1155/2009/2715402008.

[115] J. Aitchison and J. A. C. Brown, *The Lognormal Distribution*, Cambridge: Cambridge University Press, 1957.

[116] J. R. Magnus and H. Neudecker, *Matrix Differential Calculus with Applications in Statistics and Economics*, 2nd ed. New York: John Wiley & Sons, 1999.